

NASA TN D-318

NASA TN D-318



7N-02
198725
P83

TECHNICAL NOTE

D-318

A WIND-TUNNEL INVESTIGATION OF THREE PROPELLERS
THROUGH AN ANGLE-OF-ATTACK RANGE

FROM 0° TO 85°

By Paul F. Yaggy and Vernon L. Rogallo

Ames Research Center
Moffett Field, Calif.

NATIONAL AERONAUTICS AND SPACE ADMINISTRATION
WASHINGTON

May 1960

(NASA-TN-D-318) A WIND-TUNNEL INVESTIGATION
OF THREE PROPELLERS THROUGH AN
ANGLE-OF-ATTACK RANGE FROM 0 DEG TO 85 DEG
(NASA) E3 P

N89-70451

Unclass
00/02 0198725

NATIONAL AERONAUTICS AND SPACE ADMINISTRATION

TECHNICAL NOTE D-318

A WIND-TUNNEL INVESTIGATION OF THREE PROPELLERS
THROUGH AN ANGLE-OF-ATTACK RANGE
FROM 0° TO 85°

By Paul F. Yaggy and Vernon L. Rogallo

SUMMARY

An investigation of propeller performance, including in-plane forces and out-of-plane moments, has been made for three propellers operating through a range of thrust-axis angles of attack from 0° (horizontal) to 85°. The operating conditions were selected to simulate those anticipated for VTOL/STOL aircraft in the take-off, landing, and transition regimes. The propellers differed widely in plan form and included one with flapping hinges.

The results of the investigation revealed that for all three propellers similar variations in the forces and moments with thrust-axis angle of attack and advance ratio were present. Further, the thrust and power were nearly constant and in-plane forces and out-of-plane moments increased approximately linearly over large ranges of thrust-axis angle of attack for constant blade angles and effective advance ratios.

INTRODUCTION

Operation of a propeller in an unsymmetrical flow field is known to produce oscillating air loads on the propeller blades which, in turn, produce propeller shaft in-plane forces and out-of-plane moments. The flow field asymmetries result, generally, from either thrust-axis tilt or from flow angles induced by the airplane lifting surfaces. The propellers on VTOL/STOL-type aircraft will encounter greater asymmetries than those on conventional aircraft, either because of large angles of thrust-axis tilt (tilting-wing or tilting-propeller types), or because of the induced upwash of high lift devices (vectored slipstream types). Since the blade loads largely dictate the propeller design and the forces and moments are significant in terms of airplane stability and control, a knowledge of the magnitudes of these parameters through a large range of thrust-axis tilt angles is required to establish design criteria.

Previous investigators (ref. 1) have presented the aerodynamic characteristics of a specific, lightly loaded propeller over a very wide range of operating conditions. The present investigation was directed

toward more heavily loaded, higher solidity propellers operating at lower advance ratios and high tilt angles, that is, conditions expected to be typical of VTOL/STOL aircraft in the take-off, transition, and landing regimes. Tests were made of three full-scale propellers of different design over a range of thrust-axis angles of attack from 0° to 85° and advance ratios ranging from 0 to 1.8. The tests were conducted in the Ames 40- by 80-Foot Wind Tunnel.

NOTATION

B number of blades

b propeller blade chord, ft

$$c_e \text{ propeller equivalent chord, } \frac{\int_0^R br^2 dr}{\int_0^R r^2 dr}, \text{ ft}$$

c_{ld} propeller blade design section lift coefficient

C_m pitching-moment coefficient, $\frac{M}{\rho n^2 D^5}$

C_N normal-force coefficient, $\frac{N}{\rho n^2 D^4}$

C_P power coefficient, $2\pi C_Q$

C_Q torque coefficient, $\frac{Q}{\rho n^2 D^5}$

C_S side-force coefficient, $\frac{S}{\rho n^2 D^4}$

C_T thrust coefficient, $\frac{T}{\rho n^2 D^4}$

C_Y yawing-moment coefficient, $\frac{Y}{\rho n^2 D^5}$

D propeller diameter, ft

h maximum thickness of propeller blade section, ft

J propeller advance ratio based on streamwise component of velocity,
 $\frac{V_\infty}{nD}$

J' propeller advance ratio based on velocity component normal to propeller disk, $\frac{V_\infty \cos \alpha}{nD}$

M	propeller pitching moment, ft-lb
N	propeller normal force, lb
n	propeller rotational speed, rps
Q	propeller torque, ft-lb
r	blade section radius, ft
R	propeller tip radius, ft
S	propeller side force, lb
T	propeller thrust, lb
V_∞	velocity of free-stream tunnel air stream, fps
x	fraction of propeller tip radius, $\frac{r}{R}$
Y	propeller yawing moment, ft-lb
α	angle of attack measured from longitudinal tunnel axis to propeller shaft axis, deg
β	propeller blade angle measured at the 0.75 R, deg
η	propeller efficiency based on free-stream tunnel velocity, $J \frac{C_T}{C_P}$
ρ	mass density of air, slugs/cu ft
σ_e	weighted propeller solidity, $\frac{B\sigma_e}{\pi R}$

The positive directions of the propeller forces and moments are indicated on figure 1.

MODEL AND APPARATUS

Propellers

The propellers selected for the investigation were greatly different in both aerodynamic and structural design. Propeller 1 was of conventional design; propeller 2 was designed to produce large normal forces with reduced shaft moments; and propeller 3 was an articulated (flapping out-of-plane only) propeller designed to eliminate shaft moments. The physical characteristics of these propellers are listed in the following table:

Propeller	No. 1 Curtiss C634S-C500	No. 2 Curtiss C634S-C300	No. 3 Vertol 76
Diameter	12.0 feet	10.0 feet	9.5 feet
Number of blades	3	3	3
Blade construction	Hollow steel	Fiberglas	Wood and steel
Airfoil sections	NACA 16 series	NACA 64 series	NACA 0009
Blade designation	858-7C4-36	X100188	Q76R1002
Activity factor/blade	150	188	178
Flapping hinge offset	---	---	3 inches

Blade plan-form curves for the three propellers are presented in figure 2.

Testing Apparatus

For the tests, the propellers were mounted on the propeller test stand in the Ames 40- by 80-Foot Wind Tunnel, as shown in figure 3. Principal features of this stand are:

1. The shroud is isolated from the wind-tunnel balance system so that only propeller forces and moments are measured.
2. Wide ranges of power and rotational speed are possible through the use of proper motor and reduction gear combinations.
3. The angle of the thrust axis can be varied continuously from 0° to 85° and 180° to 95° (the latter by mounting the propeller in a reversed position).

Instrumentation

The blades of each propeller were equipped with strain gages which permitted monitoring of the blade stresses. Thus, the maximum range of test variables as limited by stress was investigated; however, no attempt was made to study the blade-stress problem. All conditions for which data are presented in this report were within the safe operating limits specified by the manufacturer.

Power input to the propeller was measured by means of wattmeters in the supply lines to the electric motors. These wattmeters were calibrated for drive system losses and, hence, represent the true power input to the propeller.

Six-component force data were measured by the wind-tunnel balance system upon which the test stand was mounted.

TESTS

Static Tests

A
2
6
7

Data for conditions of zero advance ratio were obtained for propellers 1 and 2. The test stand was positioned at the maximum angle of attack, as shown in figure 3(a), and the tunnel access doors (essentially the entire upper half of the test section) were open to the large test chamber which formed a plenum chamber. The propeller was sufficiently far removed from the floor that there was no appreciable ground effect. This technique prevented recirculation of flow in the tunnel and assured true static conditions.

Tests at Forward Velocities

Two different techniques were employed in obtaining data at forward velocity. For propellers 1 and 2 the thrust-axis angle of attack and tunnel air velocity were held constant while the blade angle and rotational speed of the propeller were varied. For propeller 3 the tunnel air velocity, blade angle, and rotational speed were held constant while the thrust-axis angle of attack was varied. A comparison of the results of these two techniques revealed no perceptible differences in the data which could be attributed to the techniques themselves. It will be noted that the ranges of variables for propellers 2 and 3 are considerably smaller than for 1 because of structural limitations of the propeller blades.

Reduction of Data

Although six components of forces and moments were measured, only five are presented since the propeller side forces were found to be negligible.¹ The values of the pitching moment were of the same order of magnitude as the minimum value which could be sensed by the measuring device, producing a great deal of scatter in the results. Therefore, the pitching-moment variations were obtained by a somewhat indirect method, but one considered to give accurate values. This method required the assumption that the maximum value of shaft moment occurs simultaneously with the response of the propeller blade to the maximum load. With this assumption, which is in accord with limited unpublished data, it is necessary only to know the yawing moment and its phase angle relative to the azimuth angle at which maximum loading occurs in order to obtain the pitching moment, since yawing and pitching moments are simply components of the total shaft moment. This procedure was followed, using the measured yawing moment and the phase angle as determined from the blade-stress records.

¹It should be noted that for a propeller in yaw this would not be true.

It should be noted that no variations of yawing moment and pitching moment are presented for propeller 3 since the articulation essentially reduced these shaft moments to zero.

No corrections for tunnel wall constraint have been applied to the data. However, these corrections are believed to be very small because of the large ratios of tunnel cross-sectional area to propeller disk areas. Flow surveys at the plane of the propeller (propeller removed) indicated no significant induced inflow angles due to the presence of the test stand shroud; hence no stream angle corrections were applied.

Numerous data points were obtained during the tests but it was impractical to show each point on the plots. The following data are therefore presented to indicate the accuracy of the measurements on the basis of the greatest deviation of test points from the faired curves.

C_T	± 8 percent
C_P	± 7 percent
C_N	± 9 percent
C_Y	± 9 percent
C_m	± 9 percent

It is emphasized that these are maximum deviations, the average deviations being much less than these indicated values.

All moments presented are referred to the intersection of the thrust axis and the propeller plane.

RESULTS AND DISCUSSION

As was noted in the introduction, it is expected that the results of this study will be of particular interest in defining propeller performance and the direct effect of the propeller on stability and control during the transition flight phase of VTOL/STOL aircraft. Transition is defined here as that flight phase lying between pure hover, or slow vertical flight, and conventional aircraft flight; in this region the propeller might be expected to operate at low forward velocities and large angular inclinations to the air stream.

To examine the above-mentioned effects in detail requires specification of a particular vehicle and is beyond the scope of this report; the primary purpose here is to make available the information necessary for such an analysis. However, certain generalizations can be made regarding propeller characteristics likely to be encountered in transition flight and it is proposed to discuss these briefly. Although data from the study of propeller 1 will be used to illustrate these generalizations, the same conclusions could be drawn from examination of data from the studies of either of the other two propellers.

Five-component data for propeller 1 have been plotted as a function of a modified advance ratio, J' (V'/nD where $V' = V_\infty \cos \alpha$) for constant angles of attack² and several blade angles and are shown in figures 4 through 8. Several interesting conclusions can be drawn from examination of these figures. First, it will be noted that the slopes of the curves for all five components increase with increasing angle of attack. Second, it is noted that the slopes increase with disk loading (increasing β) for all but the pitching moment which increases to $\beta = 8^\circ$ and slowly decreases thereafter. Third, only moderate changes in slope are indicated up to values of α of 45° , after which the changes become quite rapid. Further, these changes in slope are more rapid at higher values of J' than at lower values.

From figures 4 through 8, data were selected at constant values of J' and β to show the variations of the five components (C_T , C_P , C_N , C_Y , C_m) with thrust-axis angle of attack. Values of β equal to 12° and 30° were selected to show the effect of increased disk loading. These results are presented in figures 9 through 13. It is evident from figures 9 and 10 that the thrust and power variations have nearly zero slope over considerable ranges of α at low values of J' and that the range of zero slope becomes less with increasing J' . Further, figures 11 through 13 show that over these ranges where the C_T and C_P variations have nearly zero slope, variations of C_N , C_Y , and C_m have nearly a constant slope. An exception is the variation of C_N at $\beta = 30^\circ$ and small values of J' . This is a range of low propeller efficiency where large oscillating torques produce nonlinear variations.

Certain other facts revealed in figures 9 through 13 are worthy of note. A break from near linearity in the variations of all five components as α is increased is evident for all values of J' . This break occurs at progressively lower values of α as J' is increased. The position of this break is not largely affected by increasing β (and thereby the disk loading) from 12° to 30° .

Viewing these observations from the standpoint of VTOL operation, it can be demonstrated that certain transition programs can lie within the regions of linear slope for the propeller forces and moments. If the point at which the thrust curves show a deviation of about 5 percent from the value at $\alpha = 0^\circ$ is taken as a limiting condition, a boundary of airspeed ($V_\infty = J' nD / \cos \alpha$) and α can be established as shown in figure 14. To simplify the illustration the boundary has been determined for constant values of β (the boundary is the same for β of 12° and 30°) and a typical value of nD , as dictated by blade tip speed.

²It should be noted that for the isolated propeller as presented here, α is the geometric angle of attack. However, for airplane installations, this angle is often affected by wing induced flow, etc., and is the effective angle of attack of the thrust axis. See reference 3 for consideration of this aspect of the problem.

Examples of two transition programs are also shown in figure 14: One is for the hypothetical airplane described in reference 2 and is based on the data obtained for propeller 1; the other is for the Vertol Model 76 airplane and is based on data obtained for propeller 3. Both are for a 1-g transition,³ and it will be noted that both lie well below the boundary curve.

The significance of these facts is that the thrust and power characteristics of the propeller for the two transition programs, and any others lying below the boundary, could have been closely approximated from data for the propellers at $\alpha = 0^\circ$. Further, if data for the in-plane forces and out-of-plane moments had been available at $\alpha = 0^\circ$ and, say, $\alpha = 15^\circ$, a linear extrapolation based on these two values would have predicted these forces and moments with accuracy acceptable for preliminary design purposes. Similar conclusions can be drawn from examinations of the data for all three propellers tested, which were of widely different plan form and geometry. Therefore, in the absence of complete data on a particular propeller, the approach outlined in the foregoing might be used to estimate the forces and moments at large angles of attack from experimental data for small angles of attack.

All the data obtained for the three propellers are shown in figures 15 through 31 for use in further evaluation of the results. These data are presented in the more conventional form of propeller parameter as a function of J' for several blade angles, all at a constant value of α .

CONCLUDING REMARKS

It has been shown that the thrust and power coefficients for given values of β and J' are nearly constant in magnitude over a large range of thrust-axis angles of attack and that the range diminishes with increasing J' . Also, over these same ranges of angles of attack, the variations of propeller normal force, yawing moment, and pitching moment are nearly linear.

The characteristic trends of the results (except those associated with blade articulation) were the same for all three propellers tested.

³For conditions at high rate of descent, the boundary could be exceeded by these airplanes. Estimates for the hypothetical airplane of NACA TN 3304 showed that descent rates in excess of 2000 fpm at a translational speed of 56 knots would exceed the boundary.

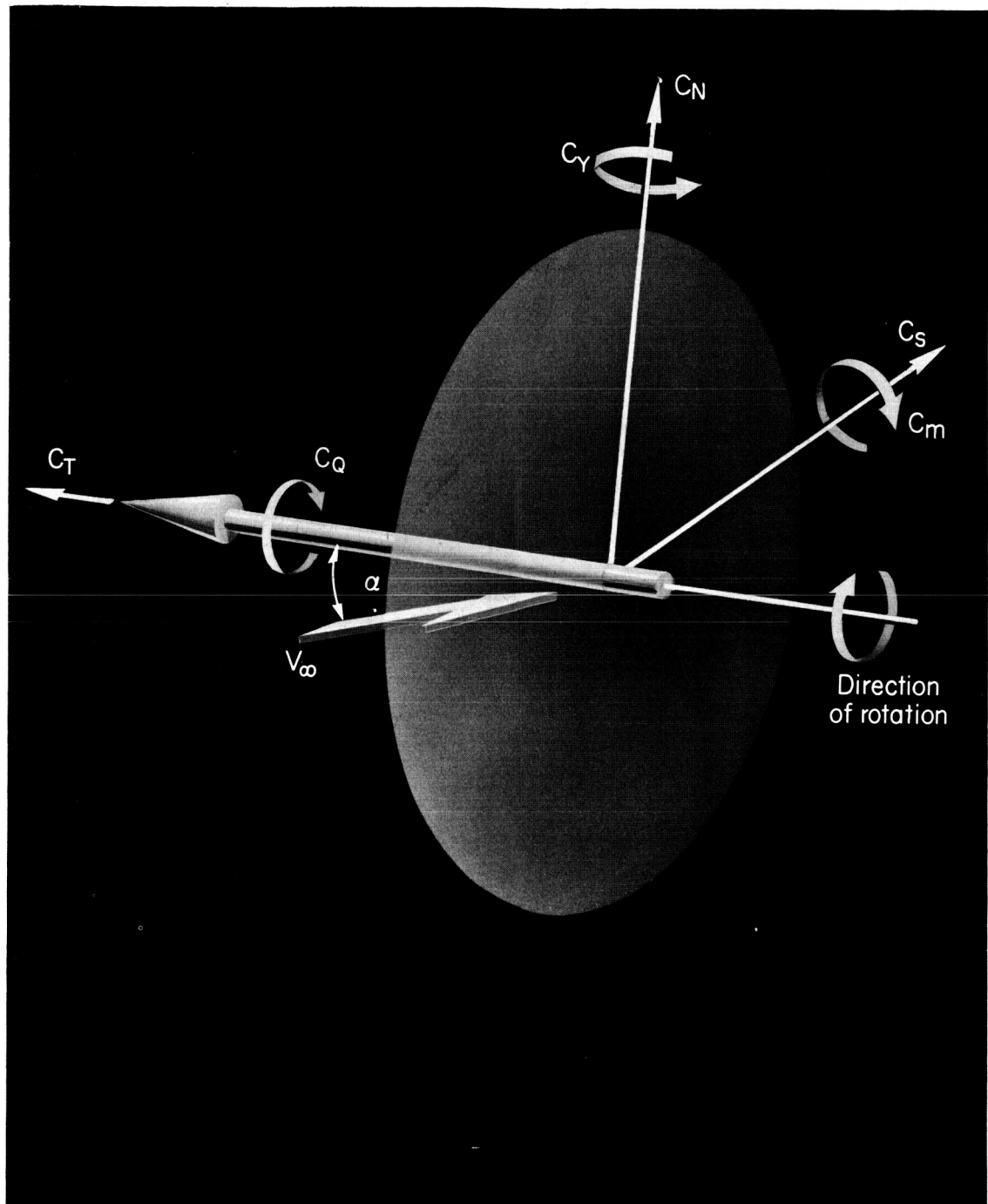
A possibility of predicting propeller forces and moments at high angles of attack and low effective advance ratios, J' , from data obtained at small angles of attack has been indicated.

Ames Research Center
National Aeronautics and Space Administration
Moffett Field, Calif., Jan. 21, 1960

A
2
6
7

REFERENCES

1. McLemore, H. Clyde, and Cannon, Michael D.: Aerodynamic Investigation of a Four-Blade Propeller Operating Through an Angle-of-Attack Range From 0° to 180°. NACA TN 3228, 1954.
2. Kuhn, Richard E., and Draper, John W.: Investigation of the Aerodynamic Characteristics of a Model Wing-Propeller Combination and of the Wing and Propeller Separately at Angles of Attack Up to 90°. NACA Rep. 1263, 1956. (Supersedes NACA TN 3304)
3. Rogallo, Vernon L., Yaggy, Paul F., and McCloud, John L., III: An Analysis of Once-Per-Revolution Oscillating Aerodynamic Thrust Loads on Single-Rotation Propellers on Tractor Airplanes at Zero Yaw. NACA Rep. 1295, 1956. (Supersedes NACA TN 3395)

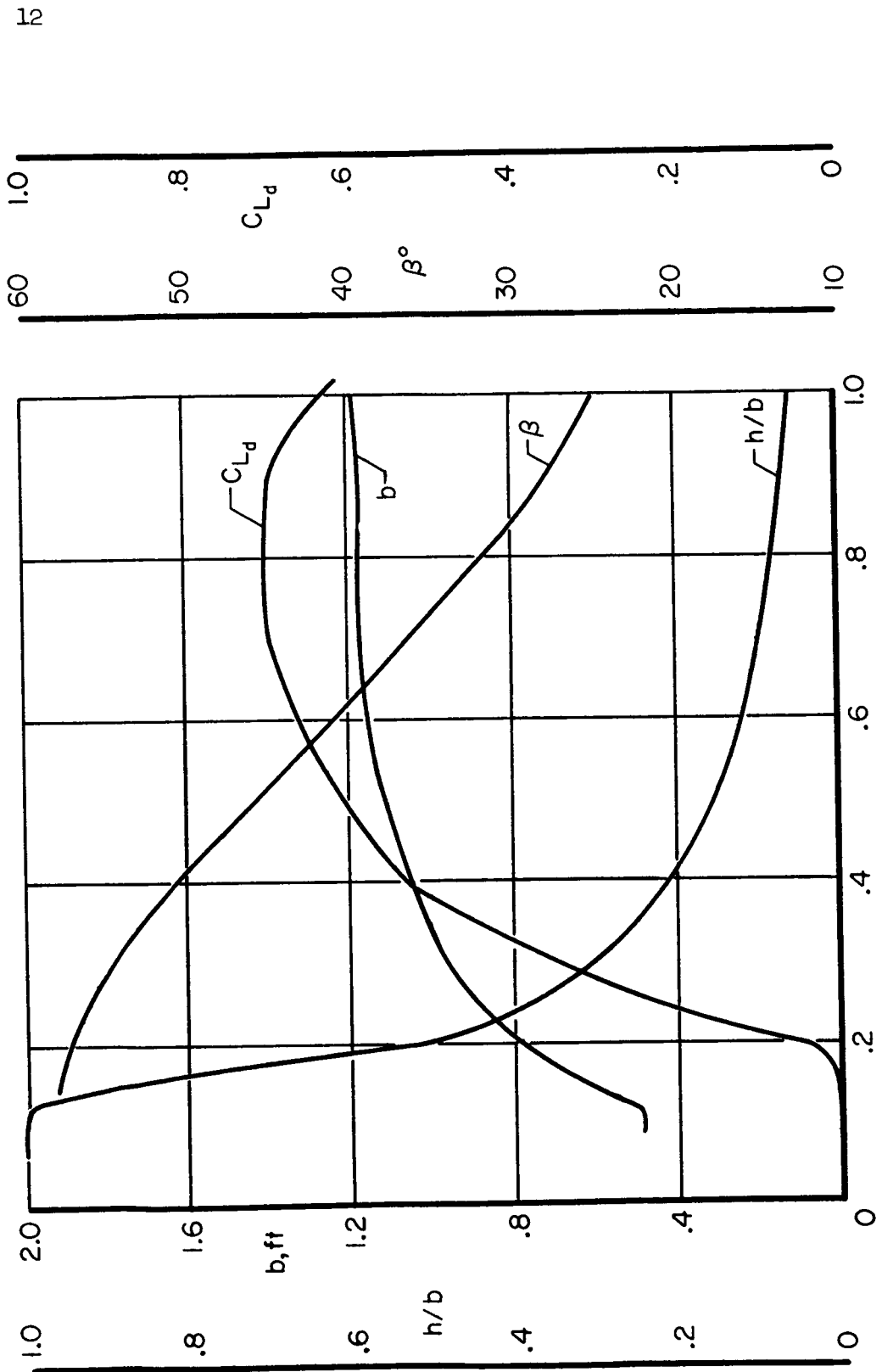


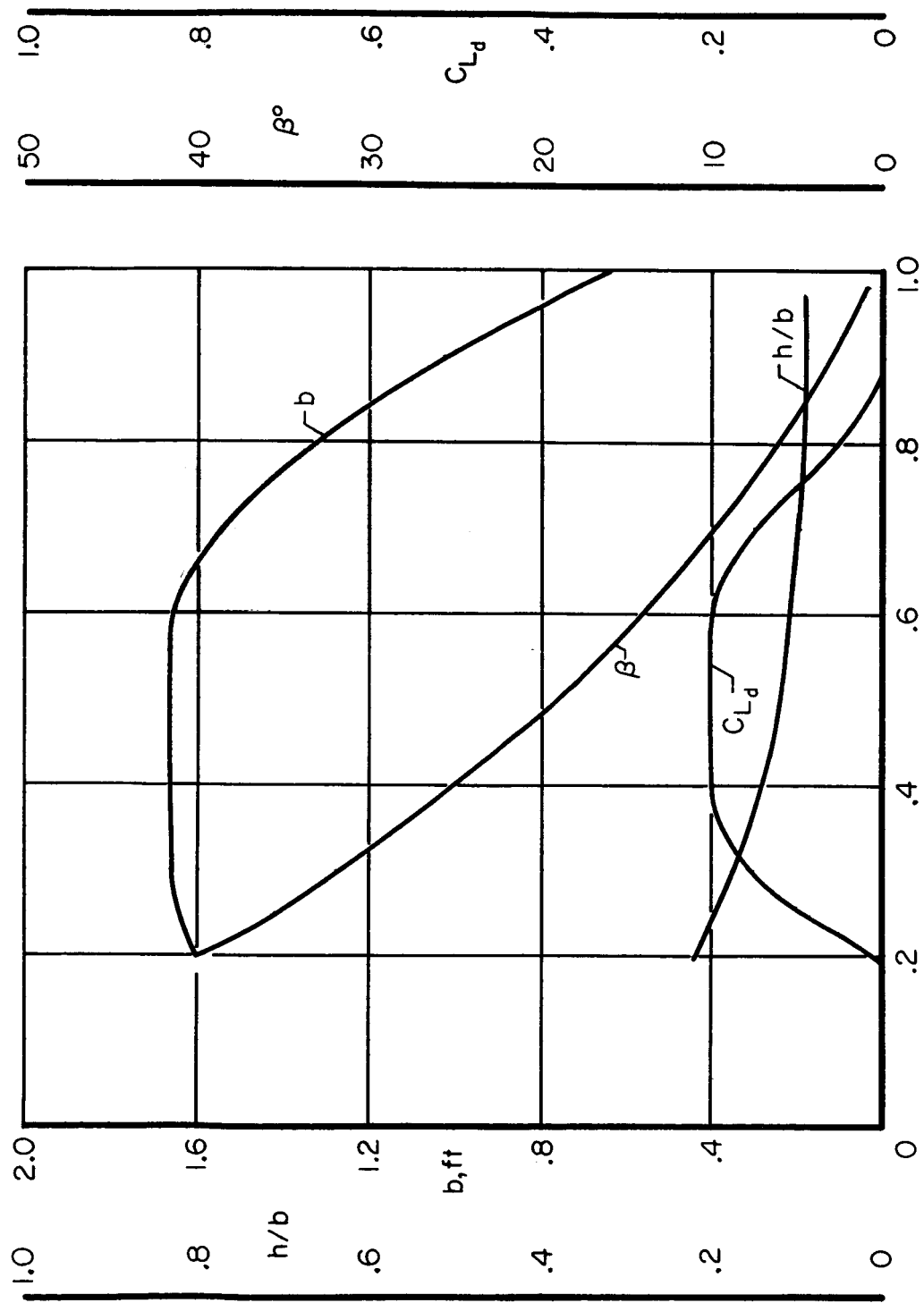
A-26029

Figure 1.- Positive directions of propeller forces and moments.

Figure 2.- Propeller blade plan-form characteristics.

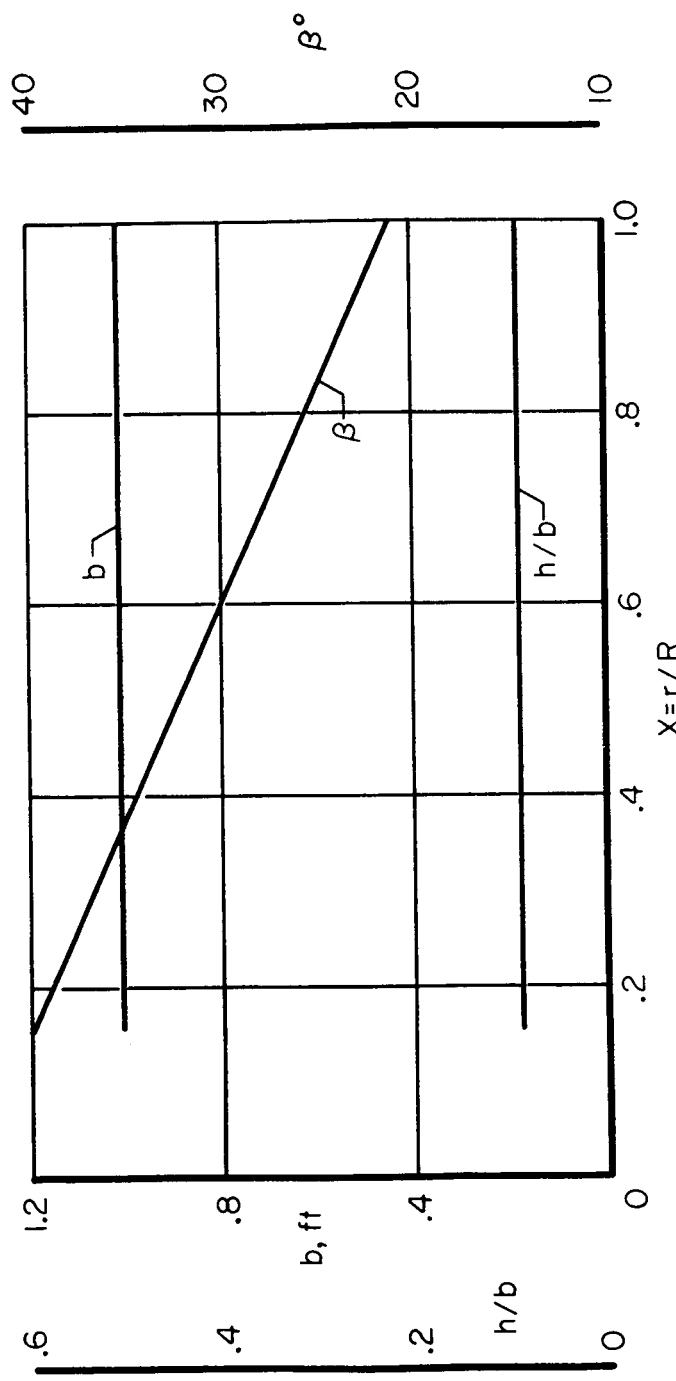
(a) Propeller number 1.





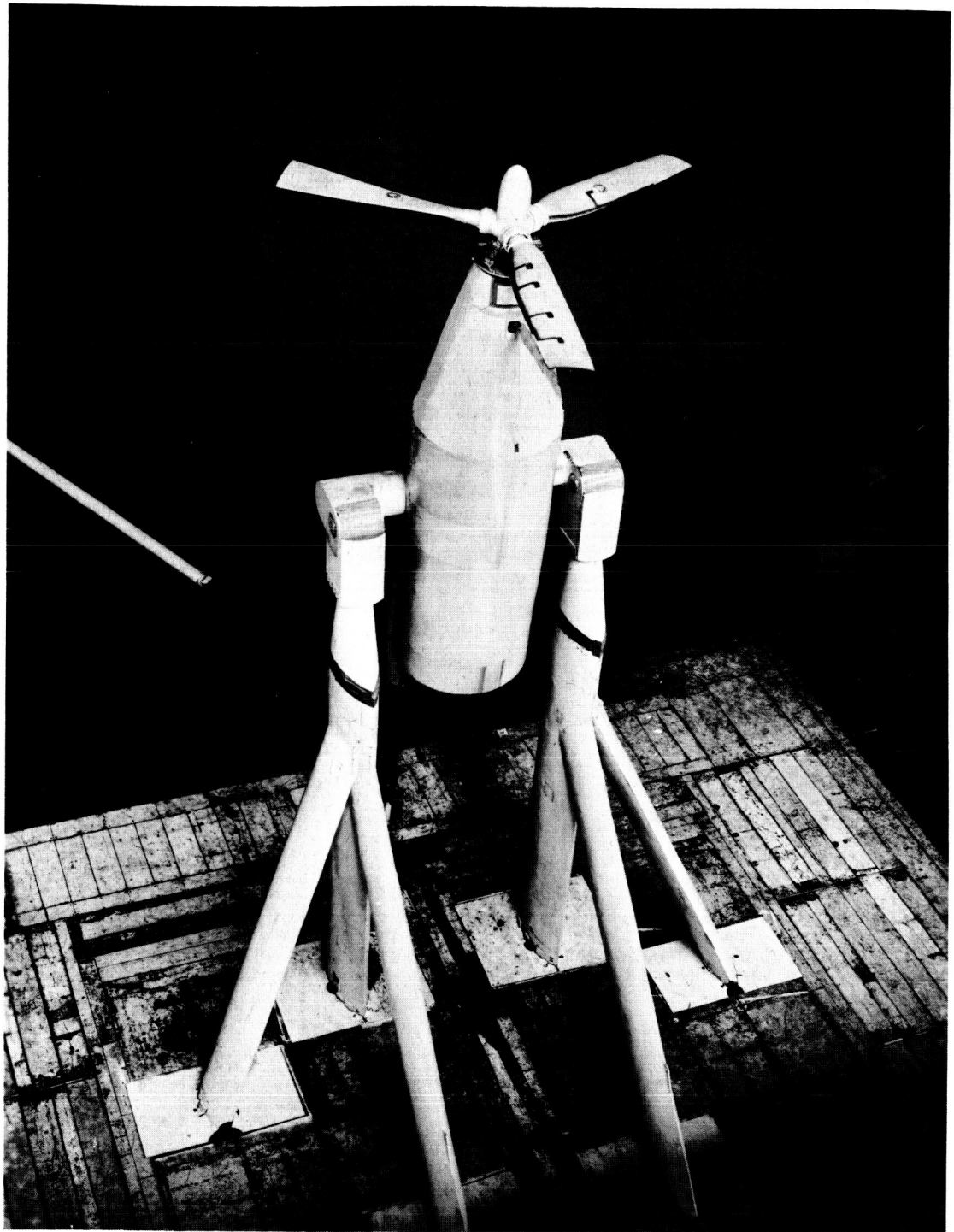
(b) Propeller number 2.

Figure 2.- Continued.



(c) Propeller number 3.

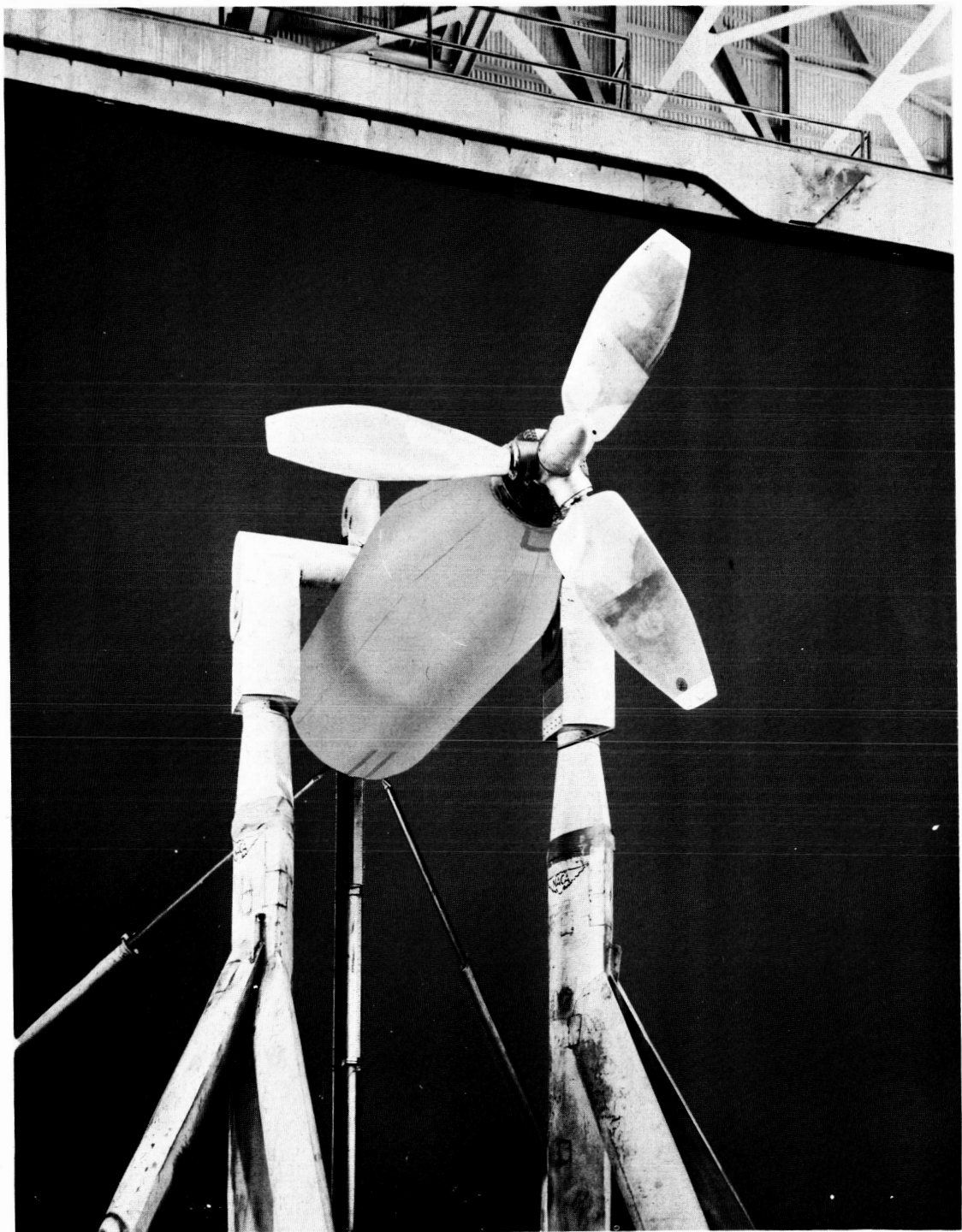
Figure 2.- Concluded.



A-24067.1

(a) Propeller number 1, $\alpha = 85^\circ$.

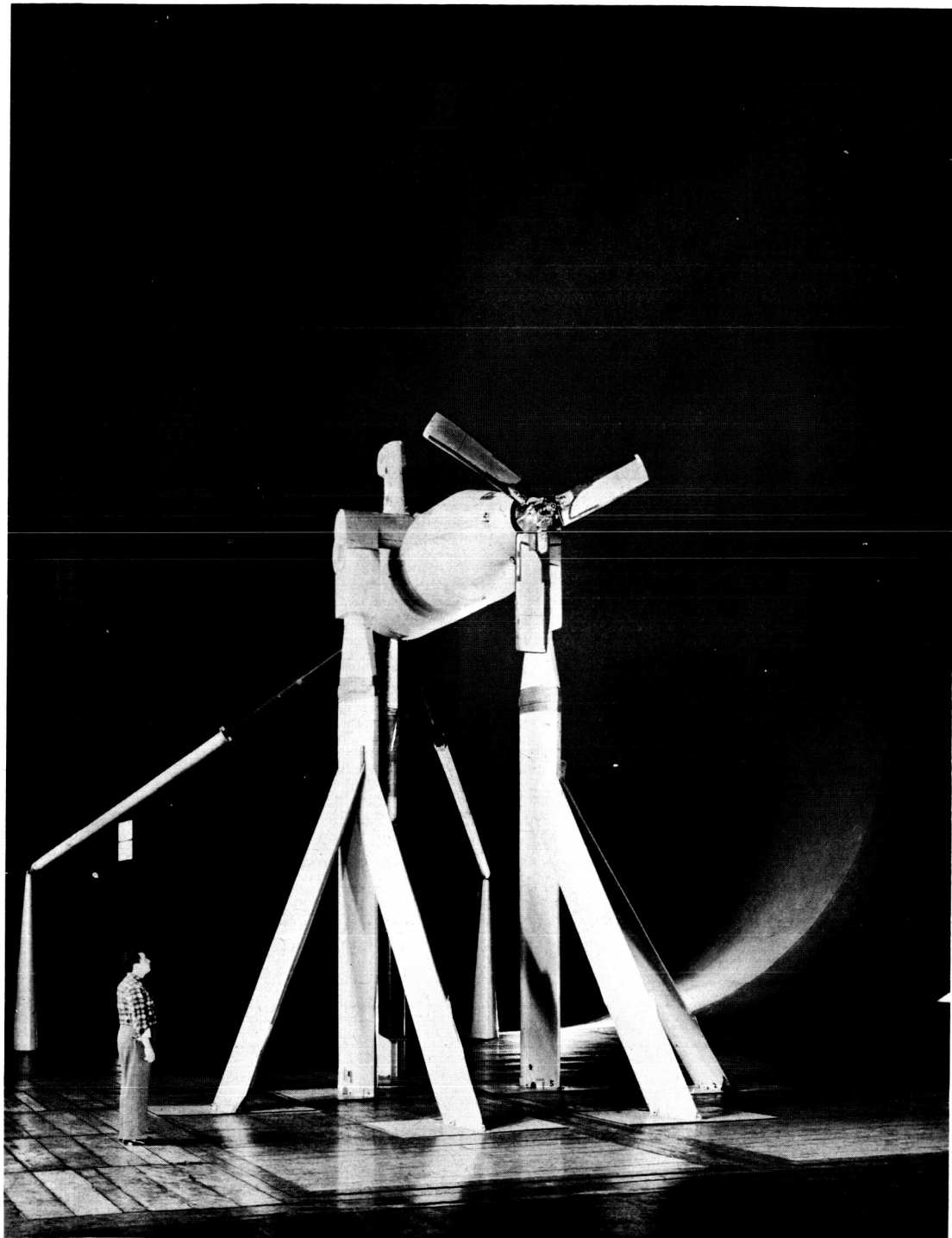
Figure 3.- Propeller and test stand installed in the Ames 40- by 80-Foot Wind Tunnel.



A-24306.1

(b) Propeller number 2, $\alpha = 0^\circ$.

Figure 3.- Continued.



A-23635.1

(c) Propeller number 3, $\alpha = 0^\circ$.

Figure 3.- Concluded.

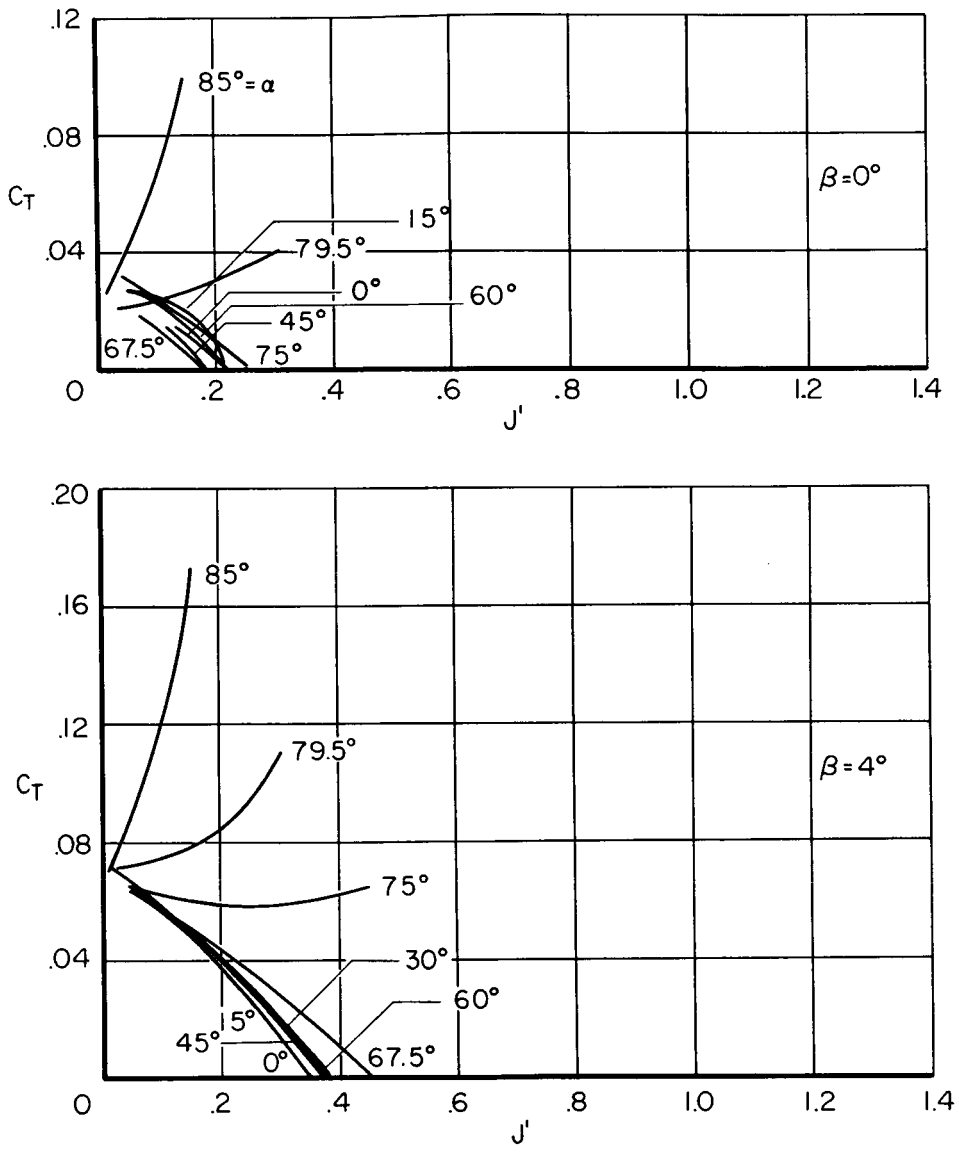
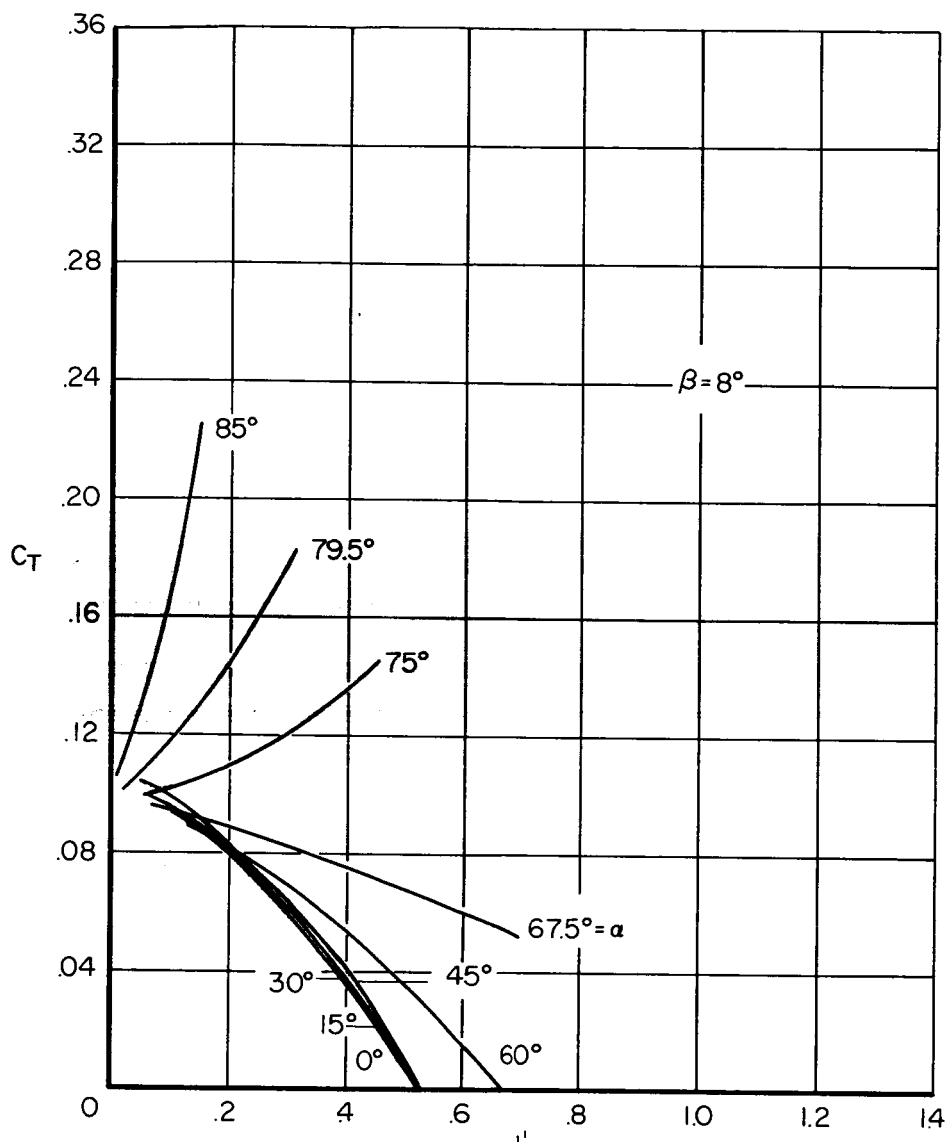
(a) $\beta = 0^\circ$ and 4°

Figure 4.- Variation of thrust coefficient C_T of propeller 1 with modified advance ratio J' for several thrust-axis angles of attack α .



(b) $\beta = 8^\circ$

Figure 4.- Continued.

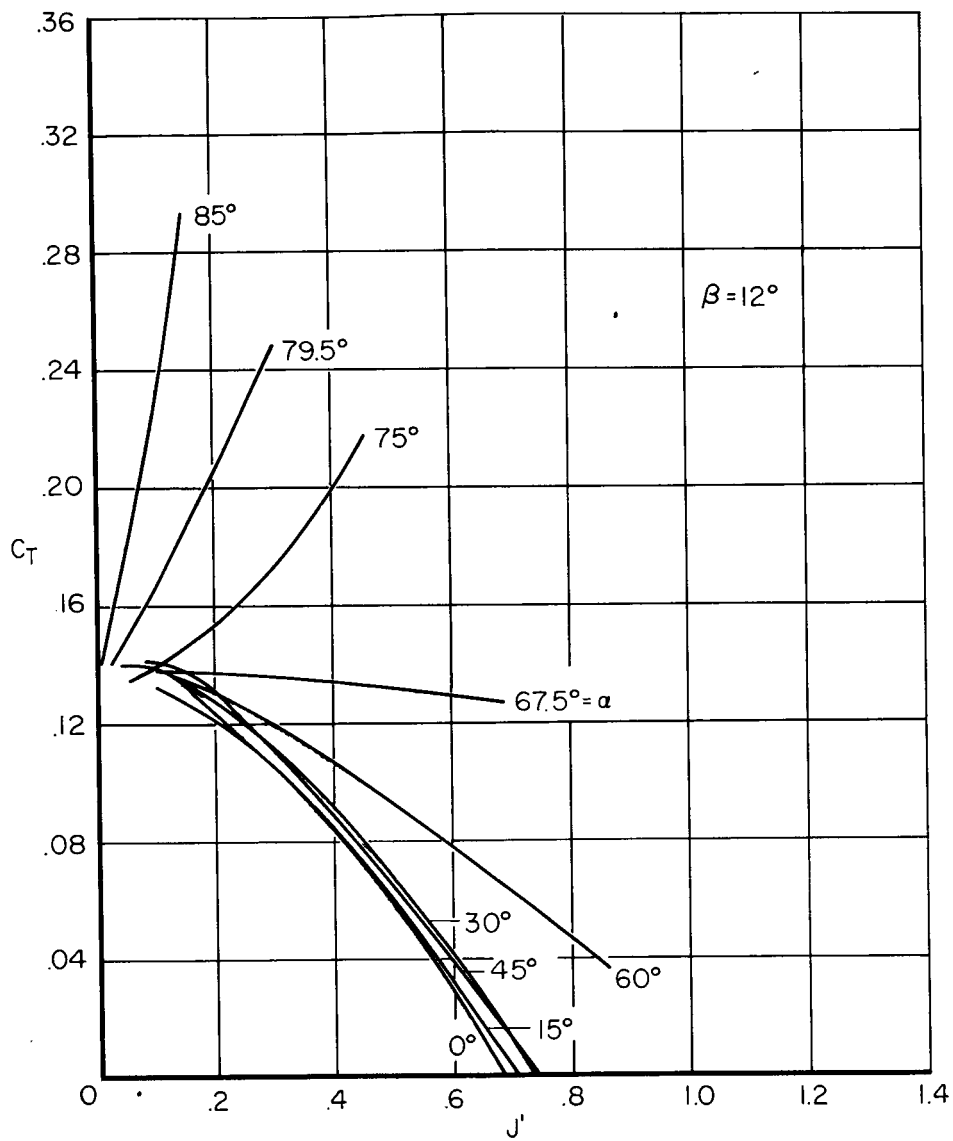
(c) $\beta = 12^\circ$

Figure 4.- Continued.

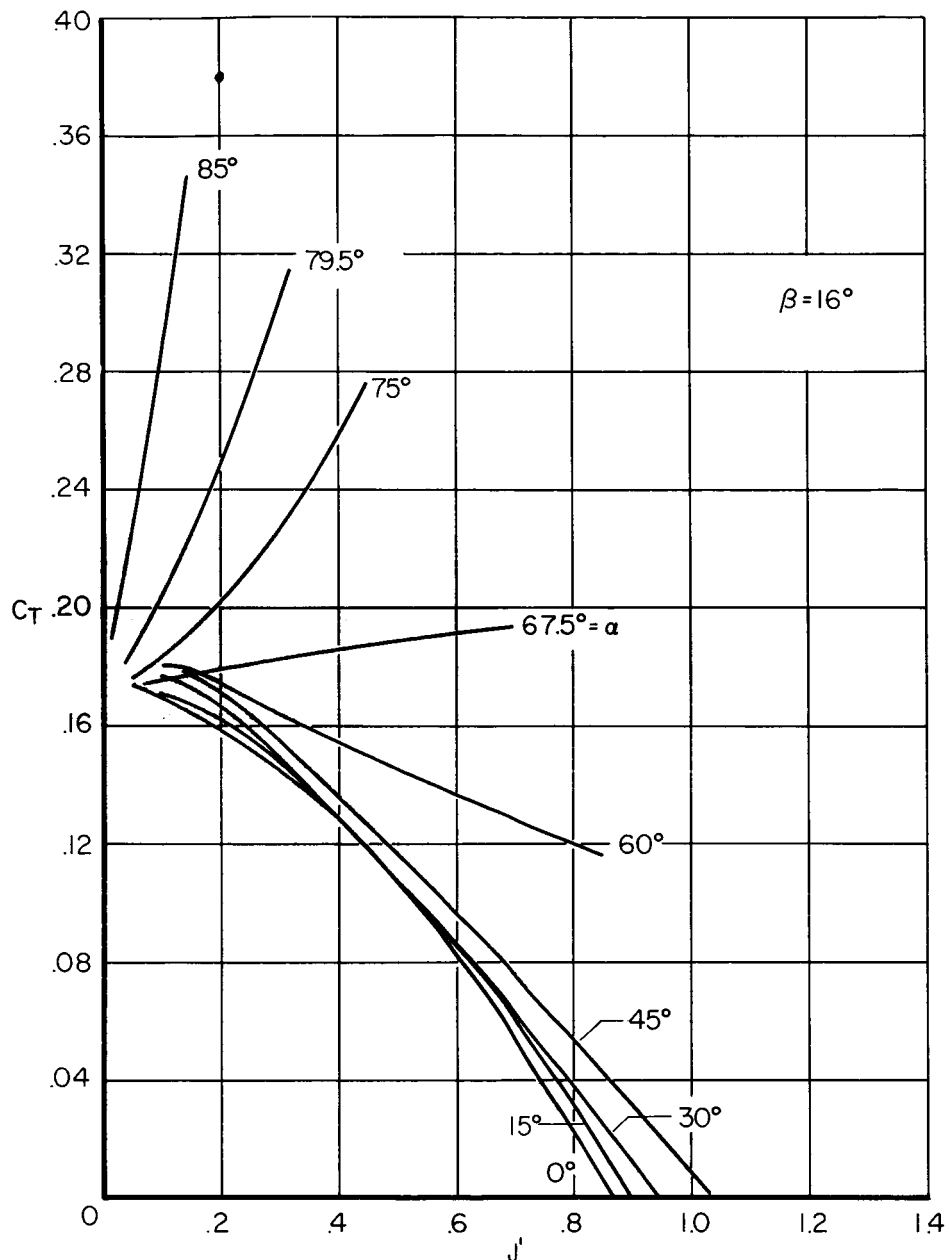
(d) $\beta = 16^\circ$

Figure 4.- Continued.

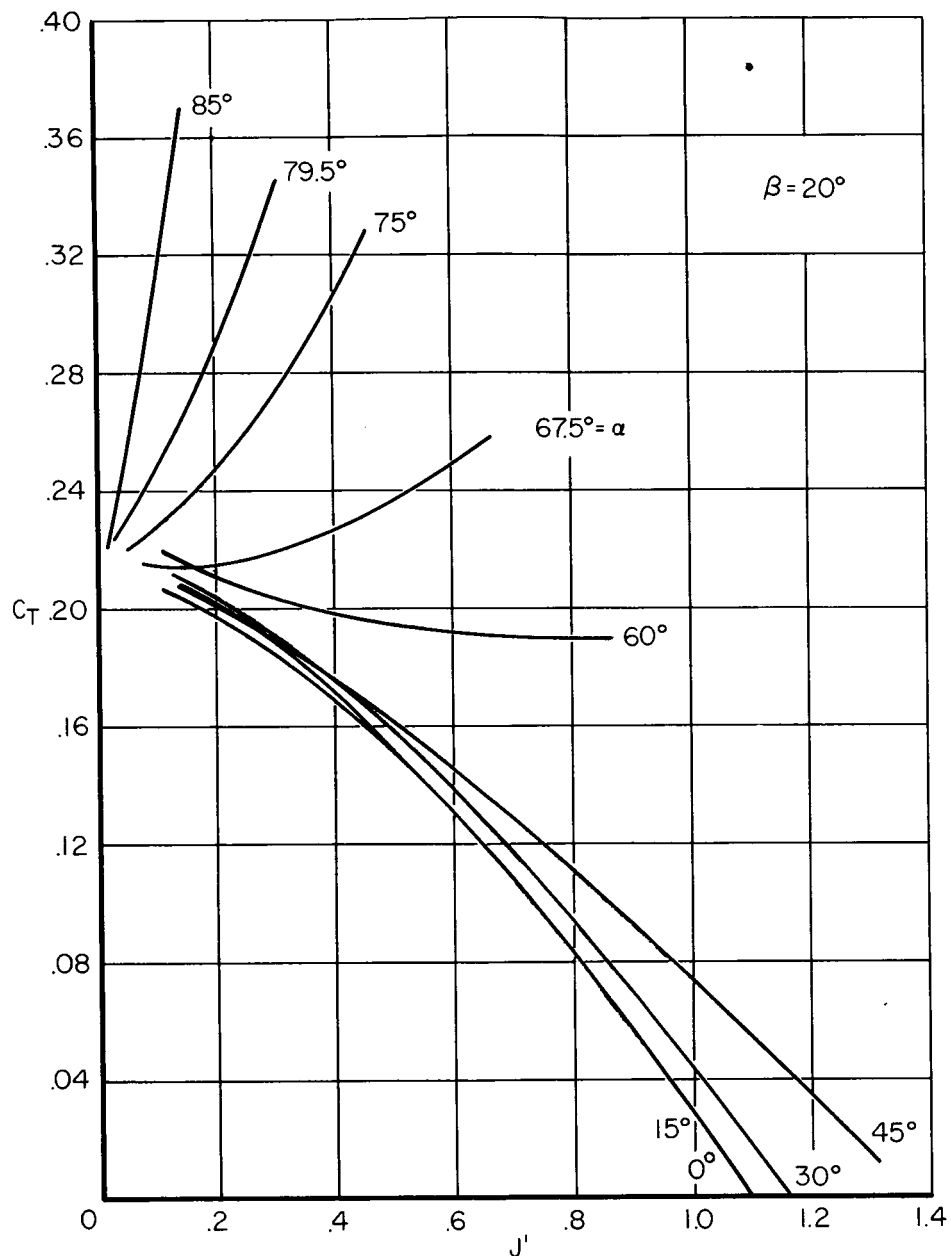
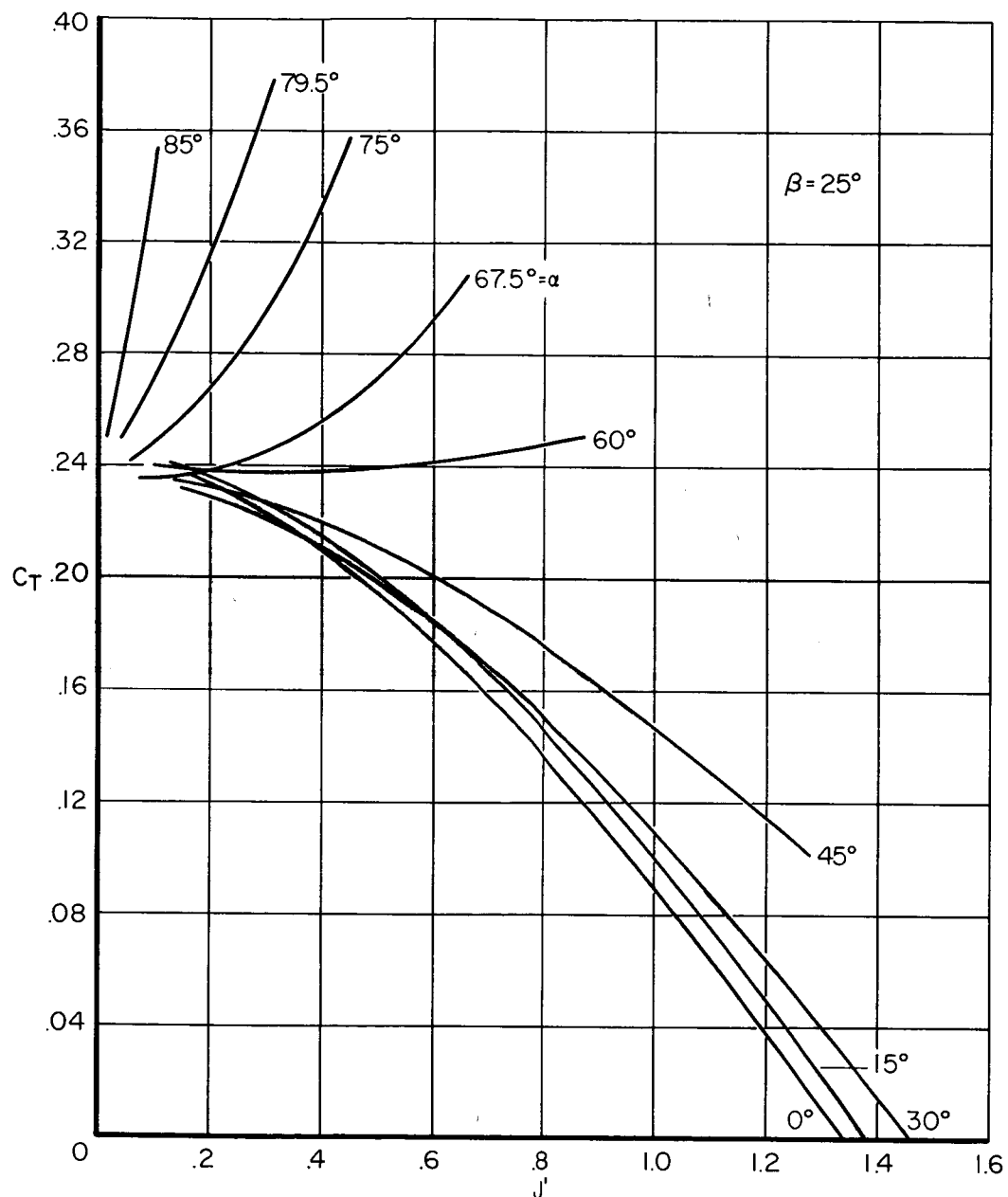
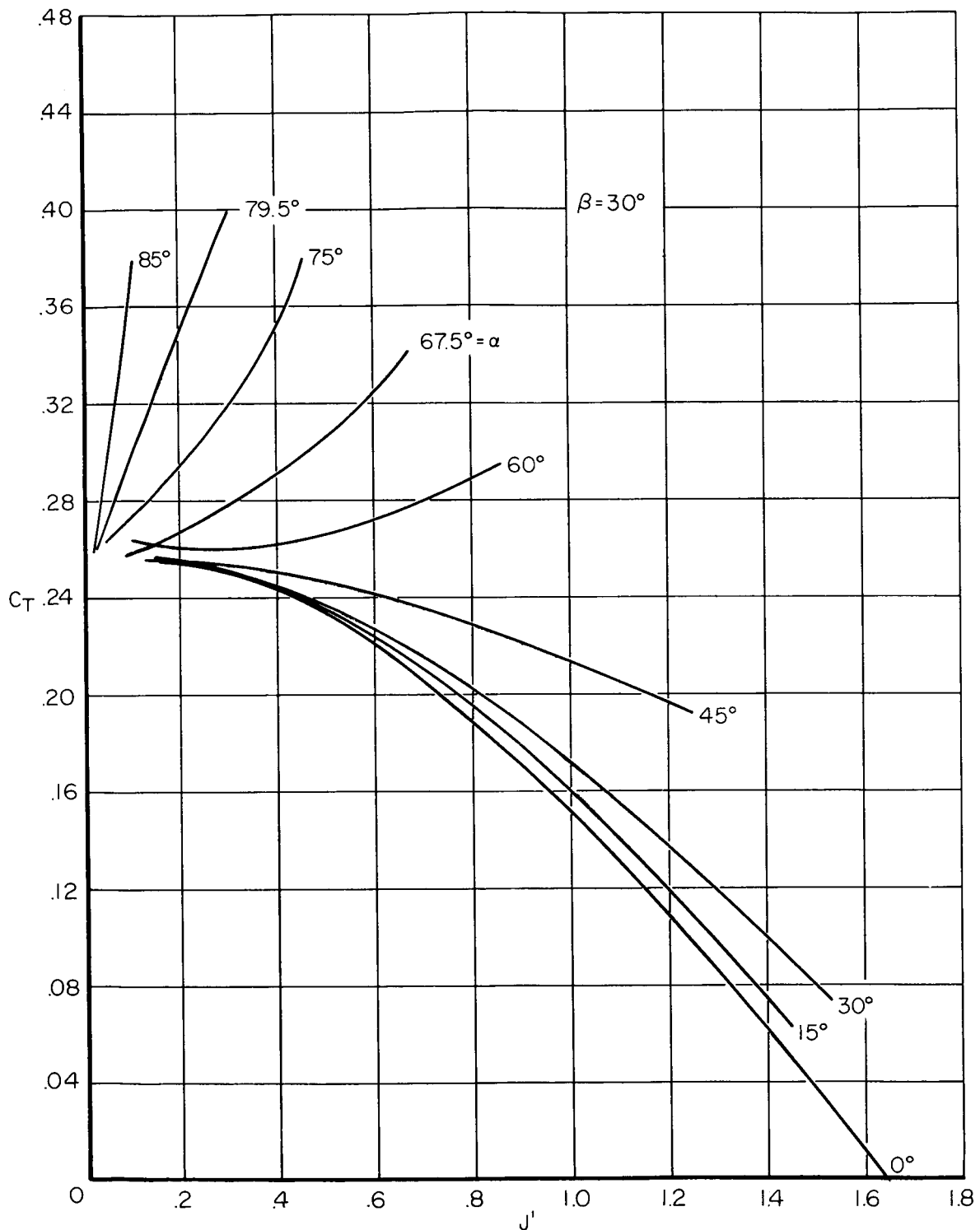
(e) $\beta = 20^\circ$

Figure 4.- Continued.



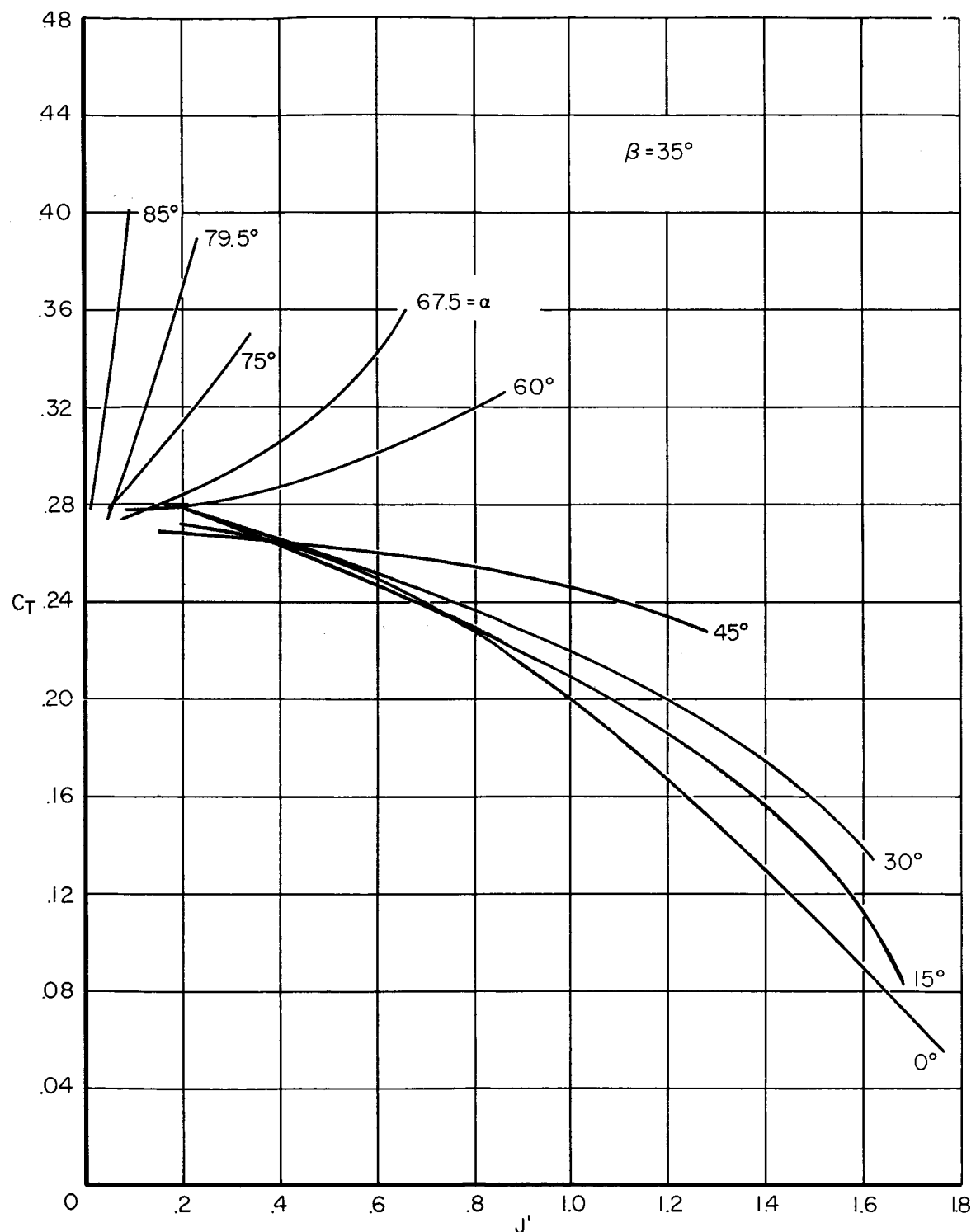
(f) $\beta = 25^\circ$

Figure 4.- Continued.



(g) $\beta = 30^\circ$

Figure 4--Continued.



(h) $\beta = 35^\circ$

Figure 4.- Continued.

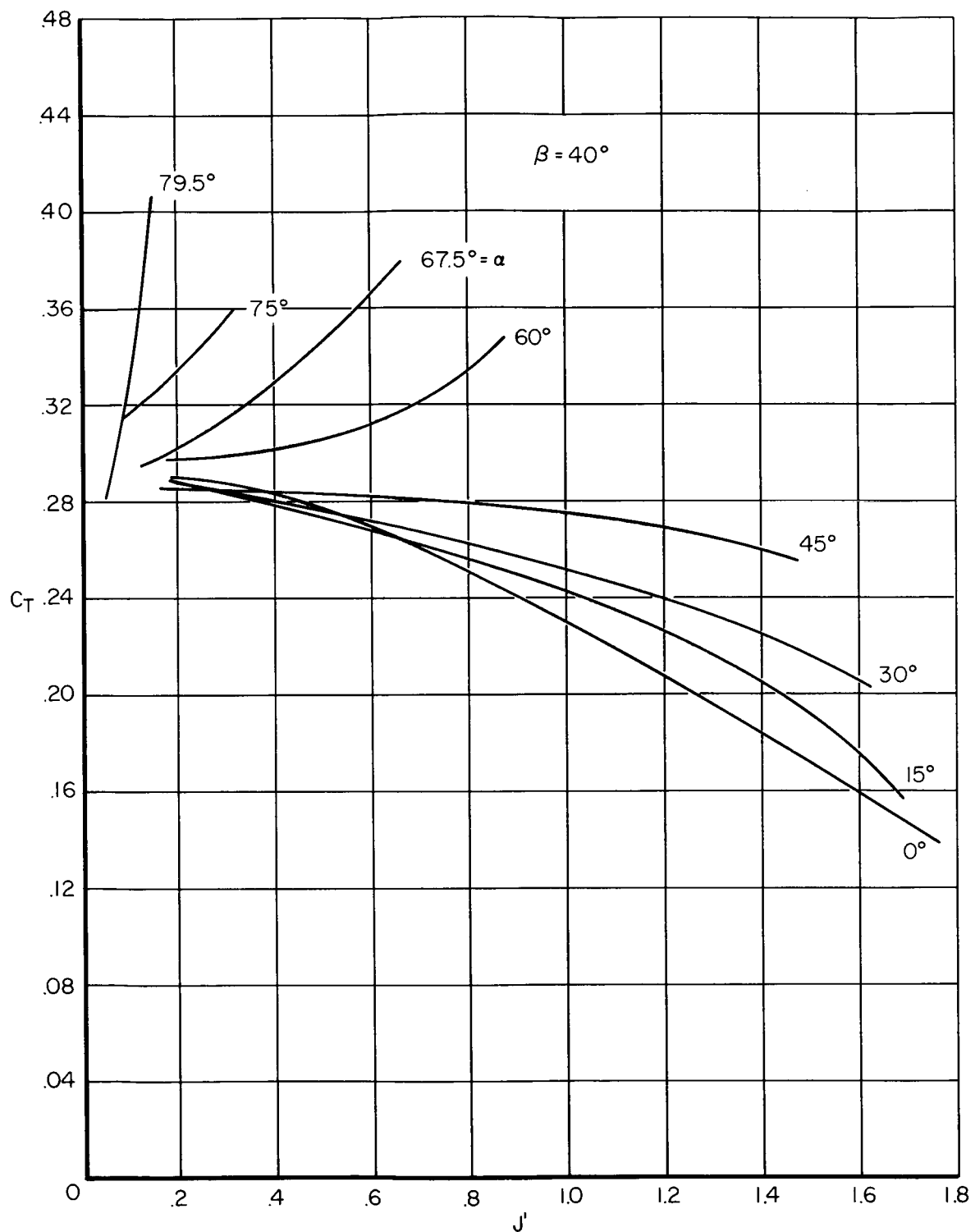
(i) $\beta = 40^\circ$

Figure 4.- Concluded.

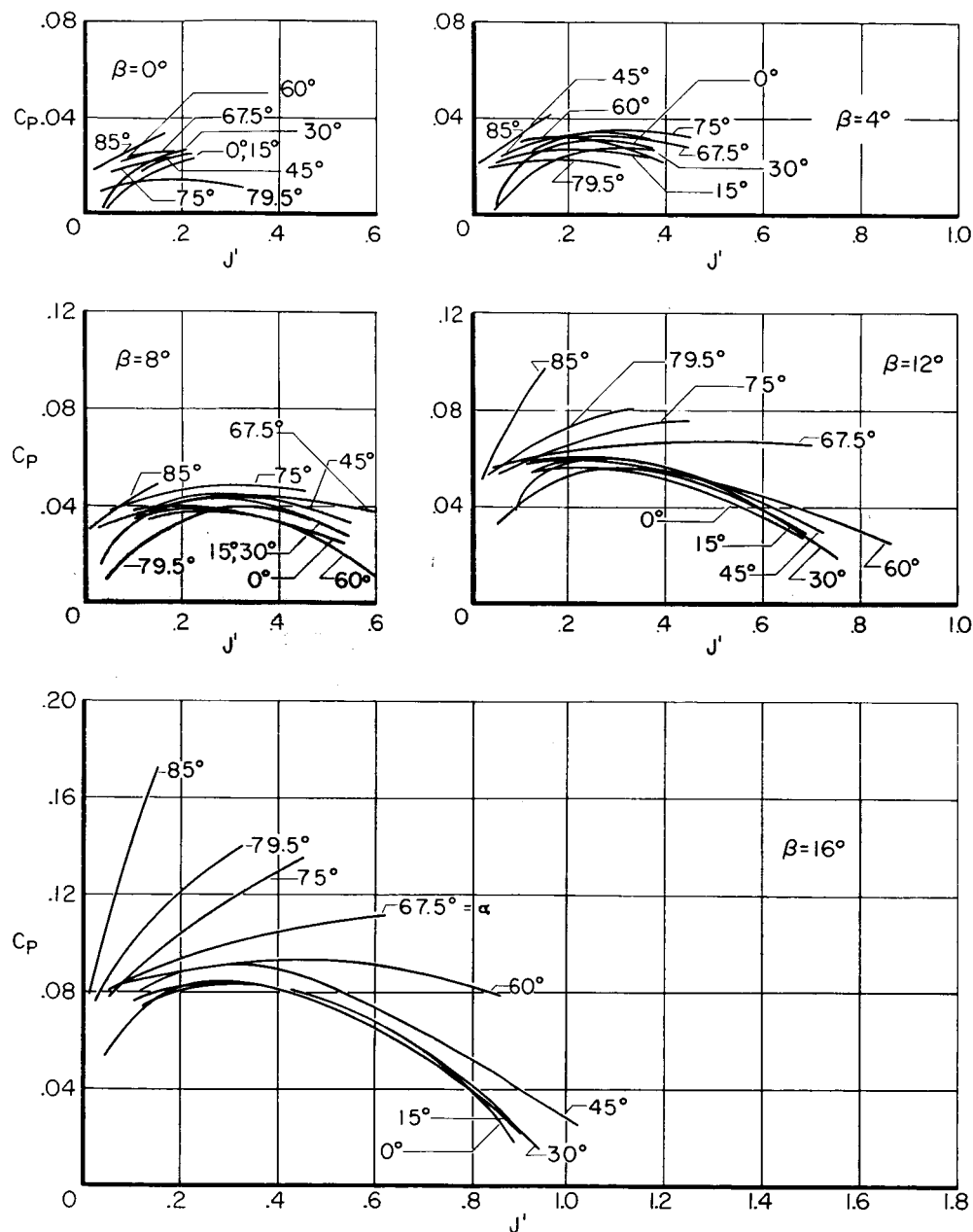
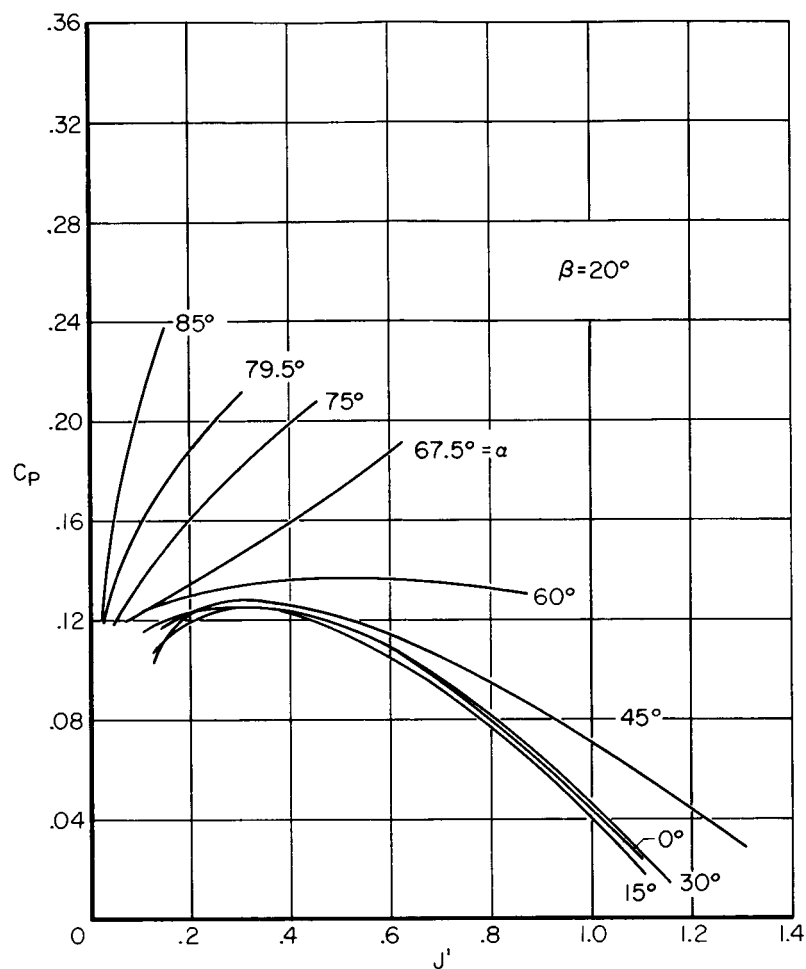
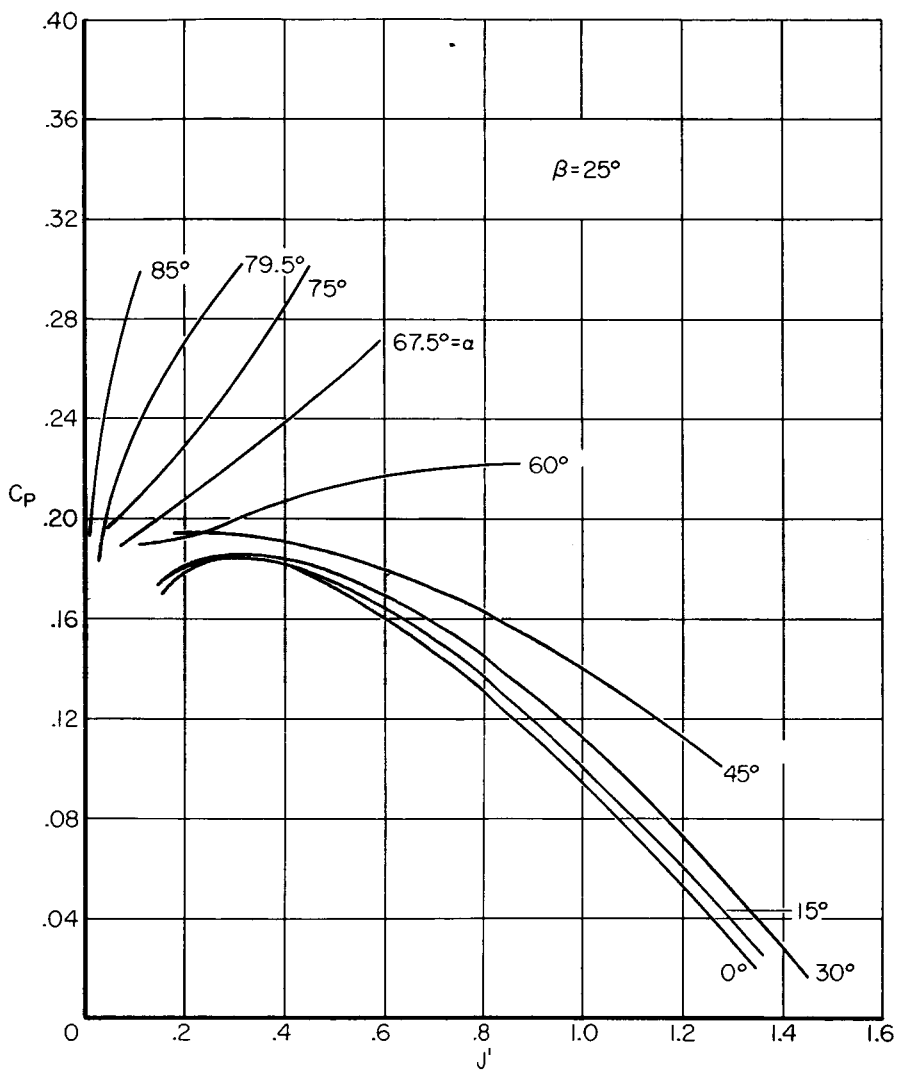
(a) $\beta = 0^\circ, 4^\circ, 8^\circ, 12^\circ, 16^\circ$

Figure 5.- Variation of power coefficient C_P of propeller 1 with modified advance ratio J' for several thrust-axis angles of attack α .



(b) $\beta = 20^\circ$

Figure 5.- Continued.



(c) $\beta = 25^\circ$

Figure 5.- Continued.

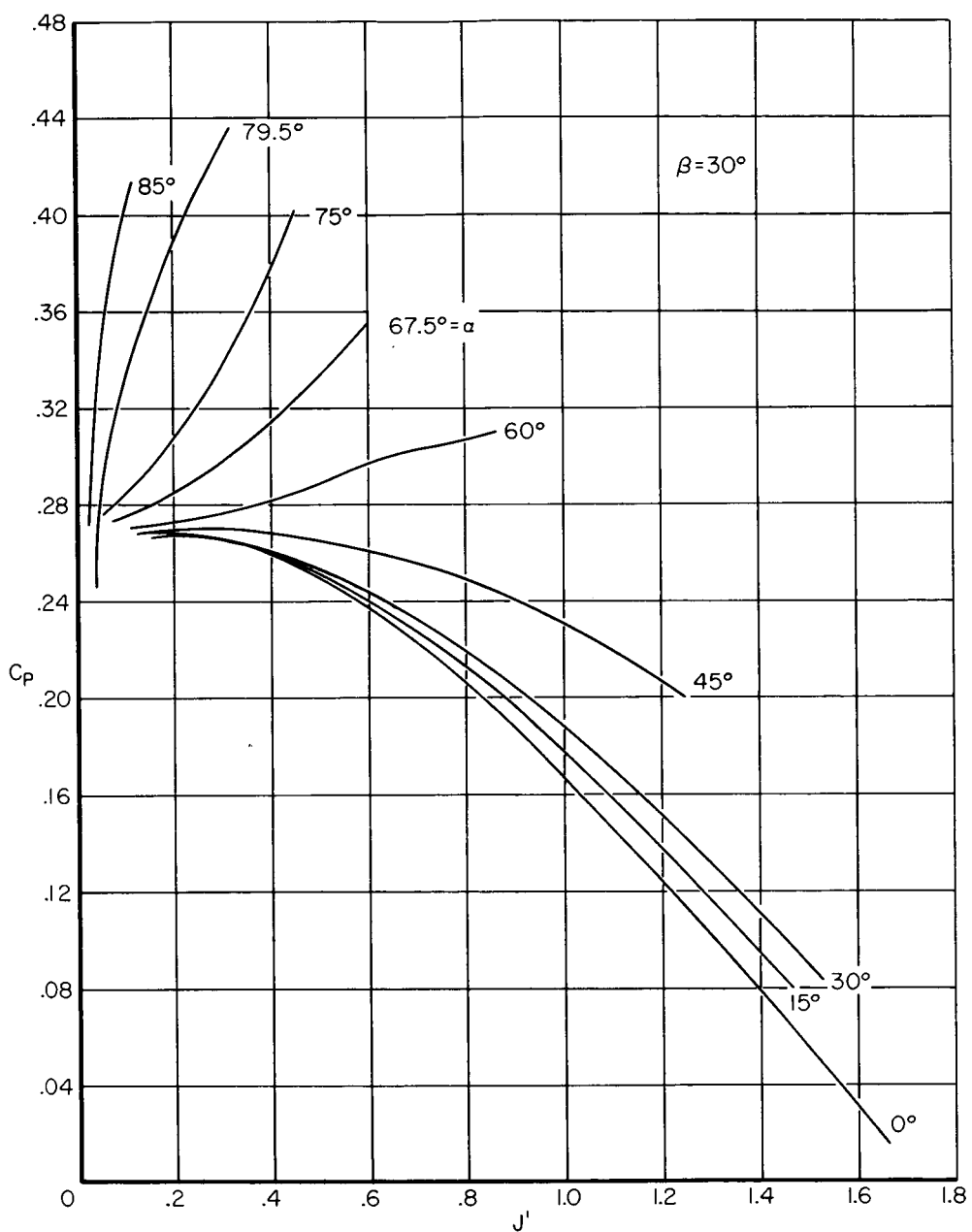
(d) $\beta = 30^\circ$

Figure 5.- Continued.

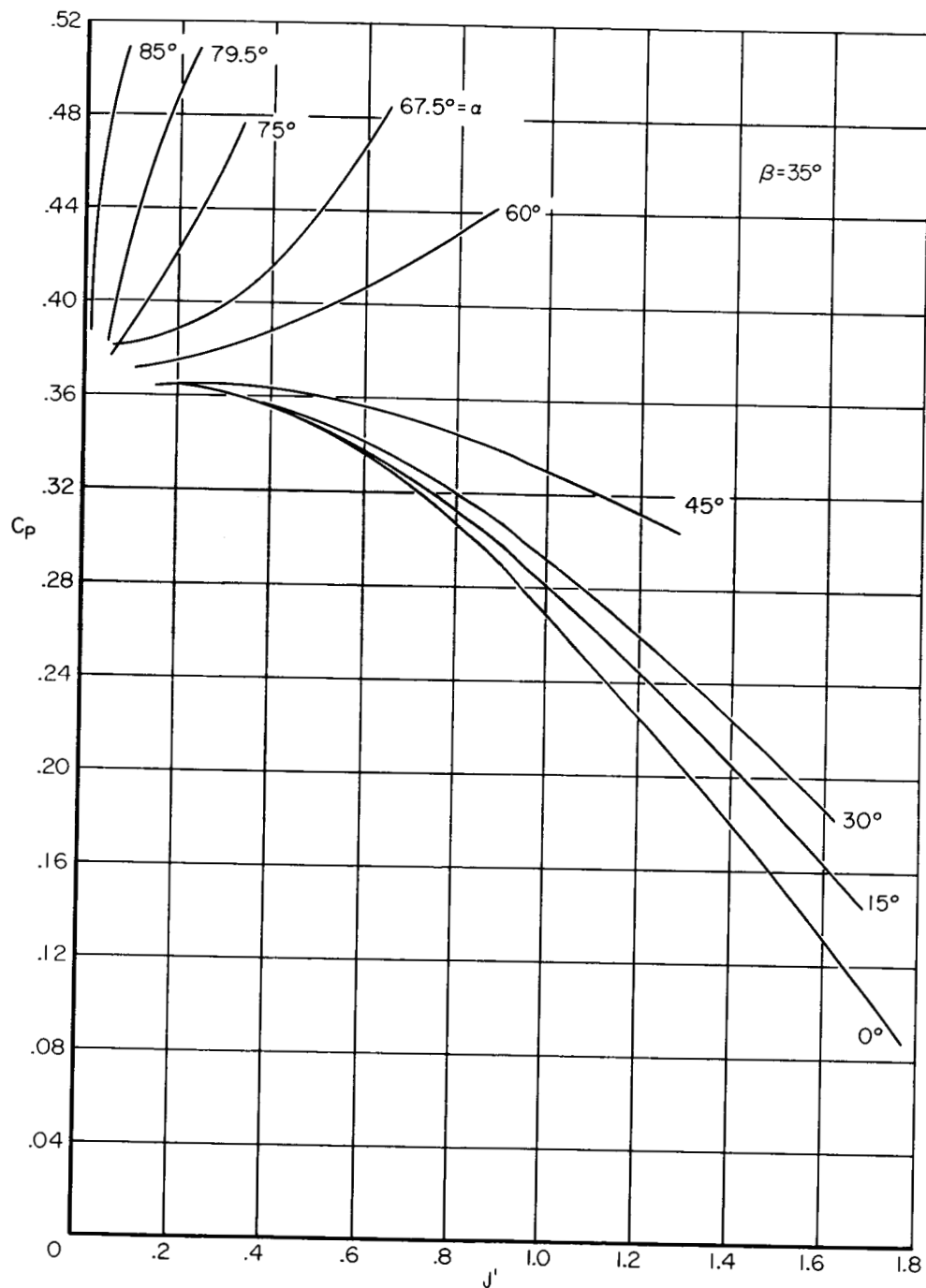
(e) $\beta = 35^\circ$

Figure 5.- Continued.

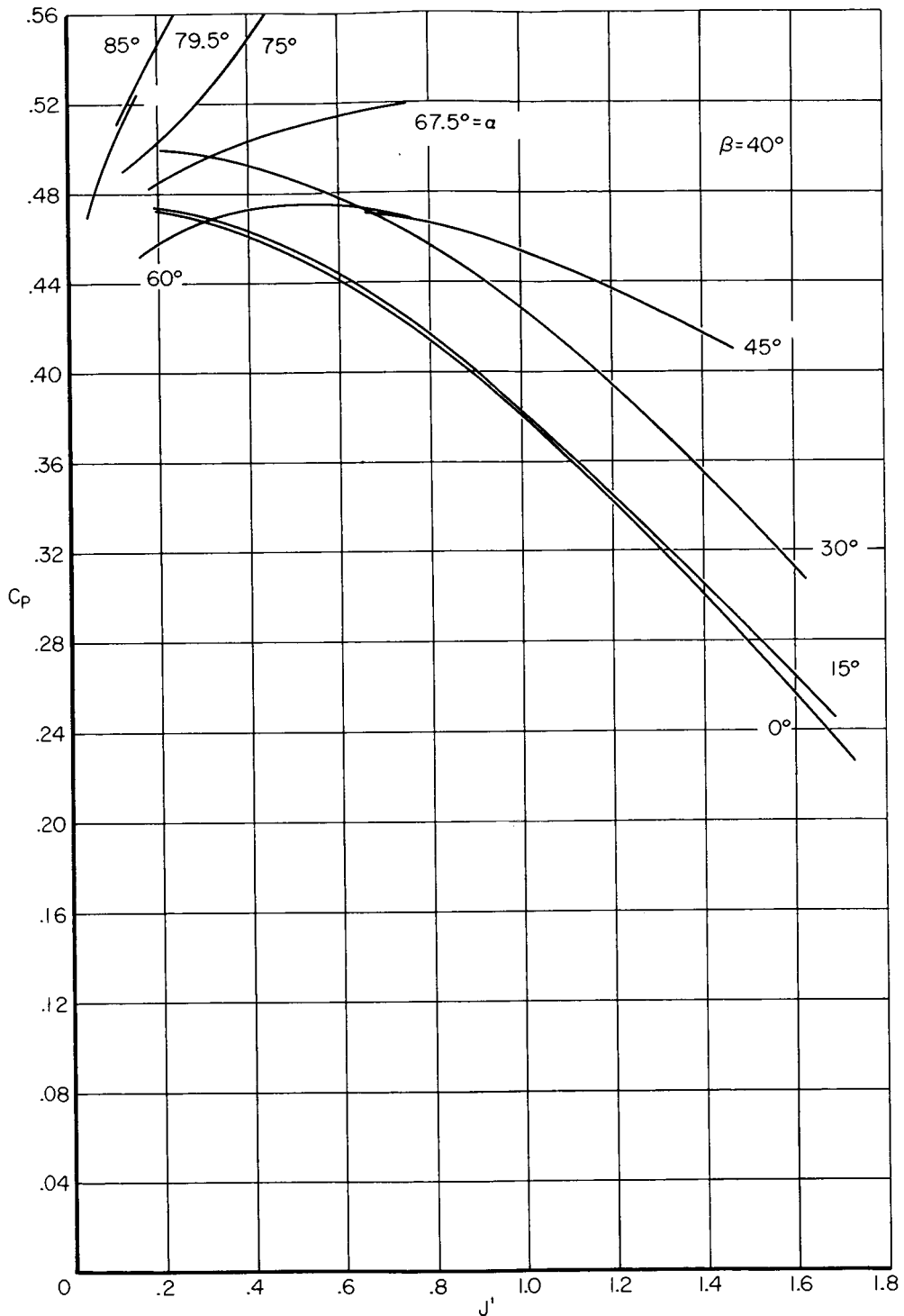
(f) $\beta = 40^\circ$

Figure 5-- Concluded.

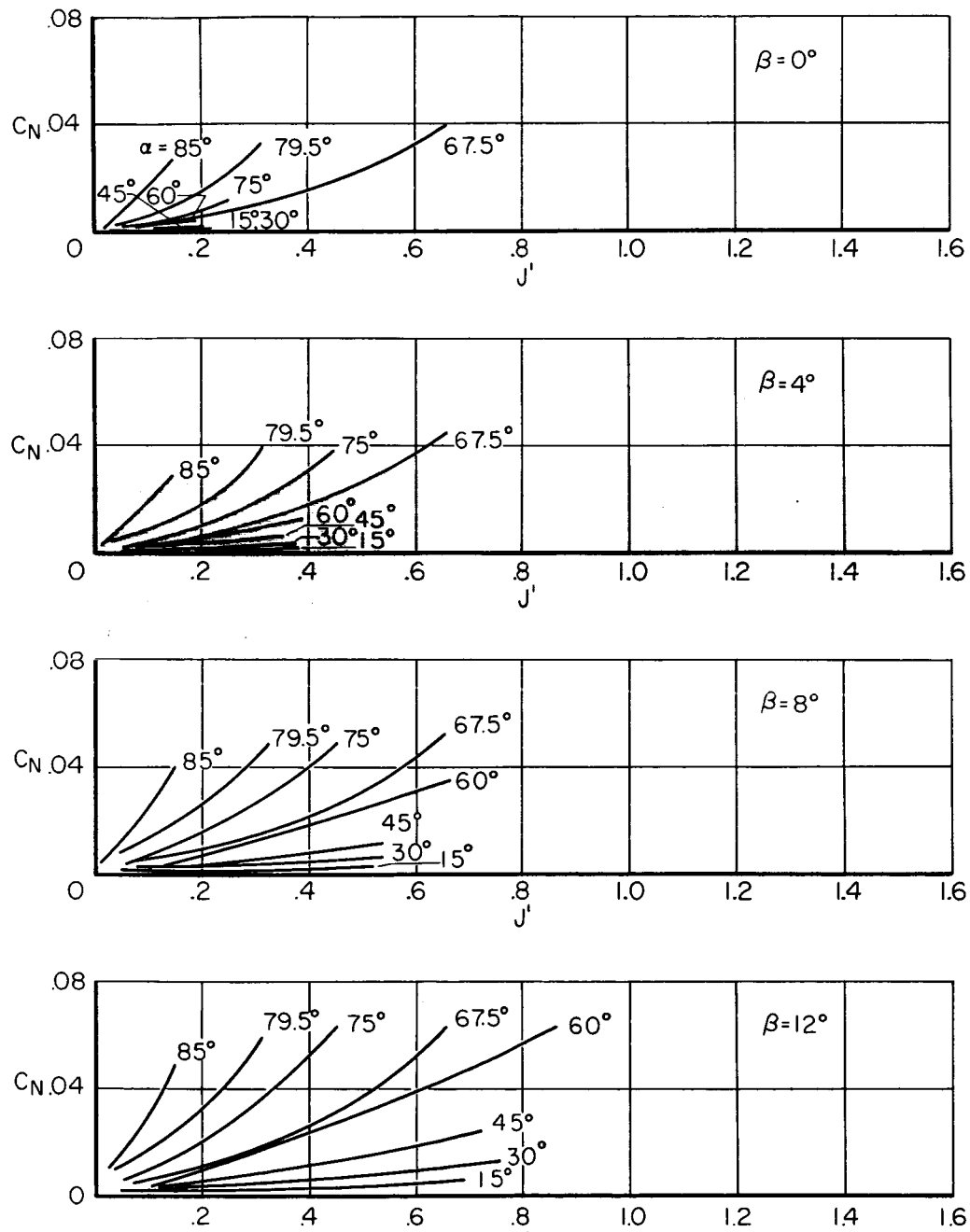
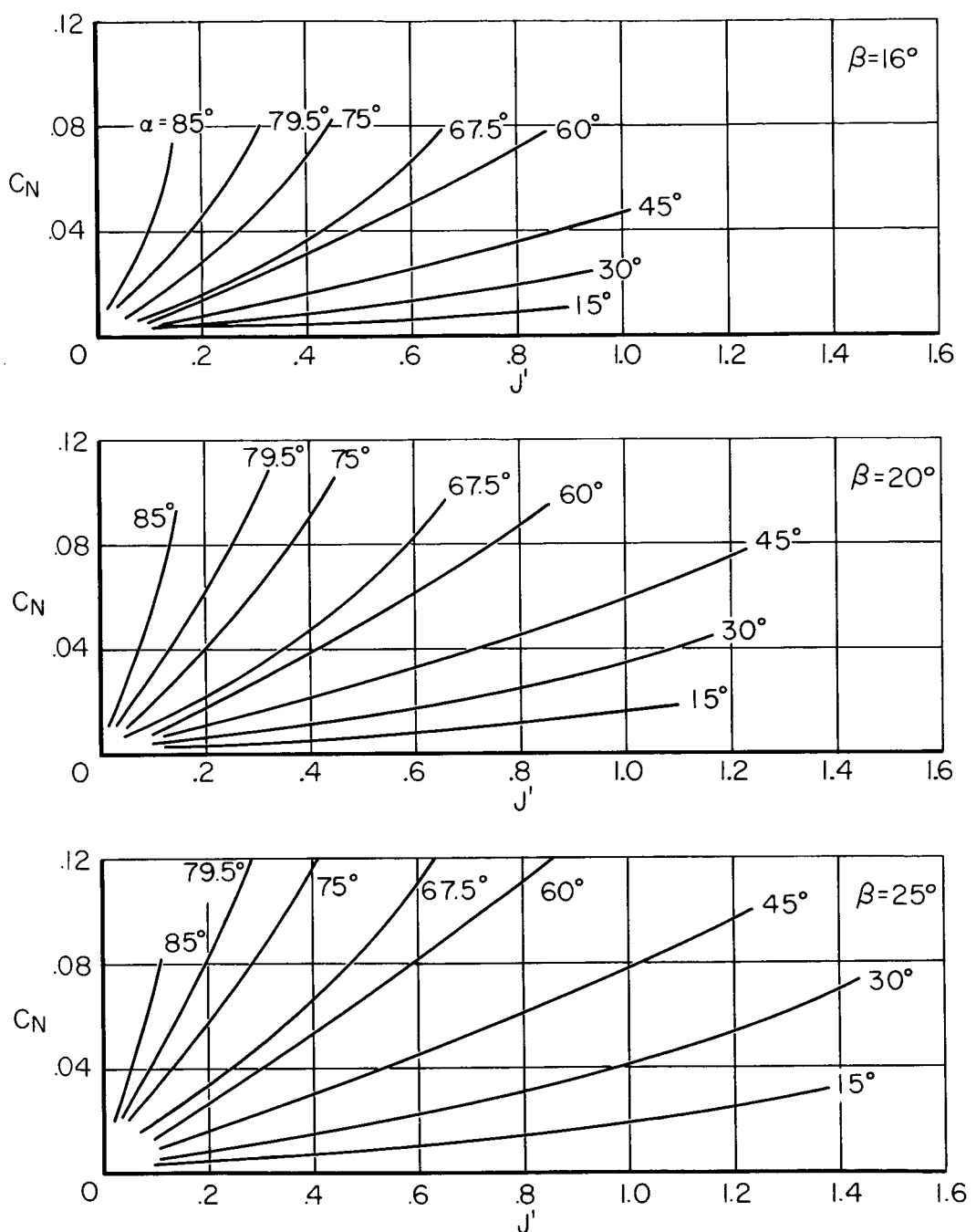
(a) $\beta = 0^\circ, 4^\circ, 8^\circ, 12^\circ$

Figure 6.- Variation of normal-force coefficient C_N of propeller 1 with modified advance ratio J' for several thrust-axis angles of attack α .



(b) $\beta = 16^\circ, 20^\circ, 25^\circ$

Figure 6.- Continued.

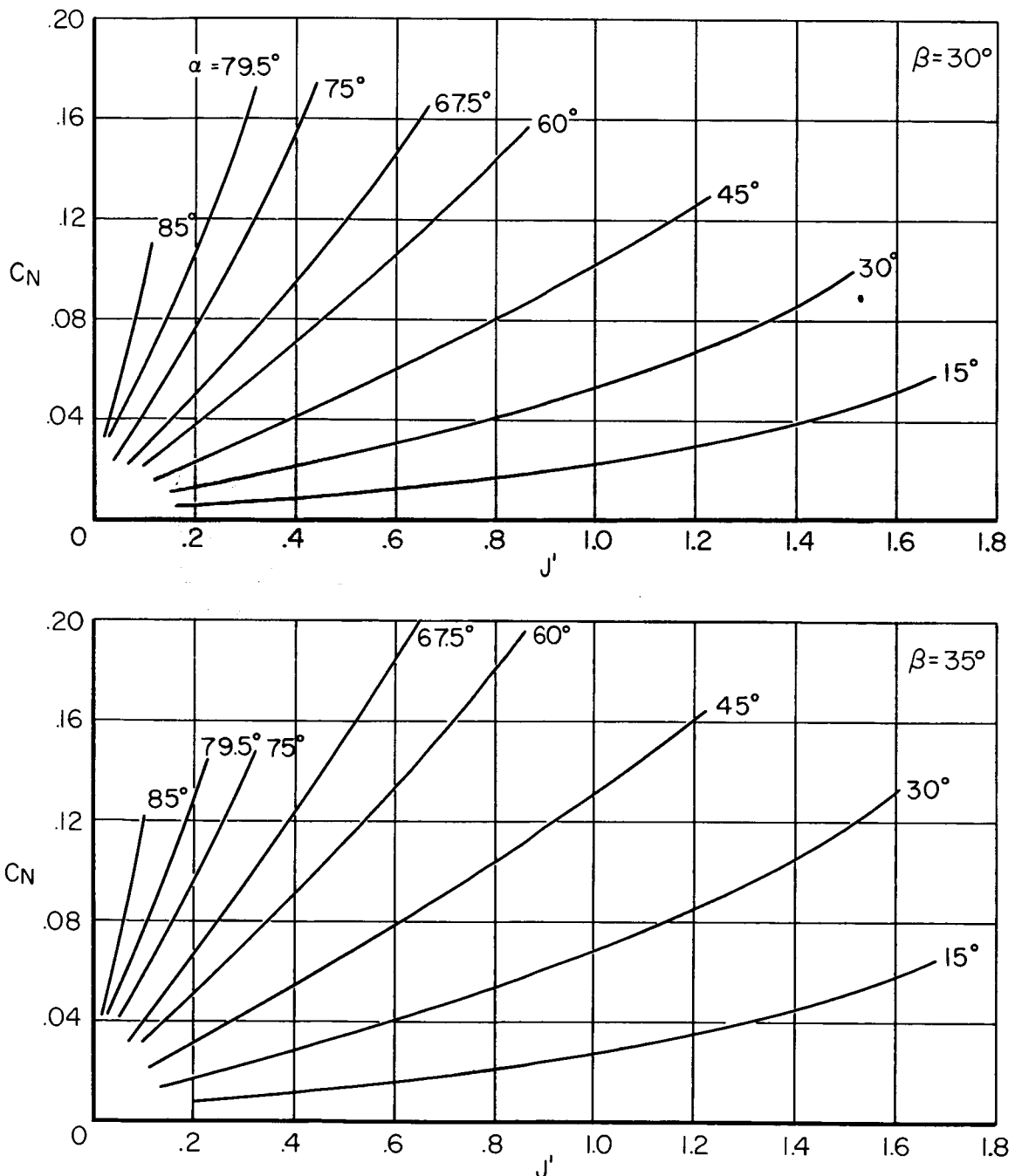
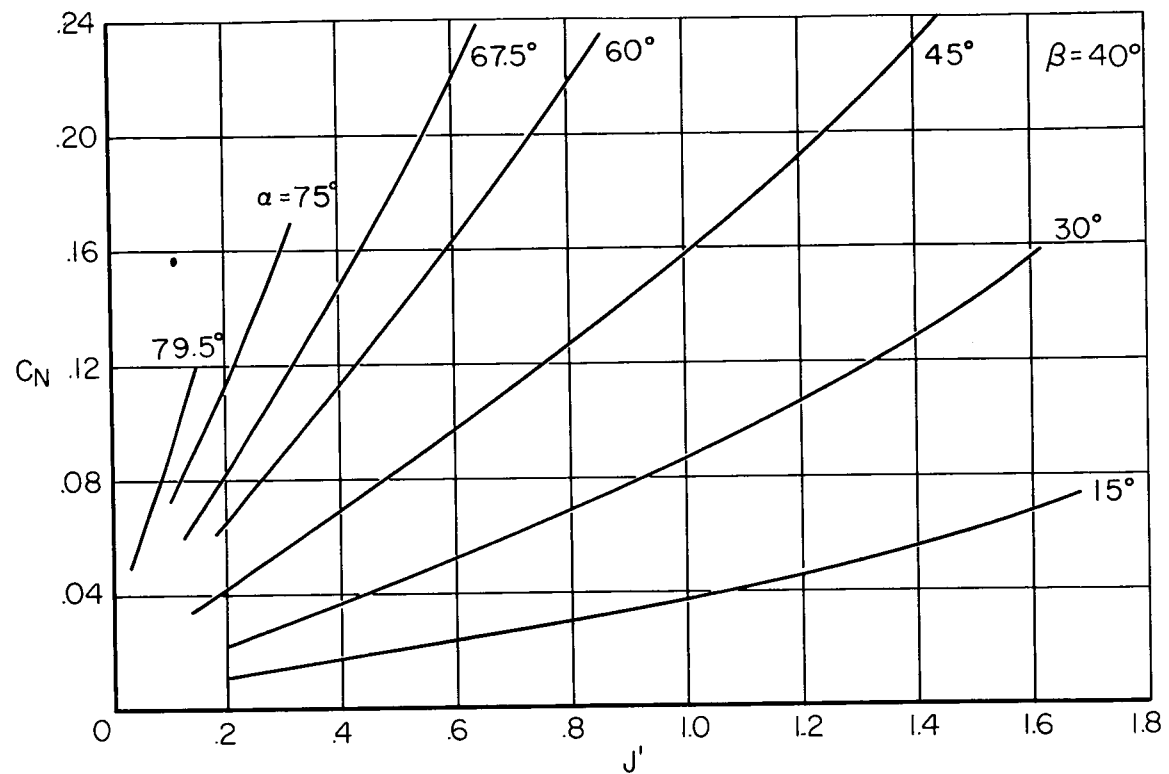
(c) $\beta = 30^\circ, 35^\circ$

Figure 6.- Continued.



(d) $\beta = 40^\circ$

Figure 6.- Concluded.

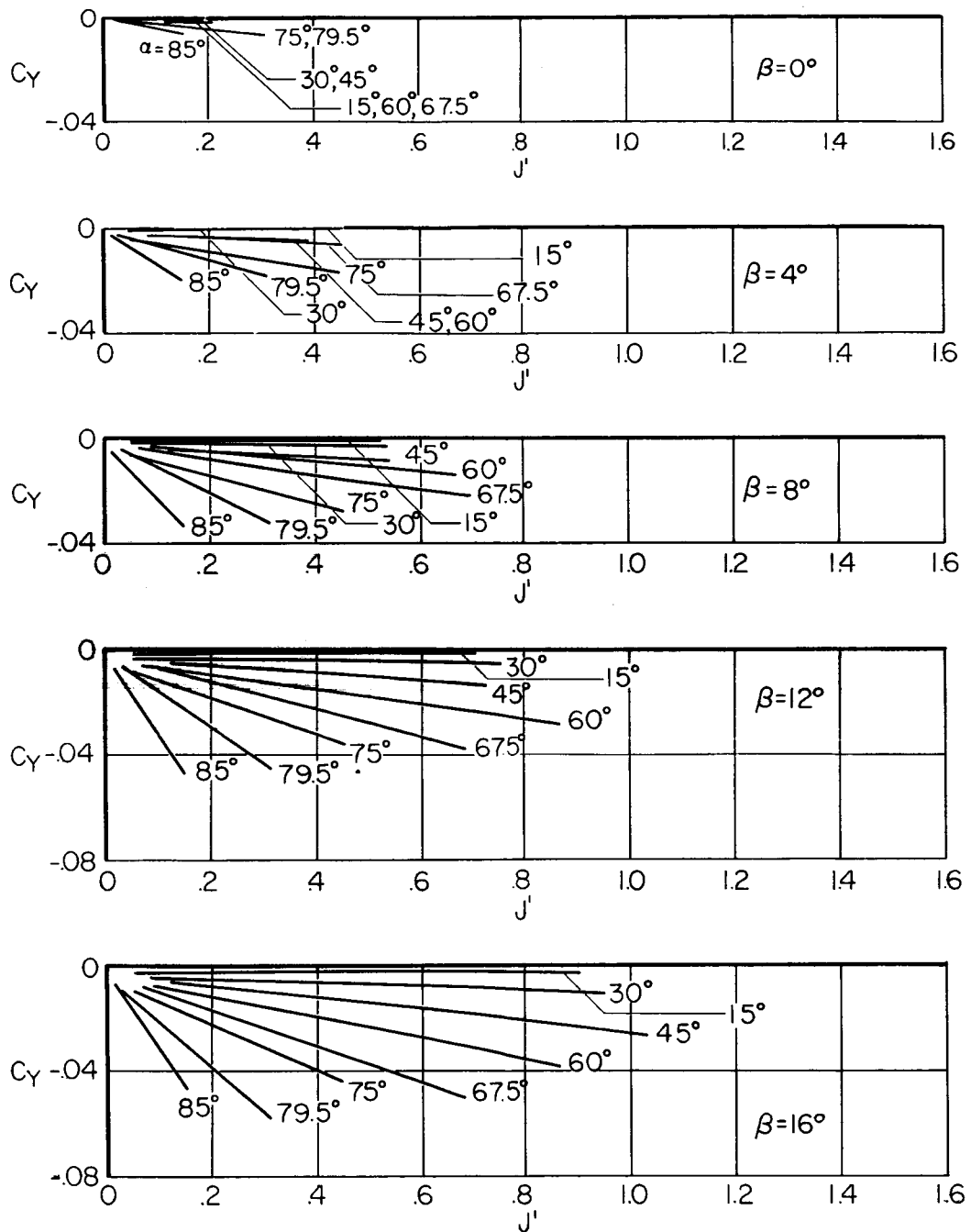
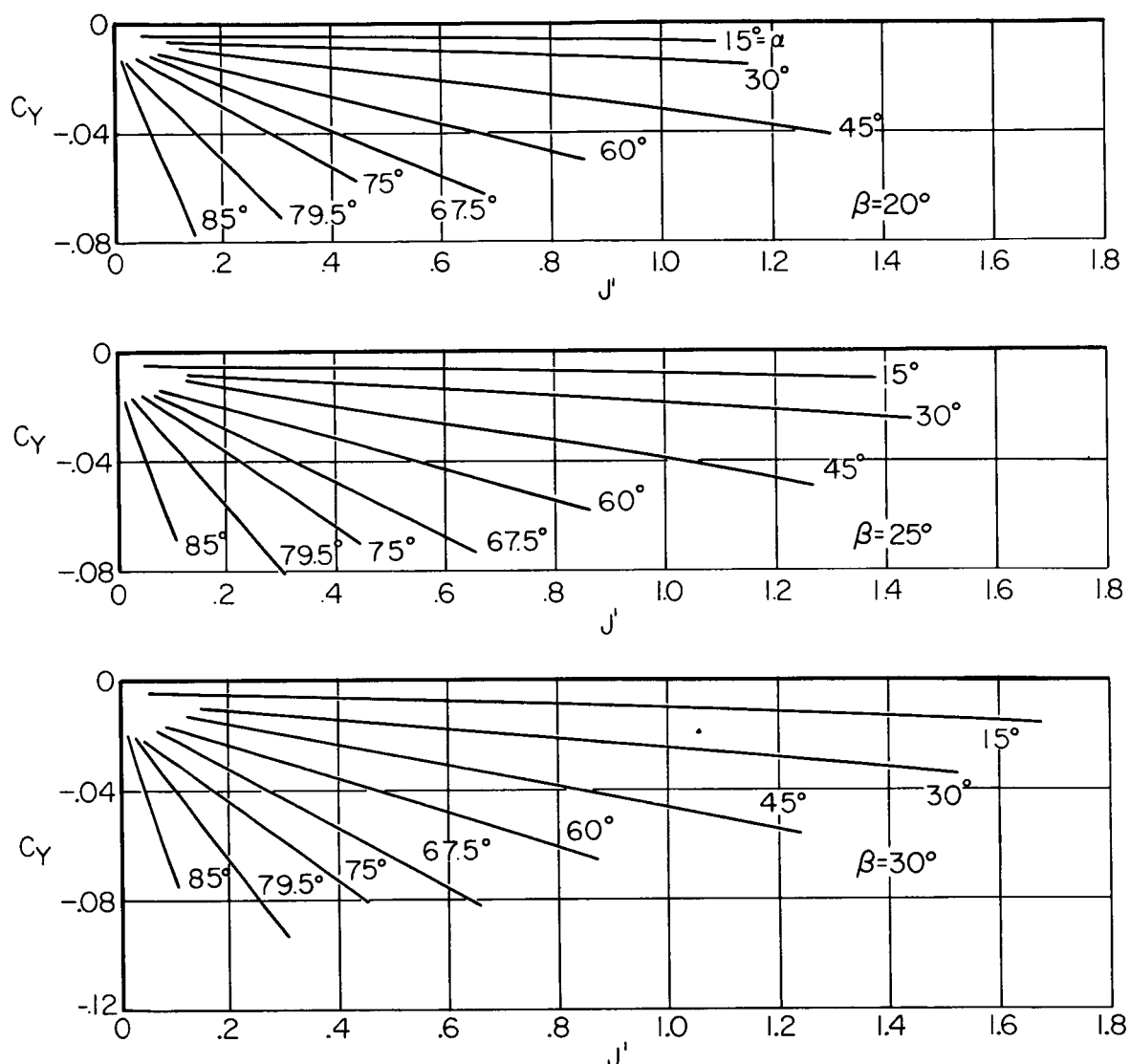
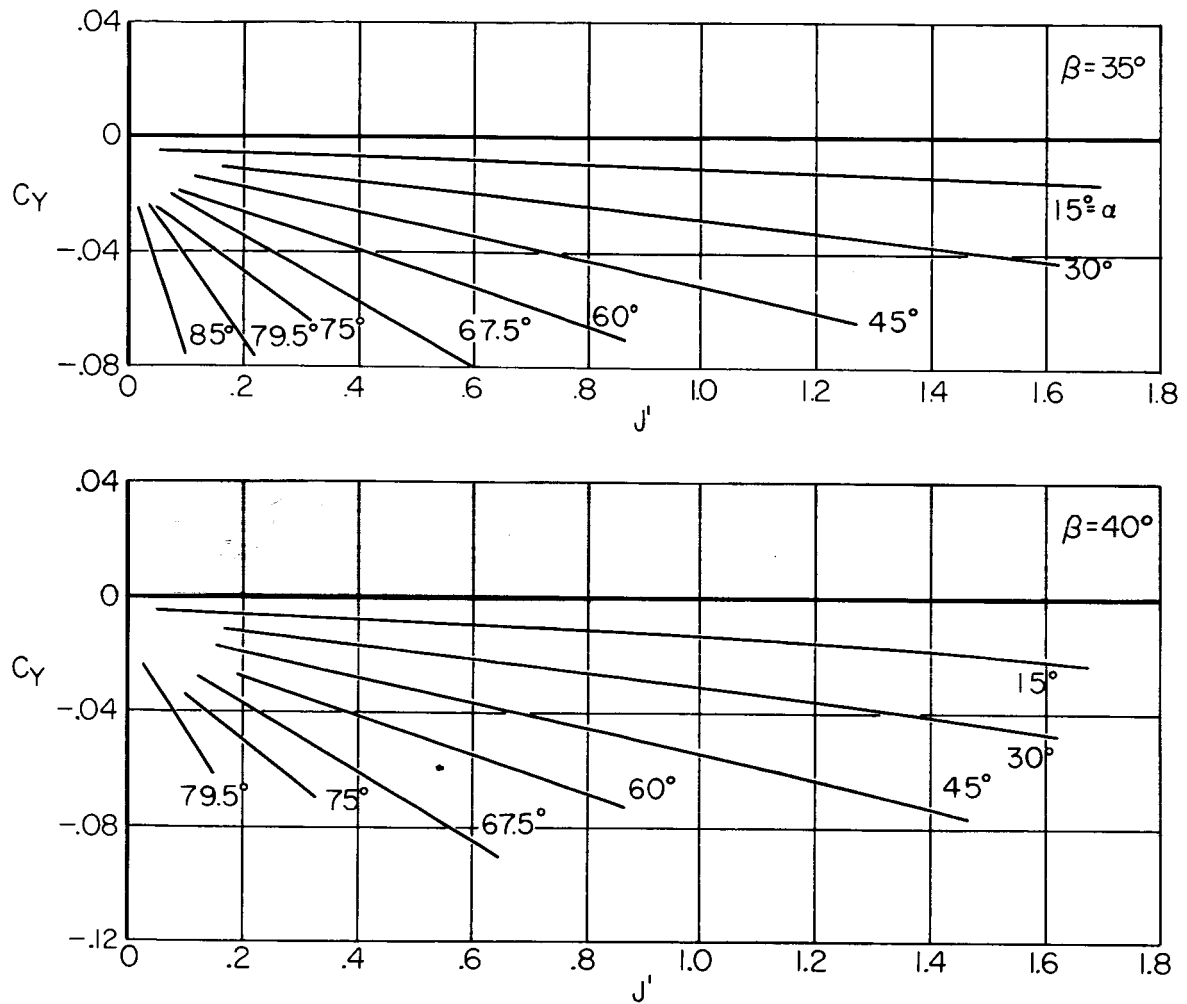
(a) $\beta = 0^\circ, 4^\circ, 8^\circ, 12^\circ, 16^\circ$

Figure 7.- Variation of yawing-moment coefficient C_Y of propeller 1 with modified advance ratio J' for several thrust-axis angles of attack α .



(b) $\beta = 20^\circ, 25^\circ, 30^\circ$

Figure 7.- Continued.



(c) $\beta = 35^\circ, 40^\circ$

Figure 7.- Concluded.

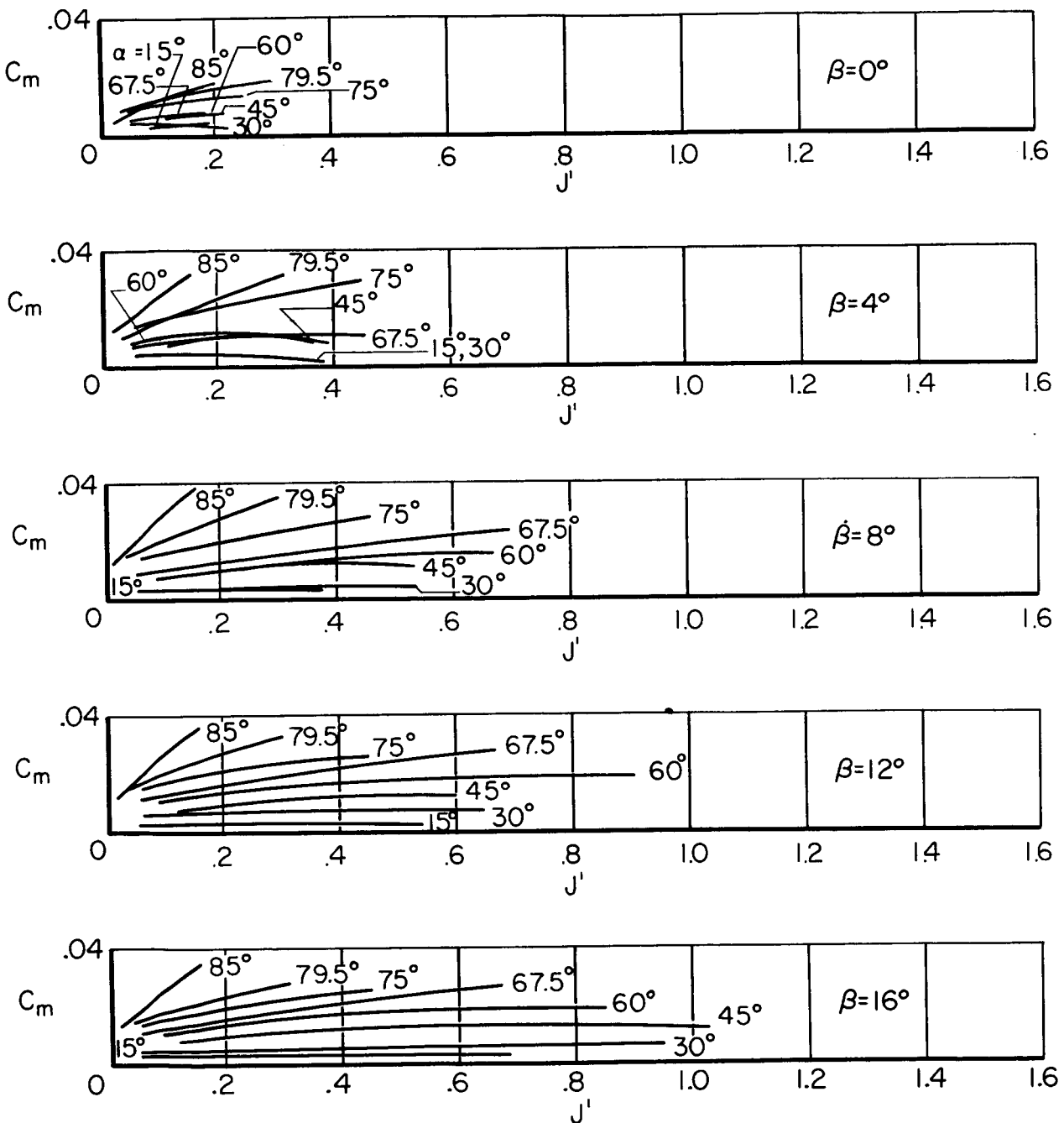
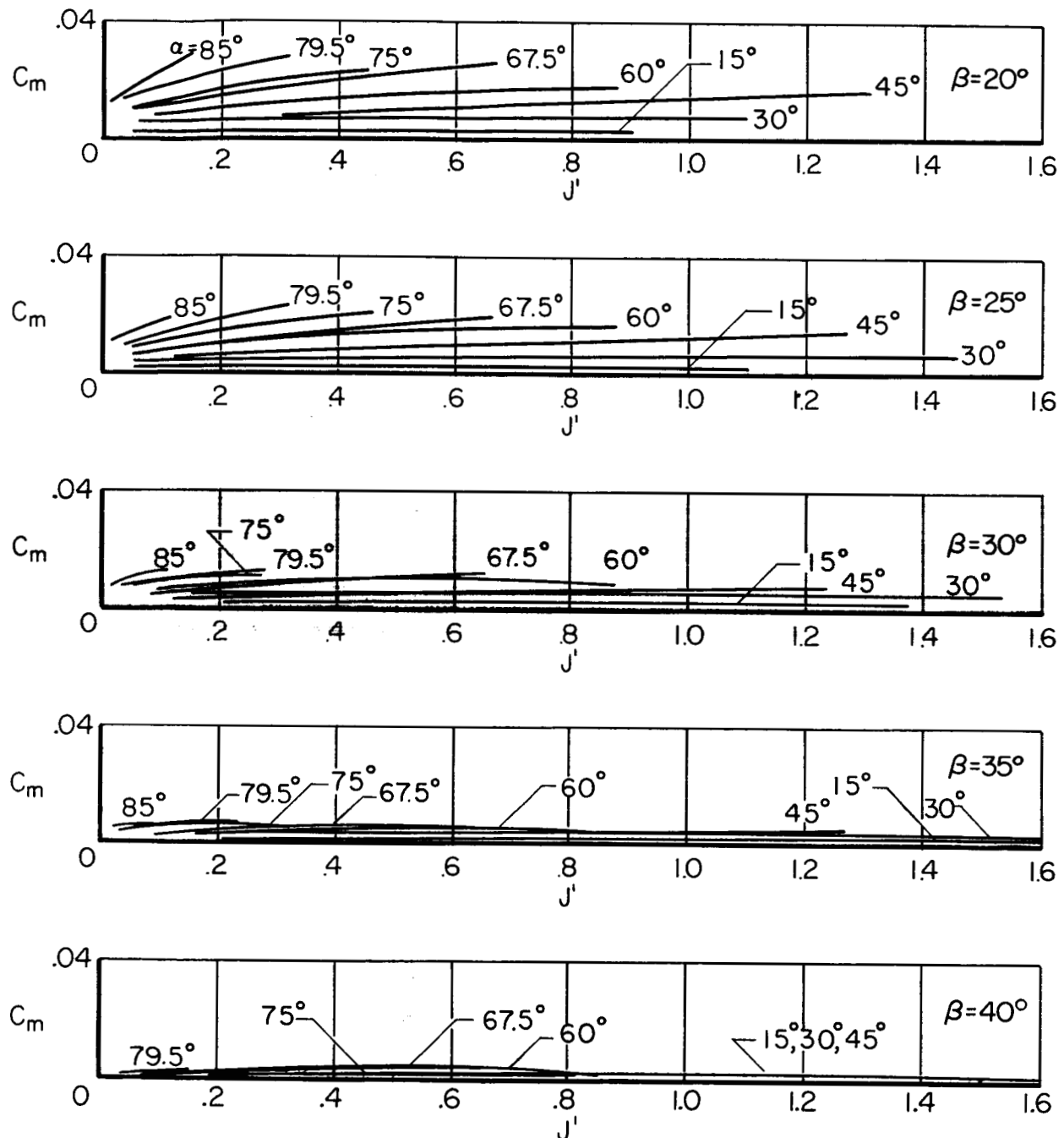
(a) $\beta = 0^\circ, 4^\circ, 8^\circ, 12^\circ, 16^\circ$

Figure 8.- Variation of pitching-moment coefficient C_m of propeller 1 with modified advance ratio J' for several thrust-axis angles of attack α .



(b) $\beta = 20^\circ, 25^\circ, 30^\circ, 35^\circ, 40^\circ$

Figure 8.- Concluded.

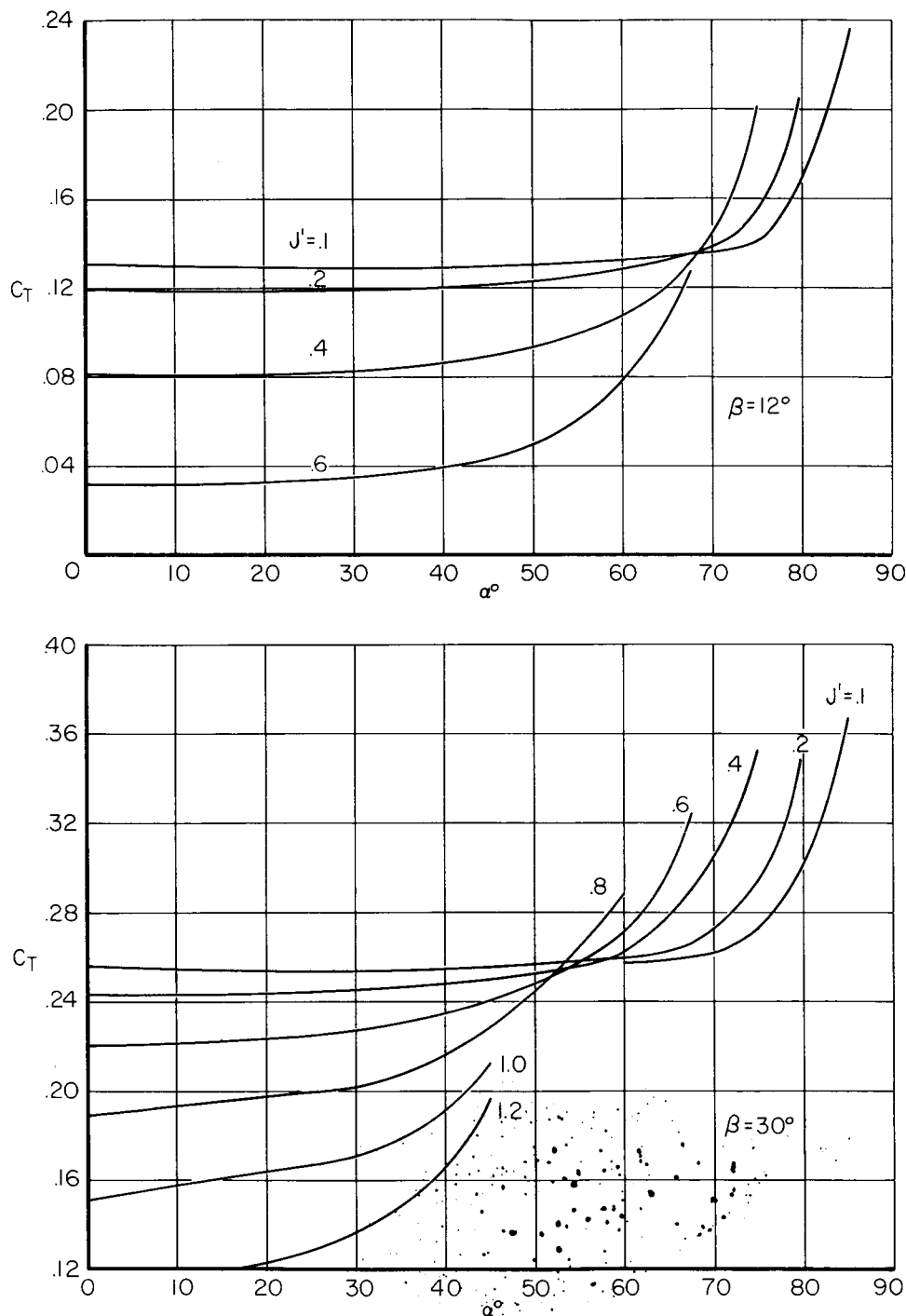


Figure 9.- Variation of thrust coefficient C_T of propeller 1 with thrust-axis angle of attack α for several values of modified advance ratio J' ; $\beta = 12^\circ$ and 30° .

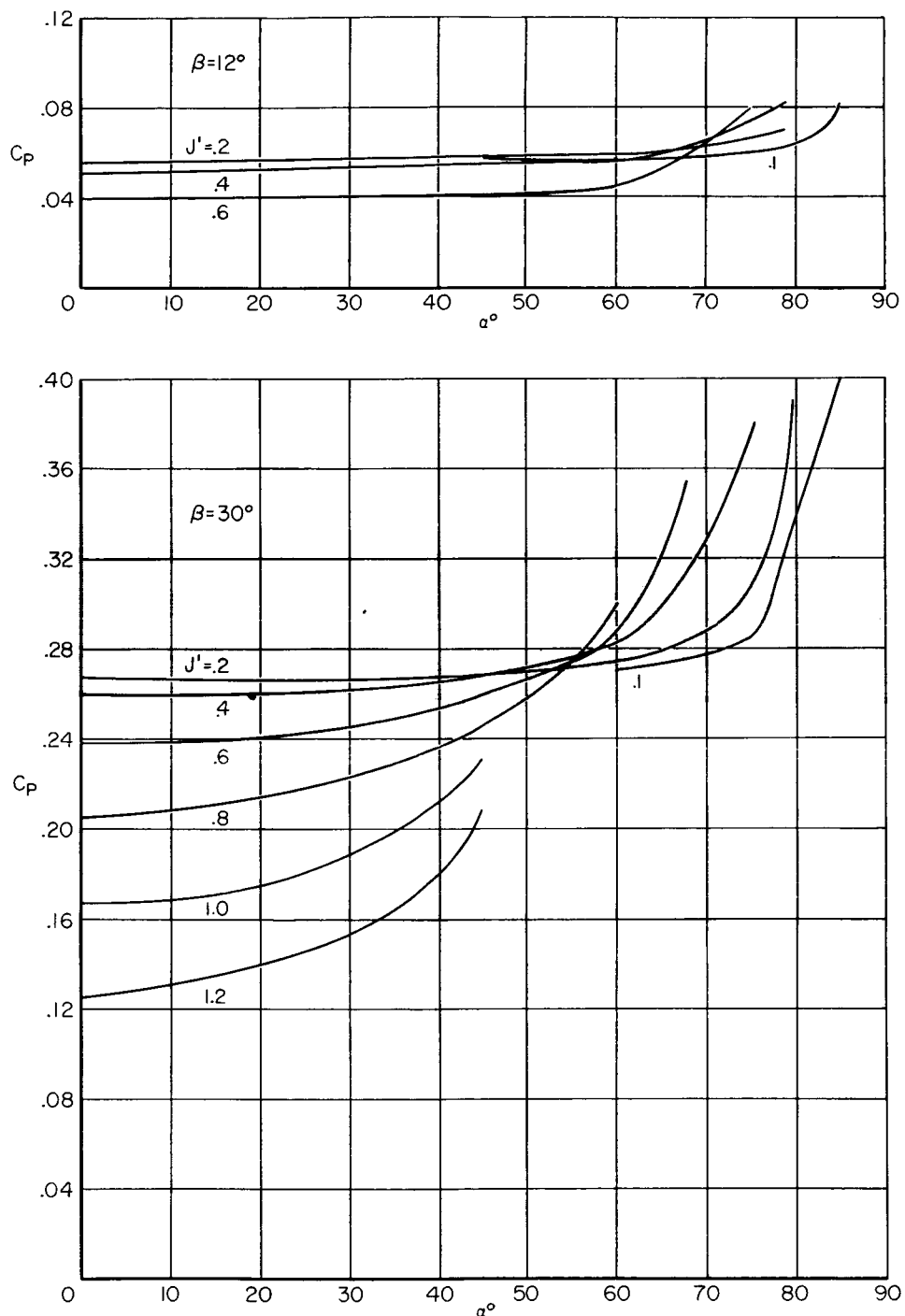


Figure 10.- Variation of power coefficient C_p of propeller 1 with thrust-axis angle of attack α for several values of modified advance ratio J' ; $\beta = 12^\circ$ and 30° .

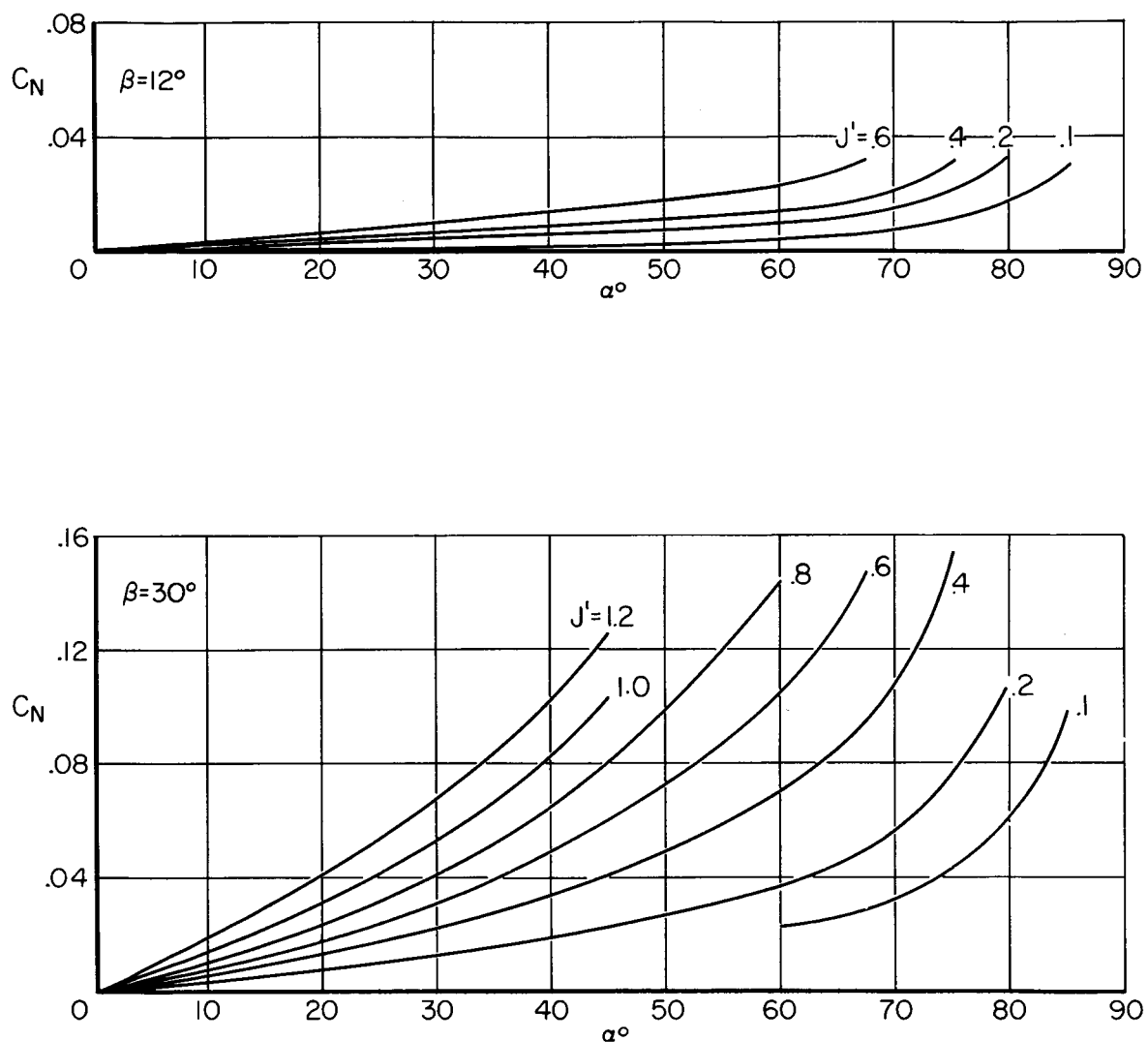


Figure 11.- Variation of normal-force coefficient C_N of propeller 1 with thrust-axis angle of attack α for several values of modified advance ratio J' ; $\beta = 12^\circ$ and 30° .

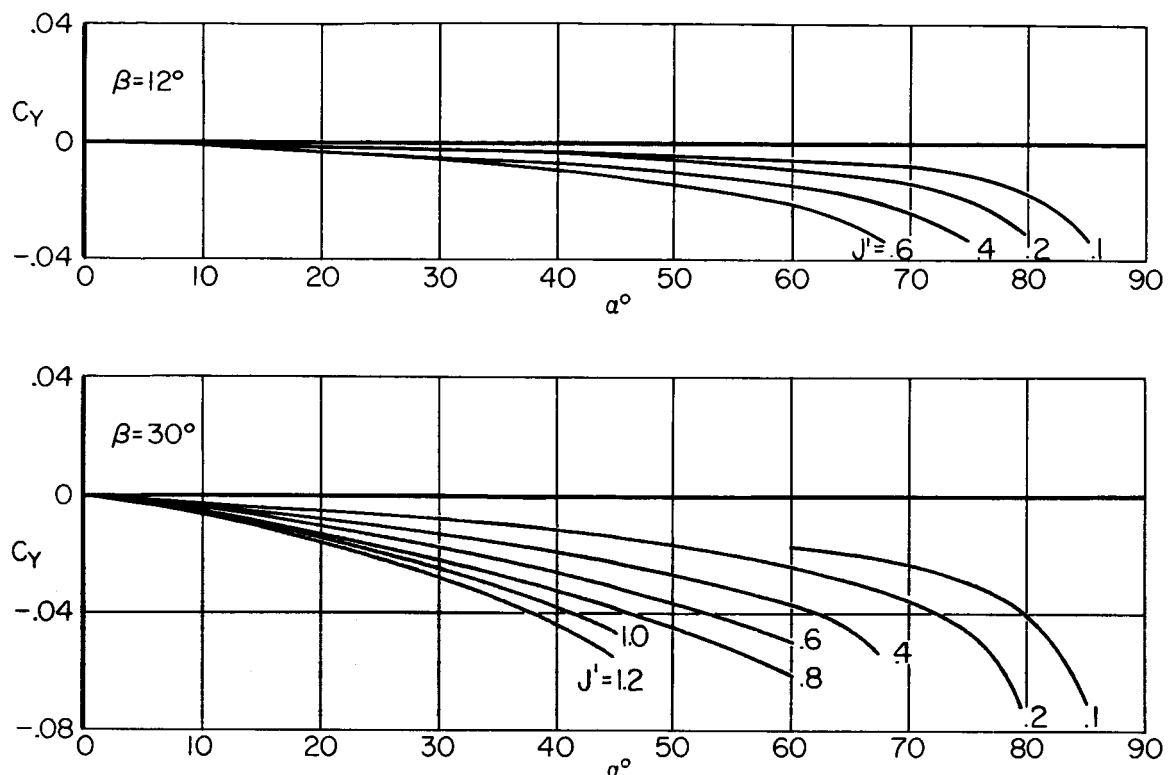


Figure 12.- Variation of yawing-moment coefficient C_Y of propeller 1 with thrust-axis angle of attack α for several modified advance ratios J' ; $\beta = 12^\circ$ and 30° .

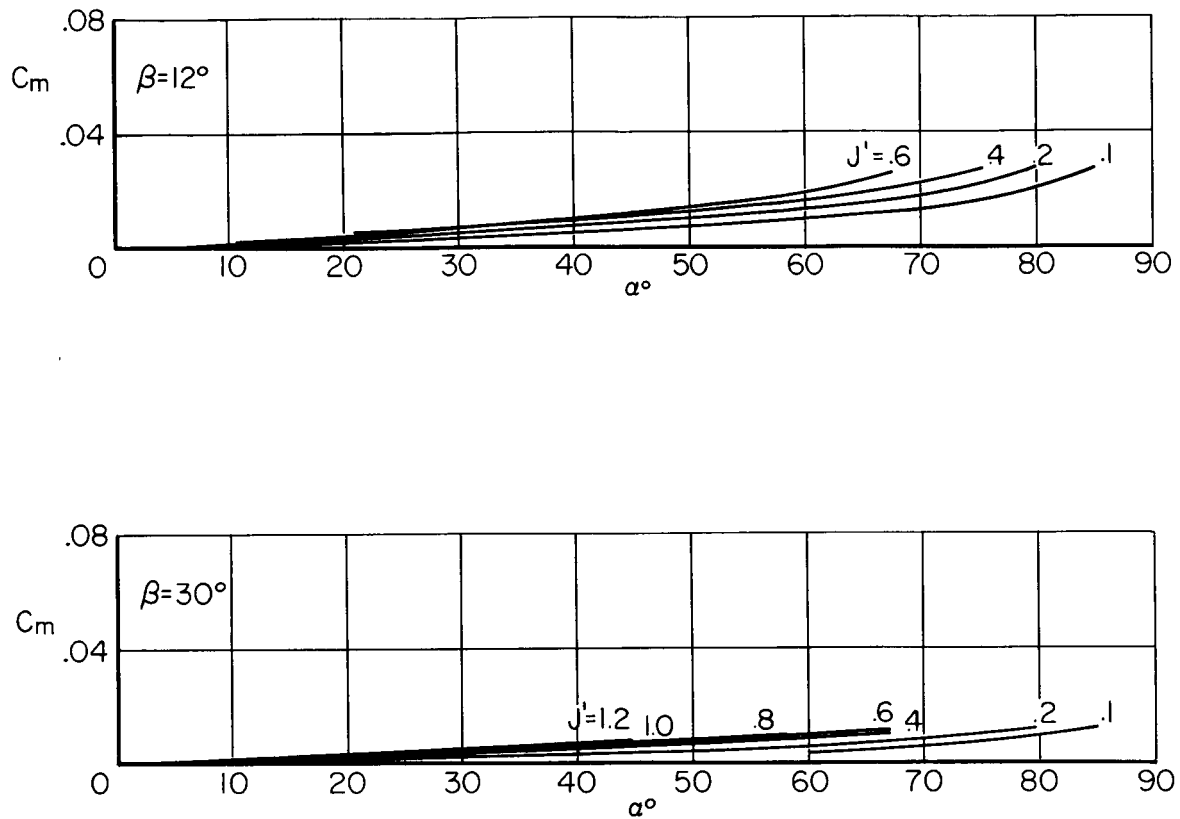


Figure 13.- Variation of pitching-moment coefficient C_m of propeller 1 with thrust-axis angle of attack α for several modified advance ratios J' ; $\beta = 12^\circ$ and 30° .

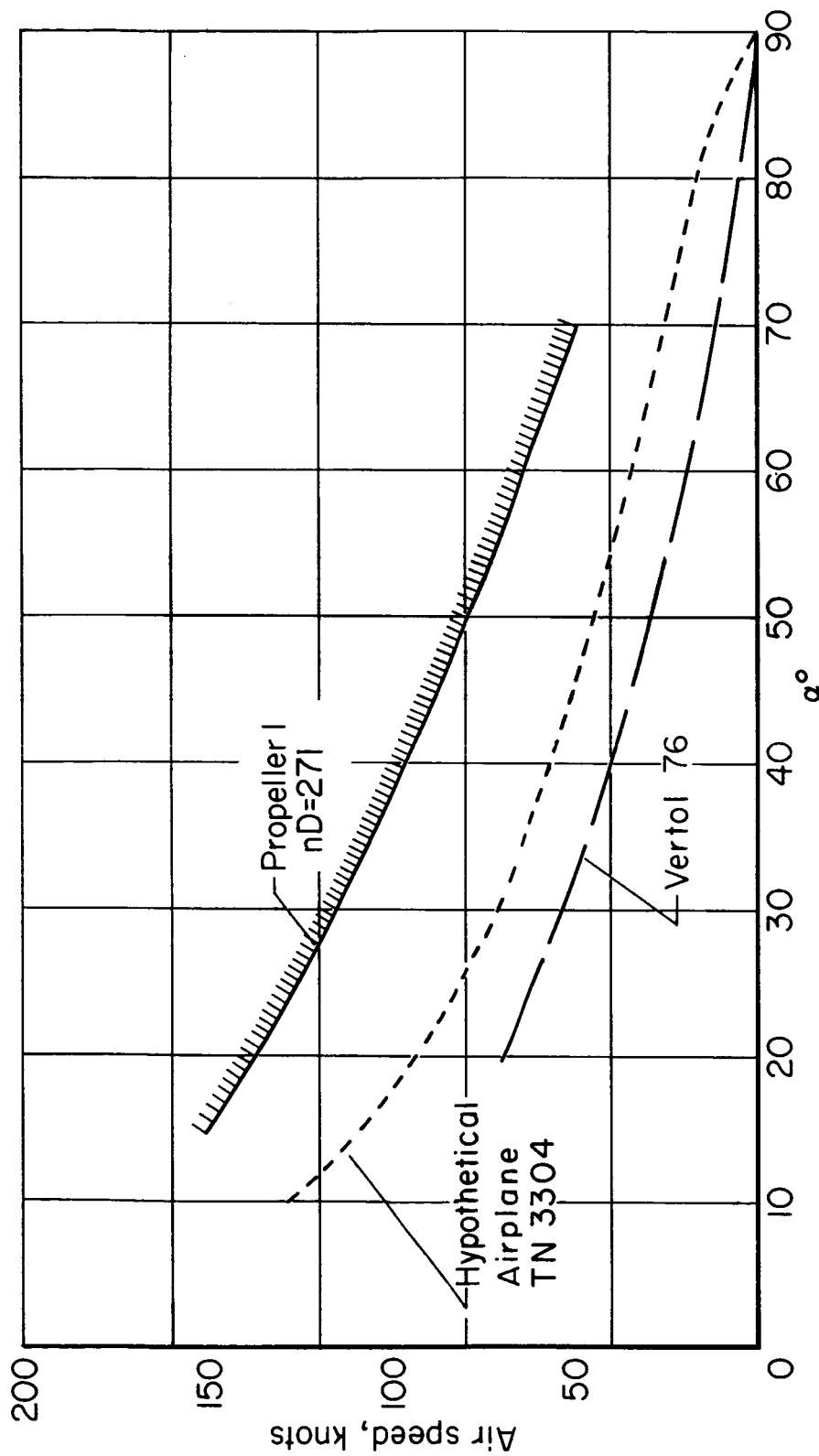
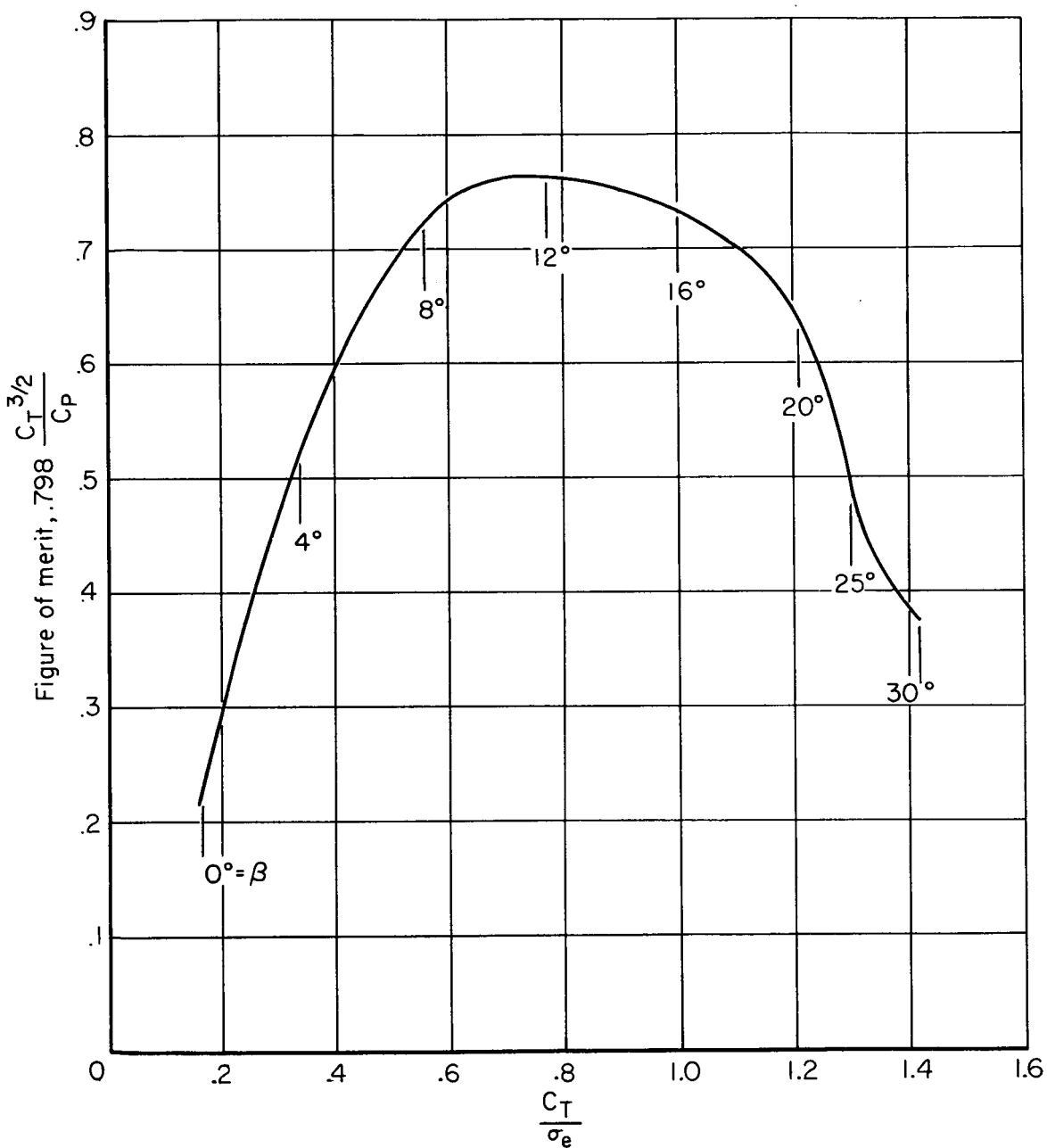


Figure 14.—Comparison of boundary curve for 5-percent increase of thrust coefficient from value at zero thrust-axis angle of attack with typical transition programs for two airplanes.



(a) Propeller 1.

Figure 15.- Figure of merit as a function of weighted thrust coefficient for the three propellers operating at static conditions.

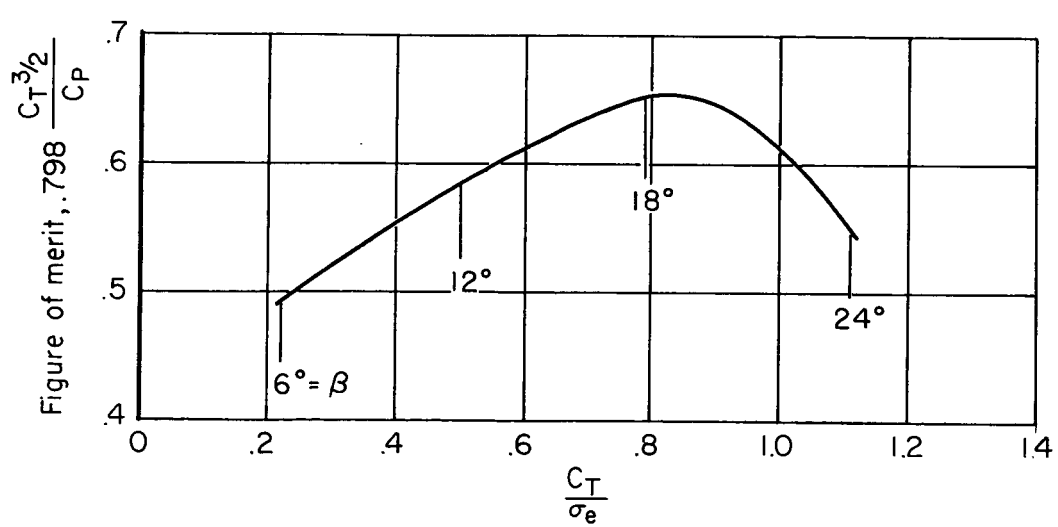
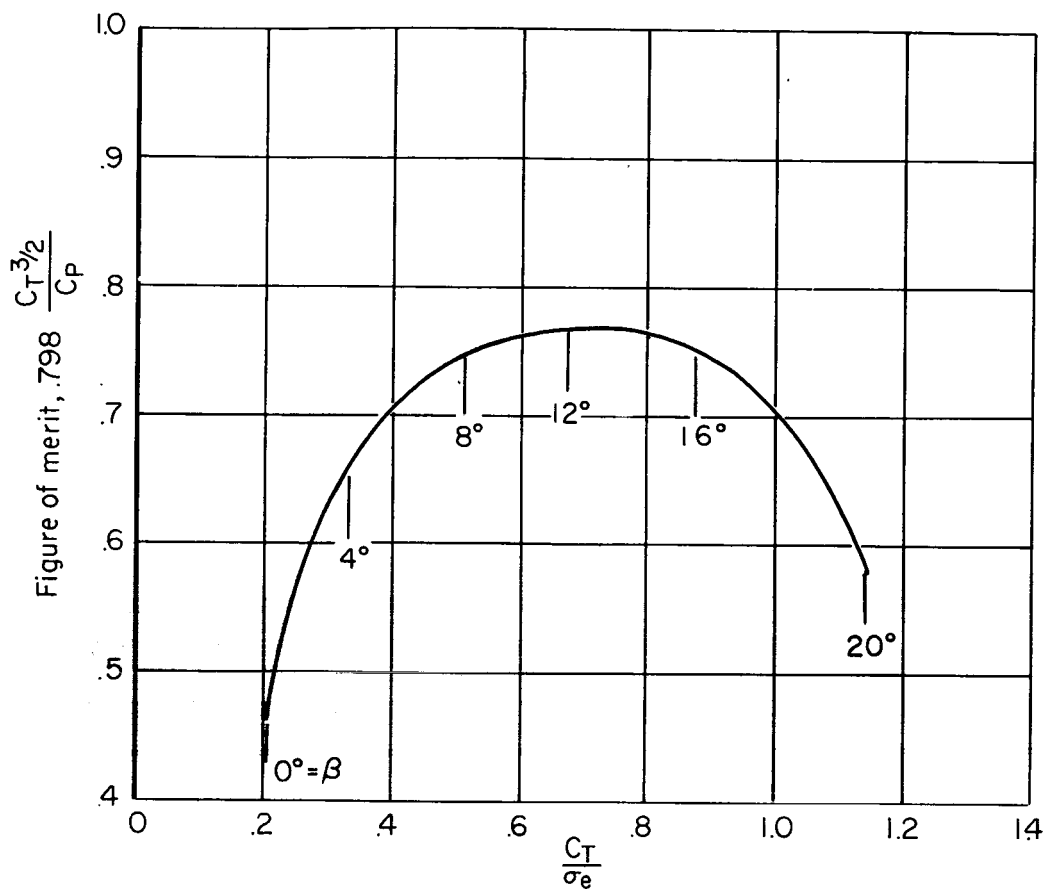
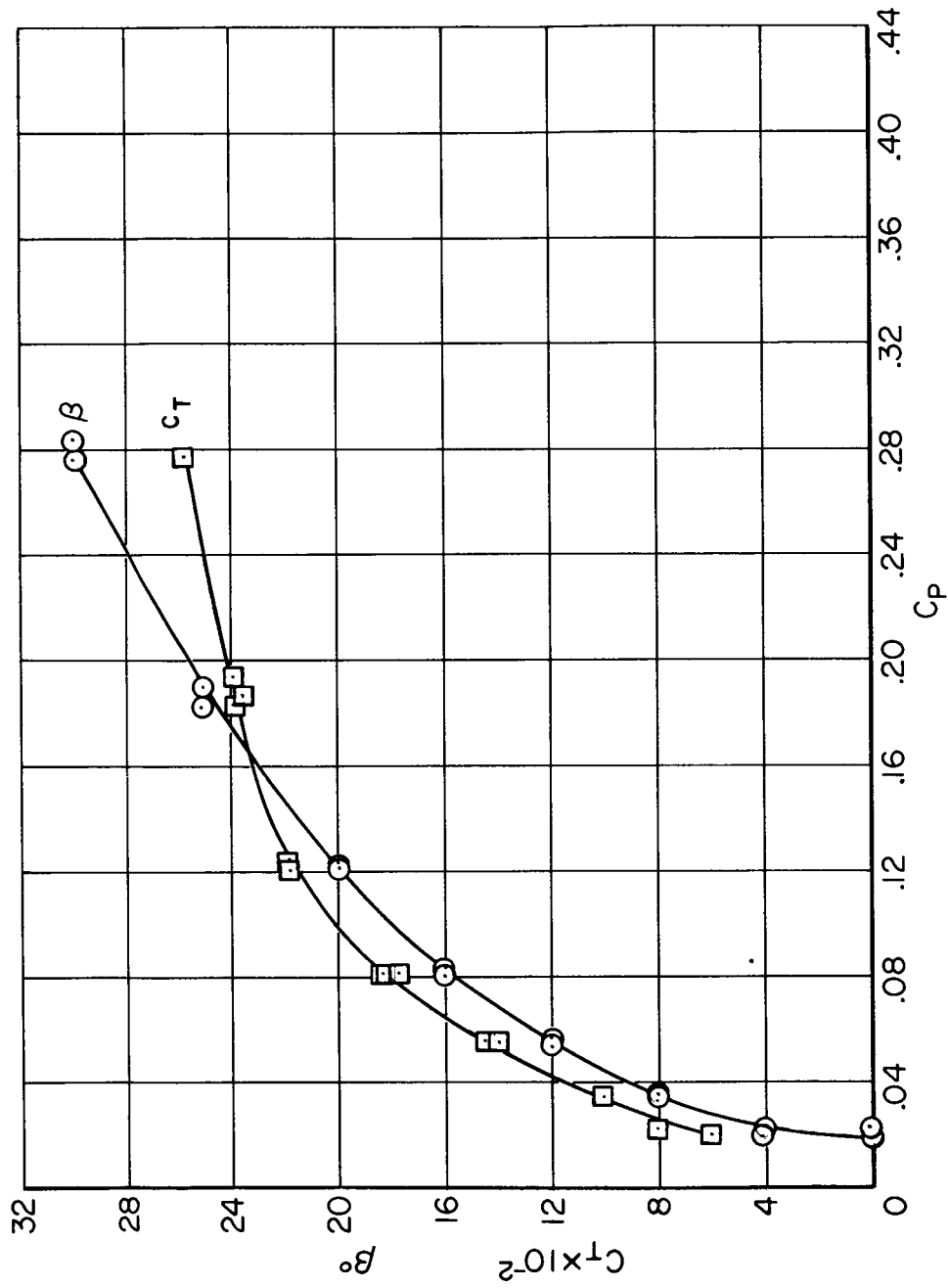


Figure 15.- Concluded.



(a) Propeller 1.

Figure 16.- Variation of thrust coefficient C_T and blade angle β with power coefficient C_P for the three propellers operating at zero advance ratio.

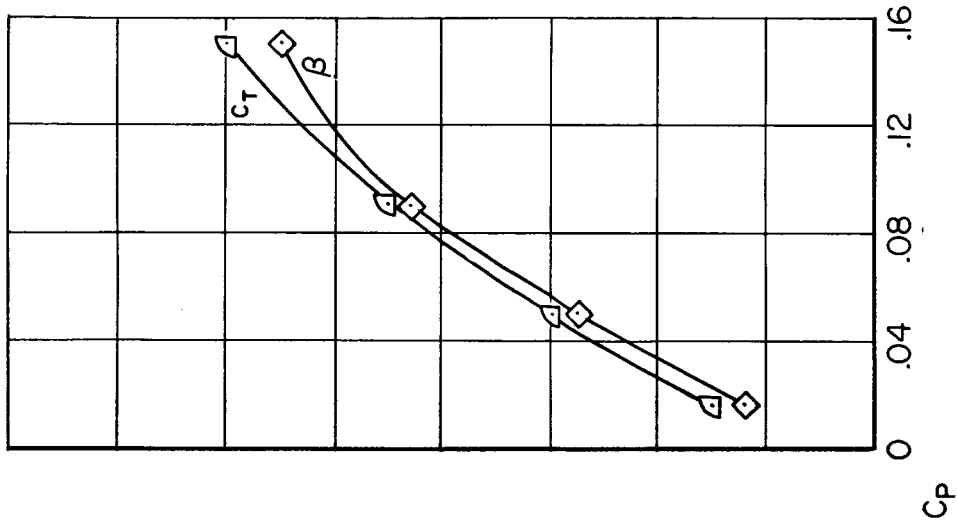
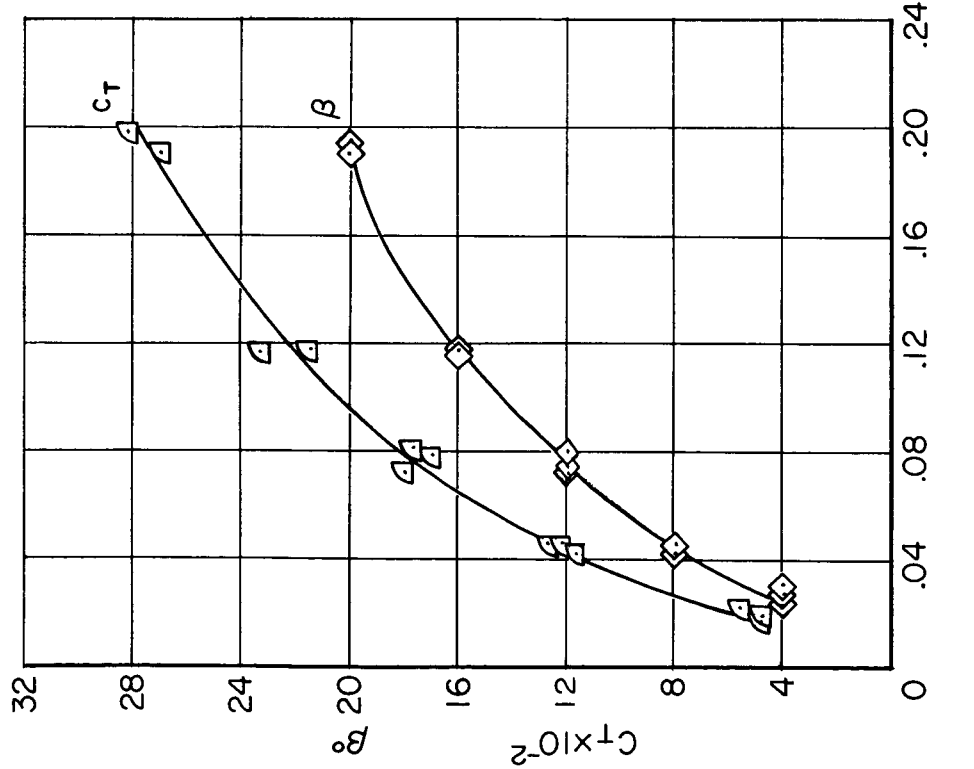


Figure 16.- Concluded.

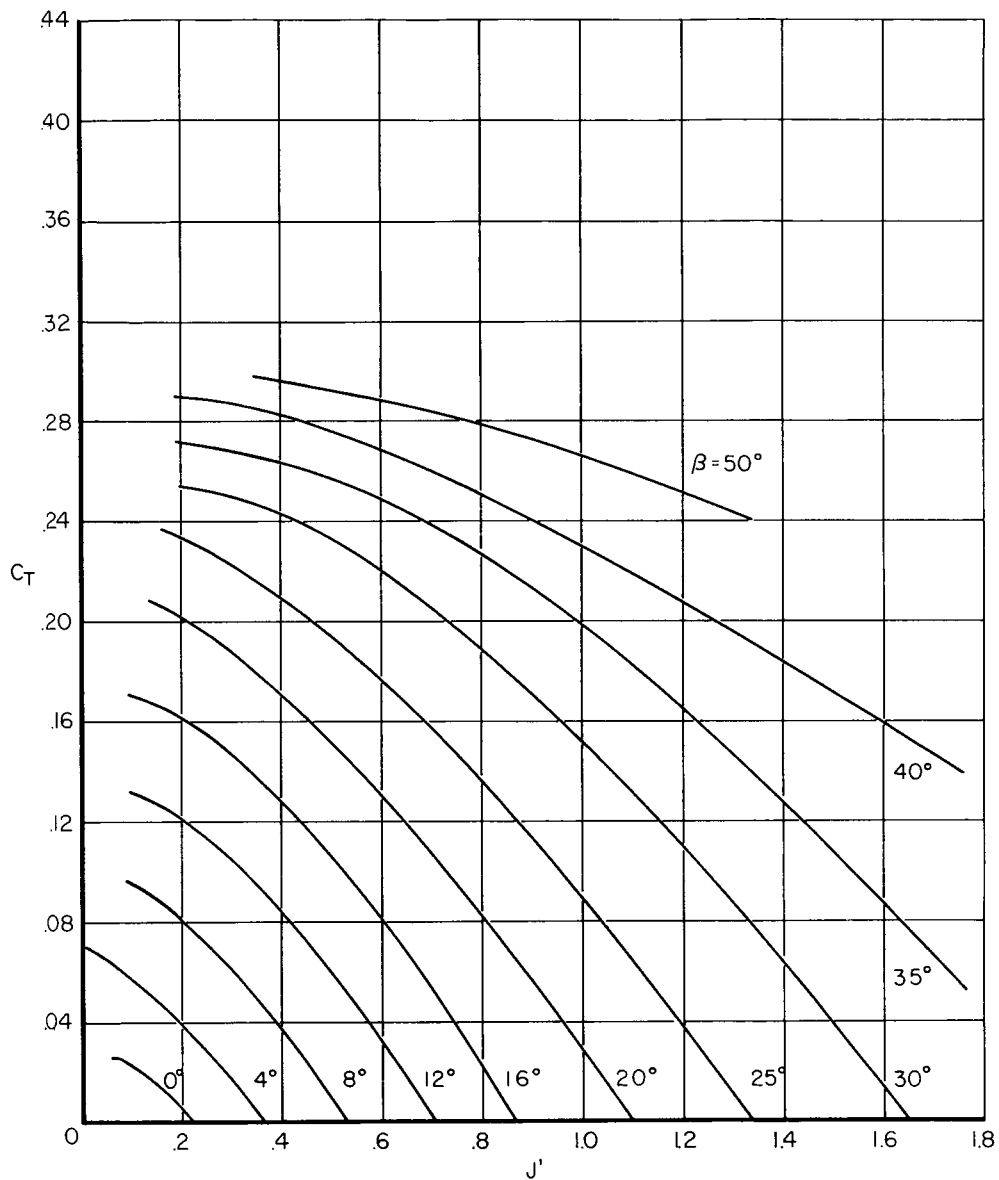
(a) Thrust coefficient C_T .

Figure 17.- Variation of the propeller performance parameters with modified advance ratio J' for several blade angles β ; $\alpha = 0^\circ$, propeller number 1.

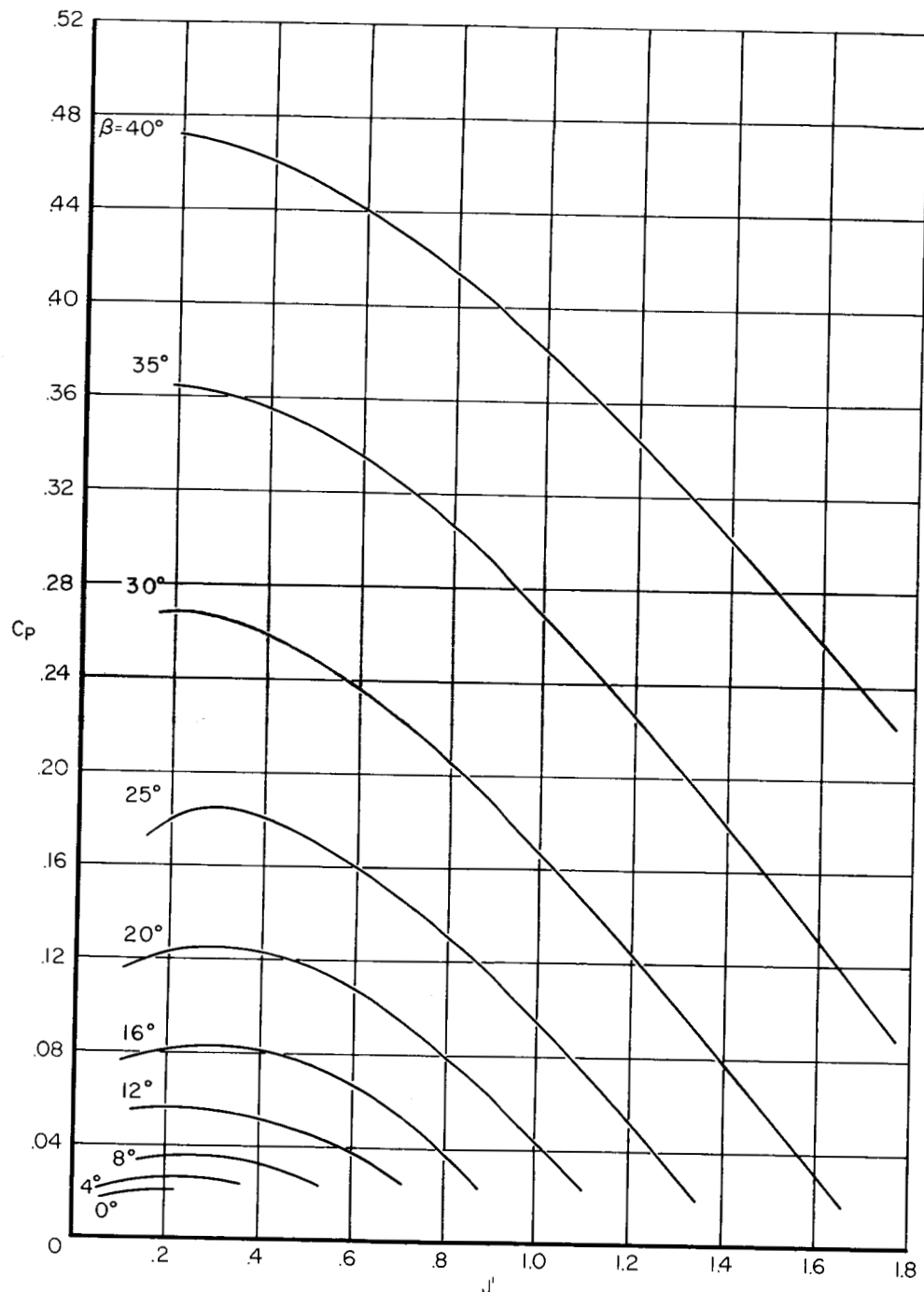
(b) Power coefficient C_P .

Figure 17.- Continued.

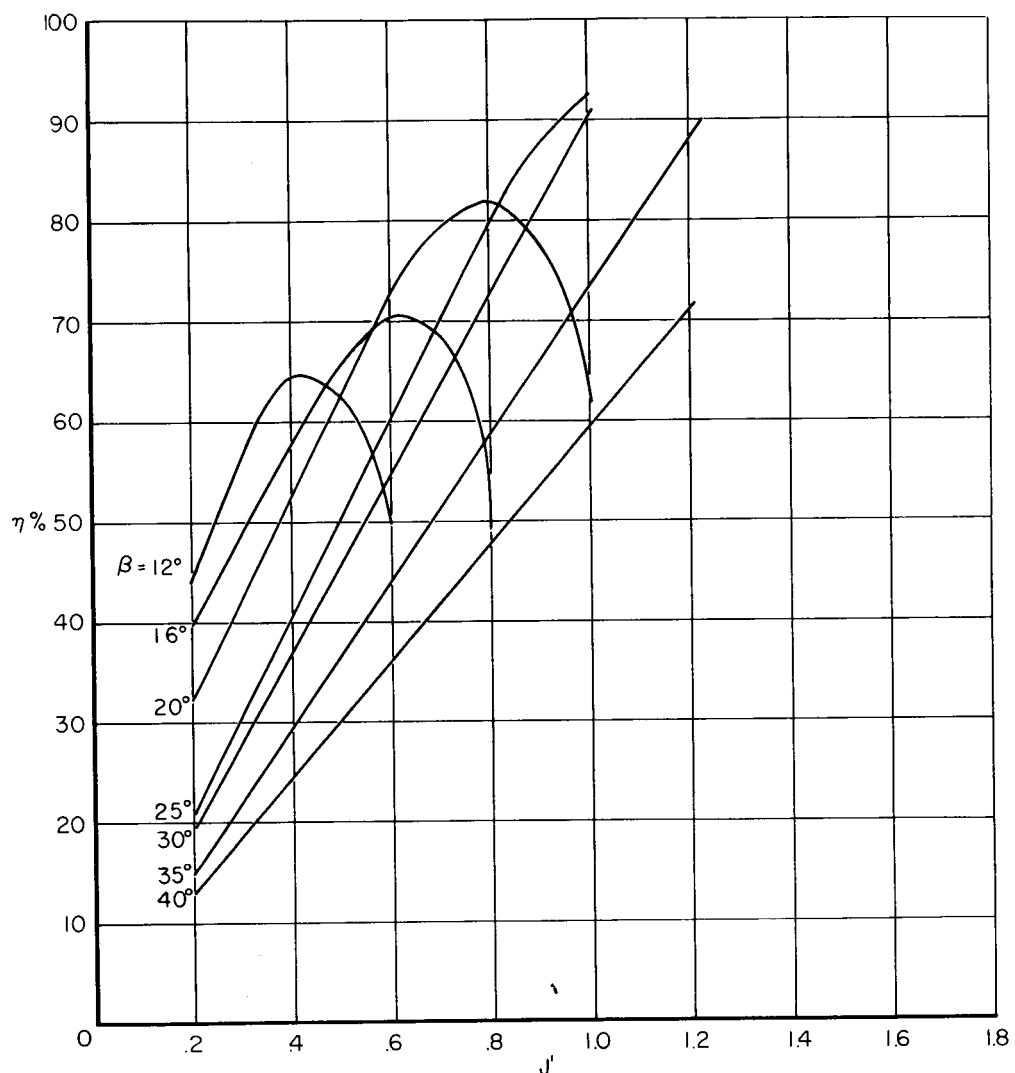
(c) Efficiency η .

Figure 17.- Concluded.

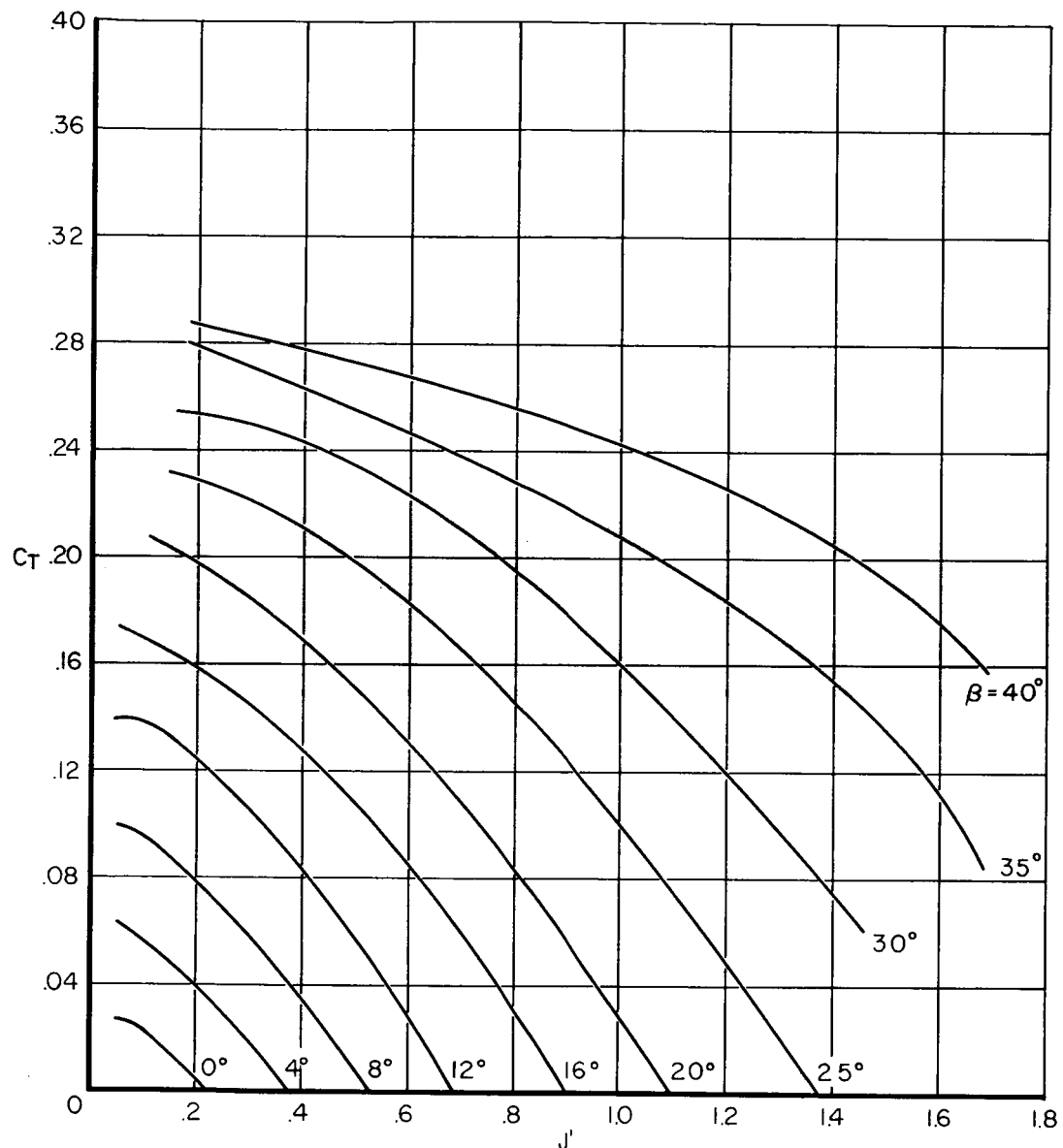
(a) Thrust coefficient C_T .

Figure 18.- Variation of the propeller performance parameters with modified advance ratio J' for several blade angles β ; $\alpha = 15^\circ$, propeller number 1.

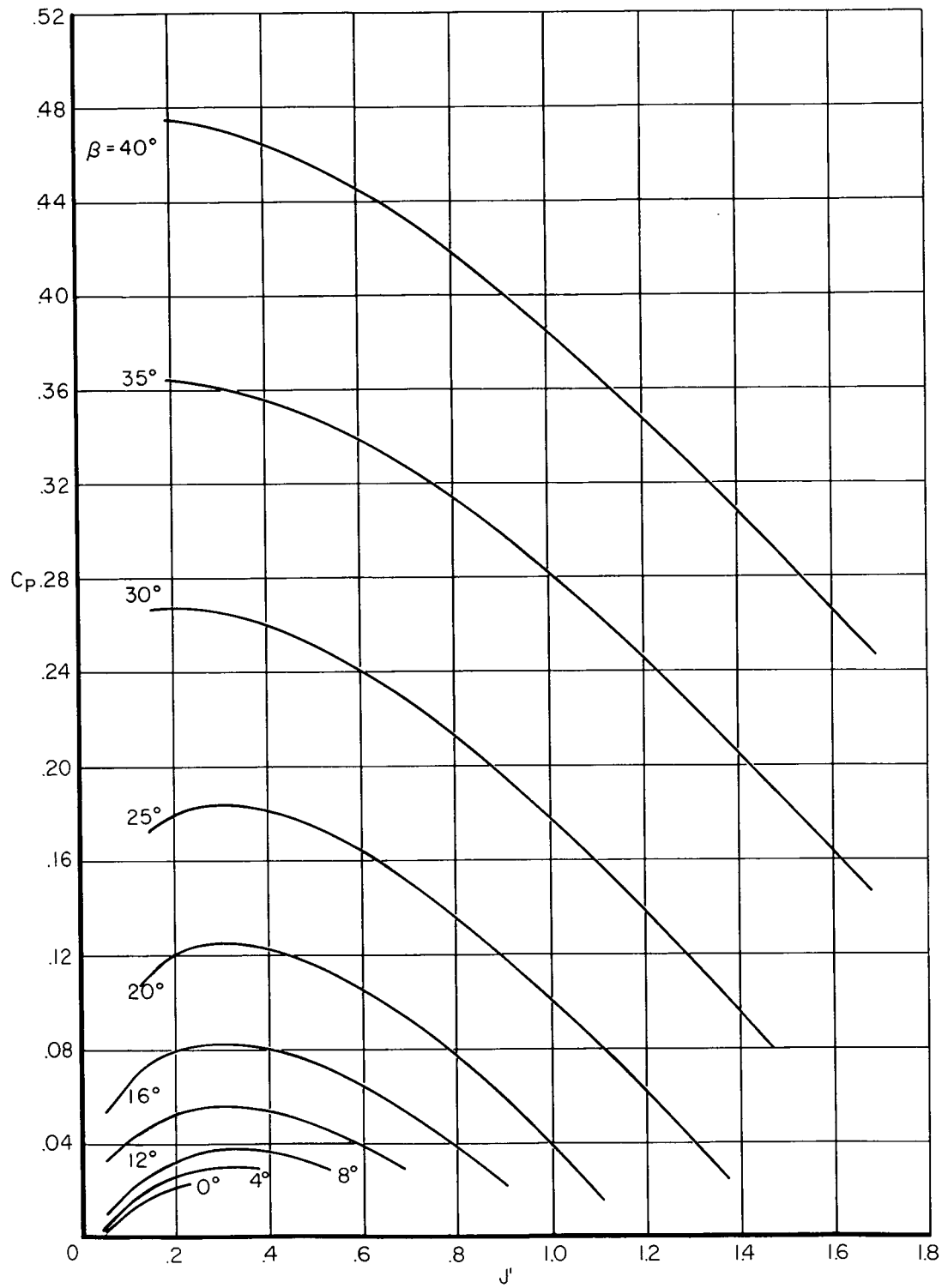
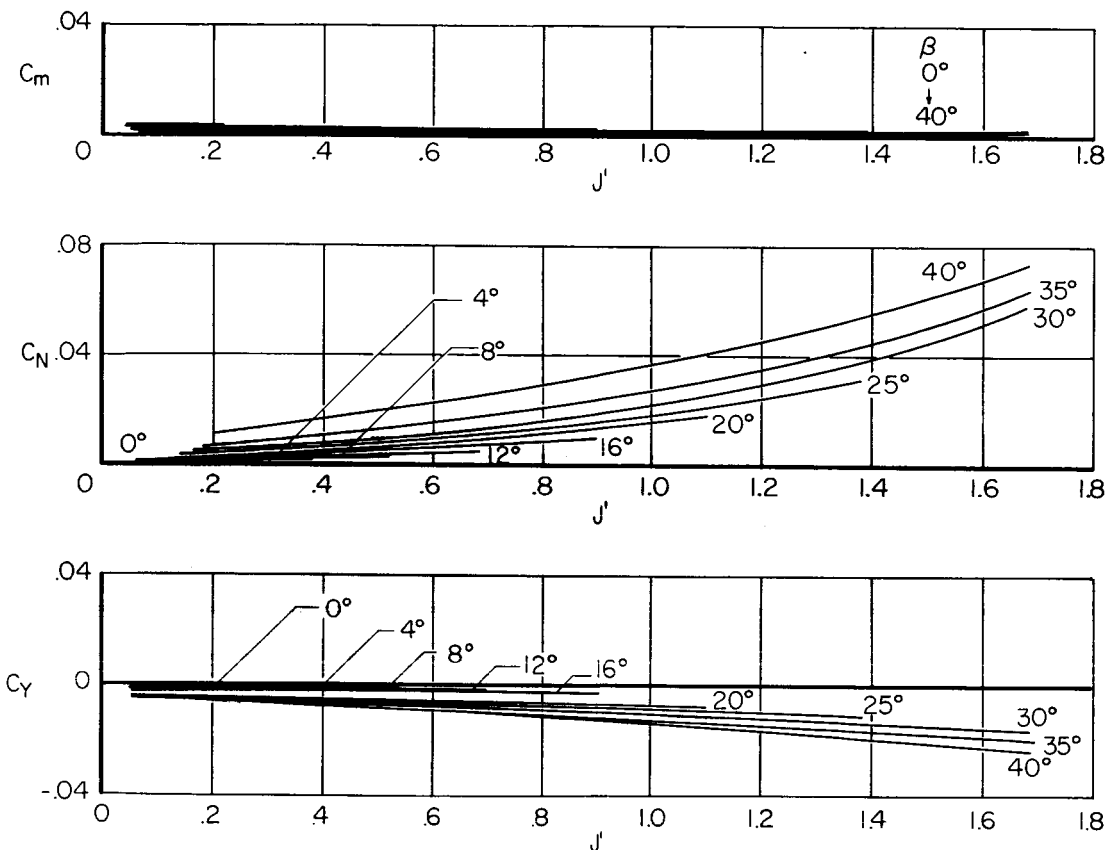
(b) Power coefficient C_P .

Figure 18.- Continued.



(c) Pitching-moment coefficient C_m ; normal-force coefficient C_N ; yawing-moment coefficient C_Y .

Figure 18.- Concluded.

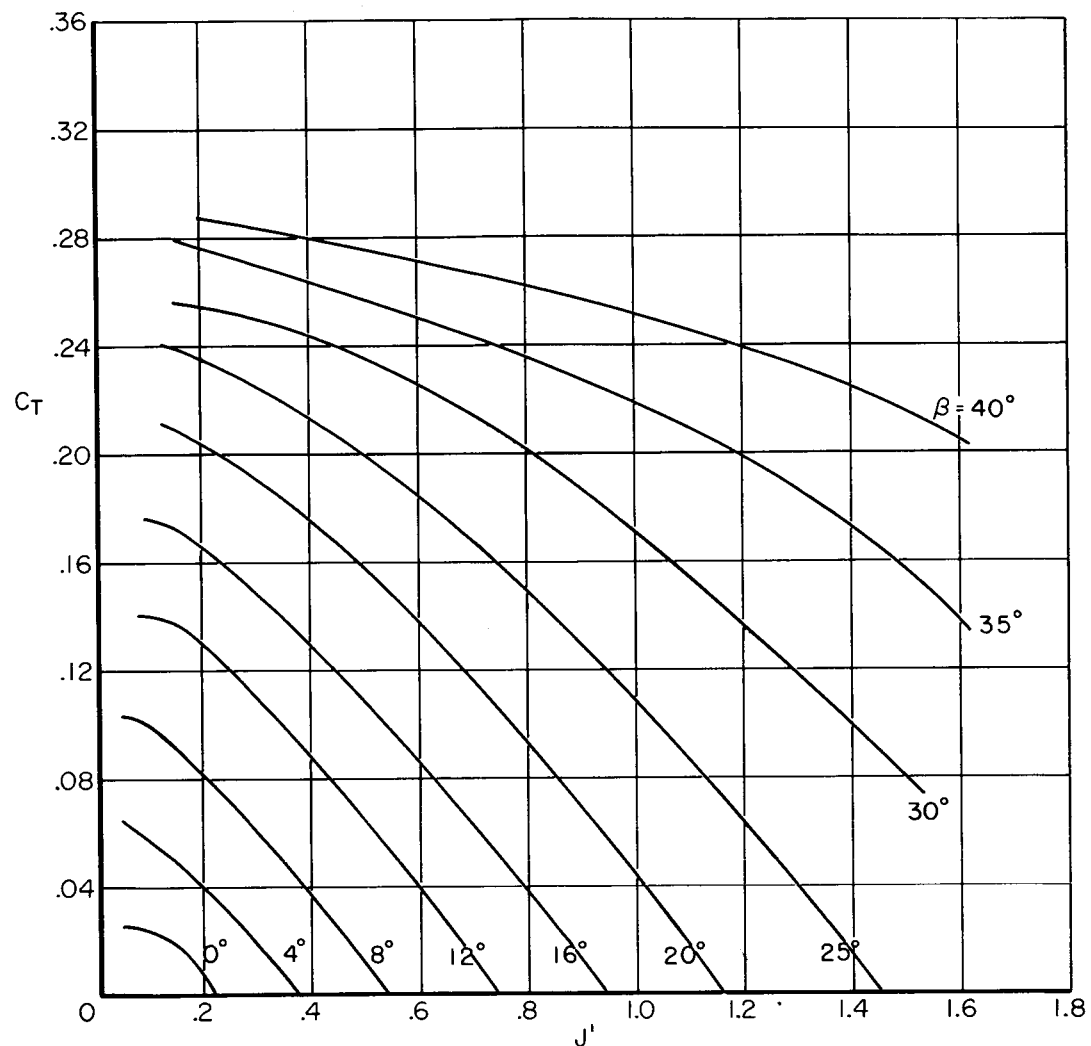
(a) Thrust coefficient C_T .

Figure 19.- Variation of the propeller performance parameters with modified advance ratio J' for several blade angles β ; $\alpha = 30^\circ$, propeller number 1.

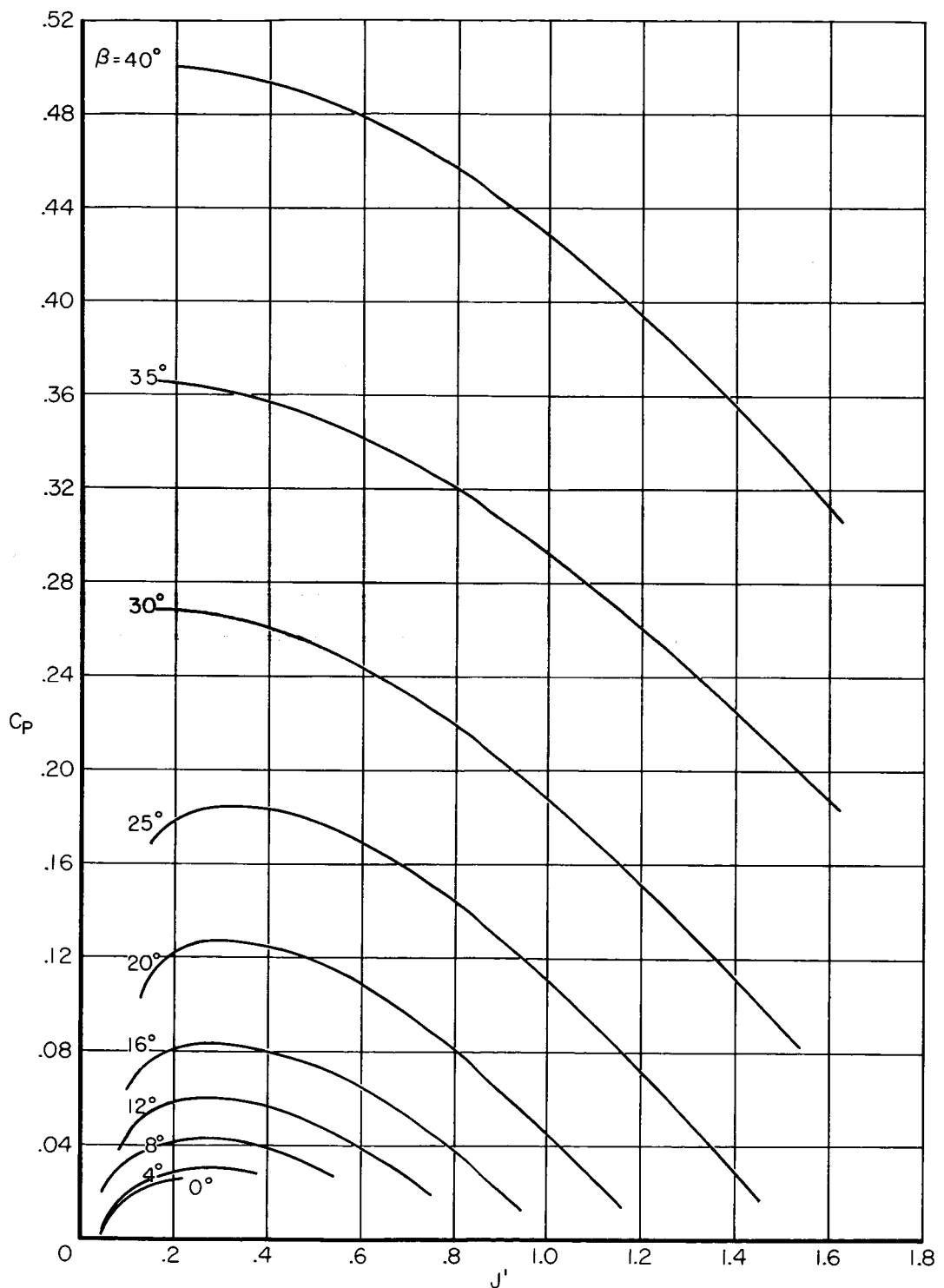
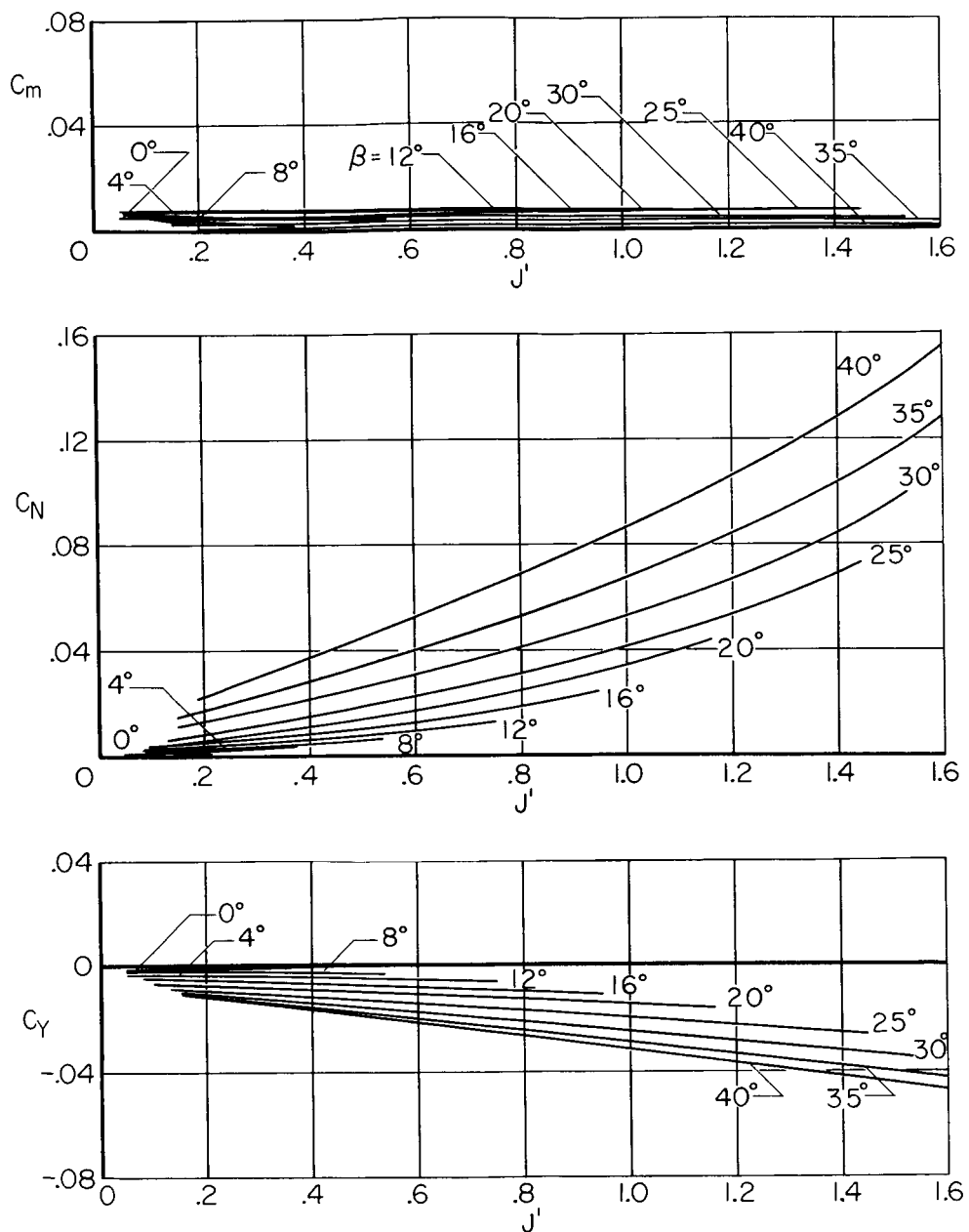
(b) Power coefficient C_P .

Figure 19.- Continued.



(c) Pitching-moment coefficient C_m ; normal-force coefficient C_N ; yawing-moment coefficient C_Y .

Figure 19.- Concluded.

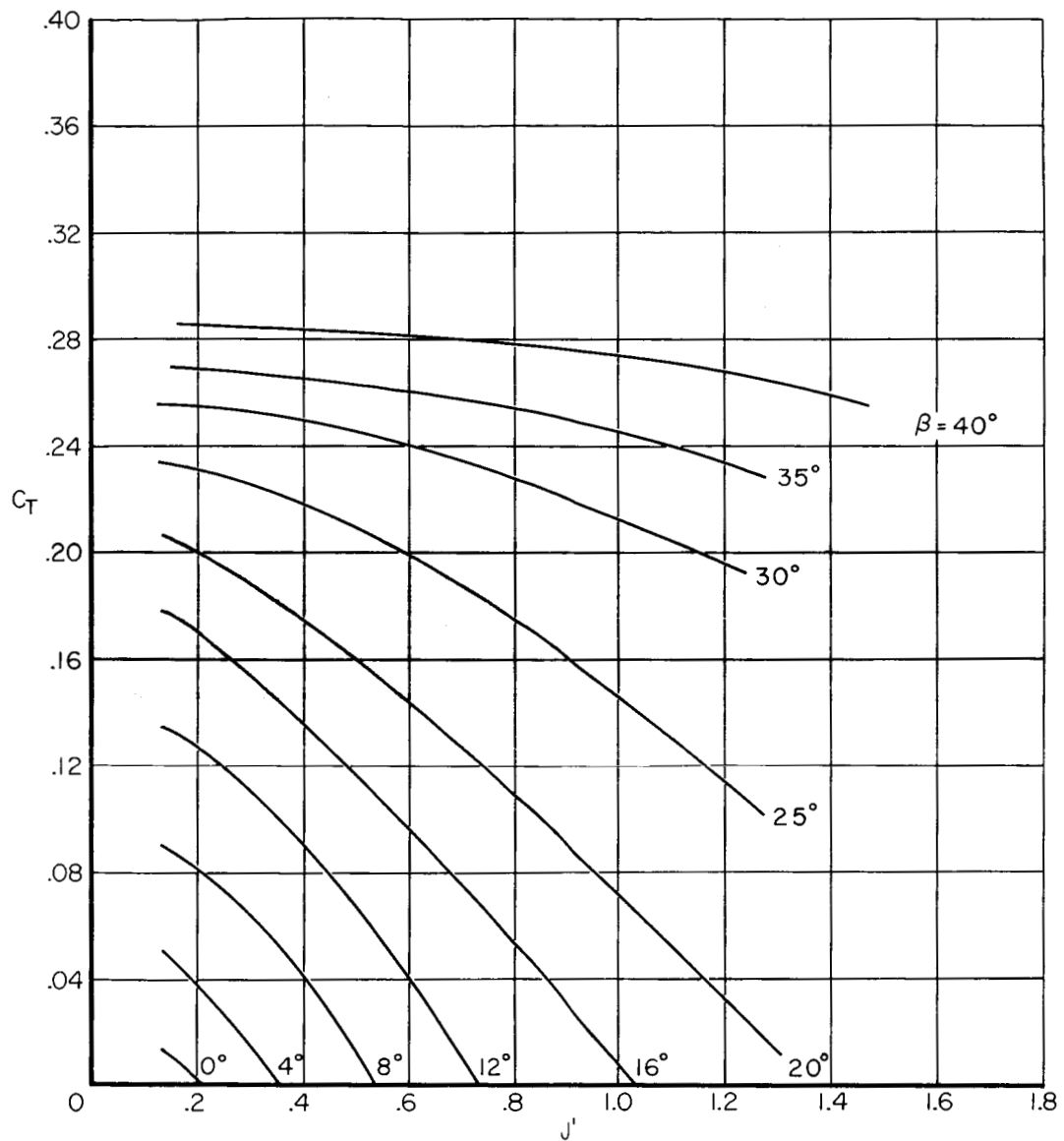
(a) Thrust coefficient C_T .

Figure 20.- Variation of the propeller performance parameters with modified advance ratio J' for several blade angles β ; $\alpha = 45^\circ$, propeller number 1.

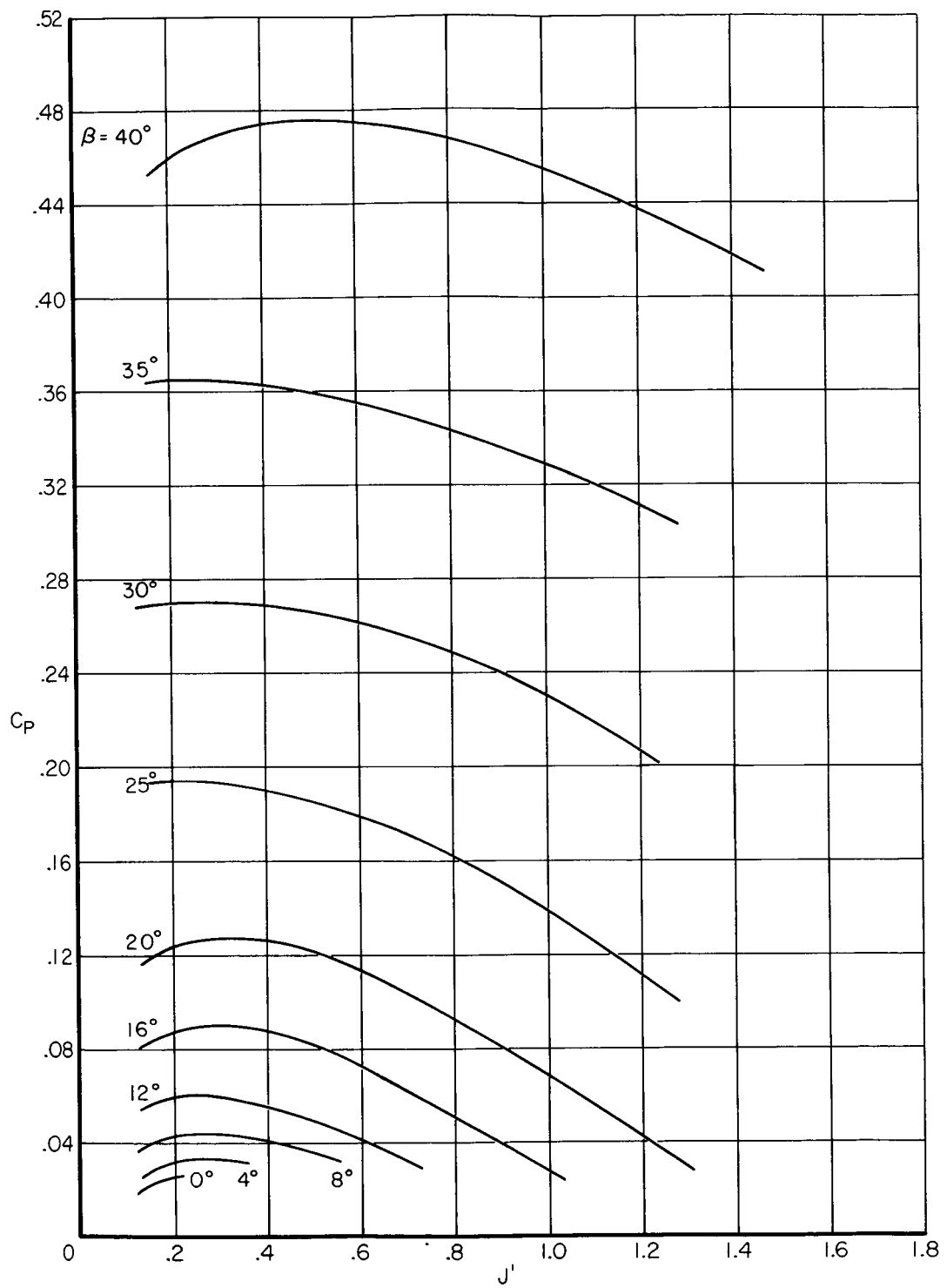
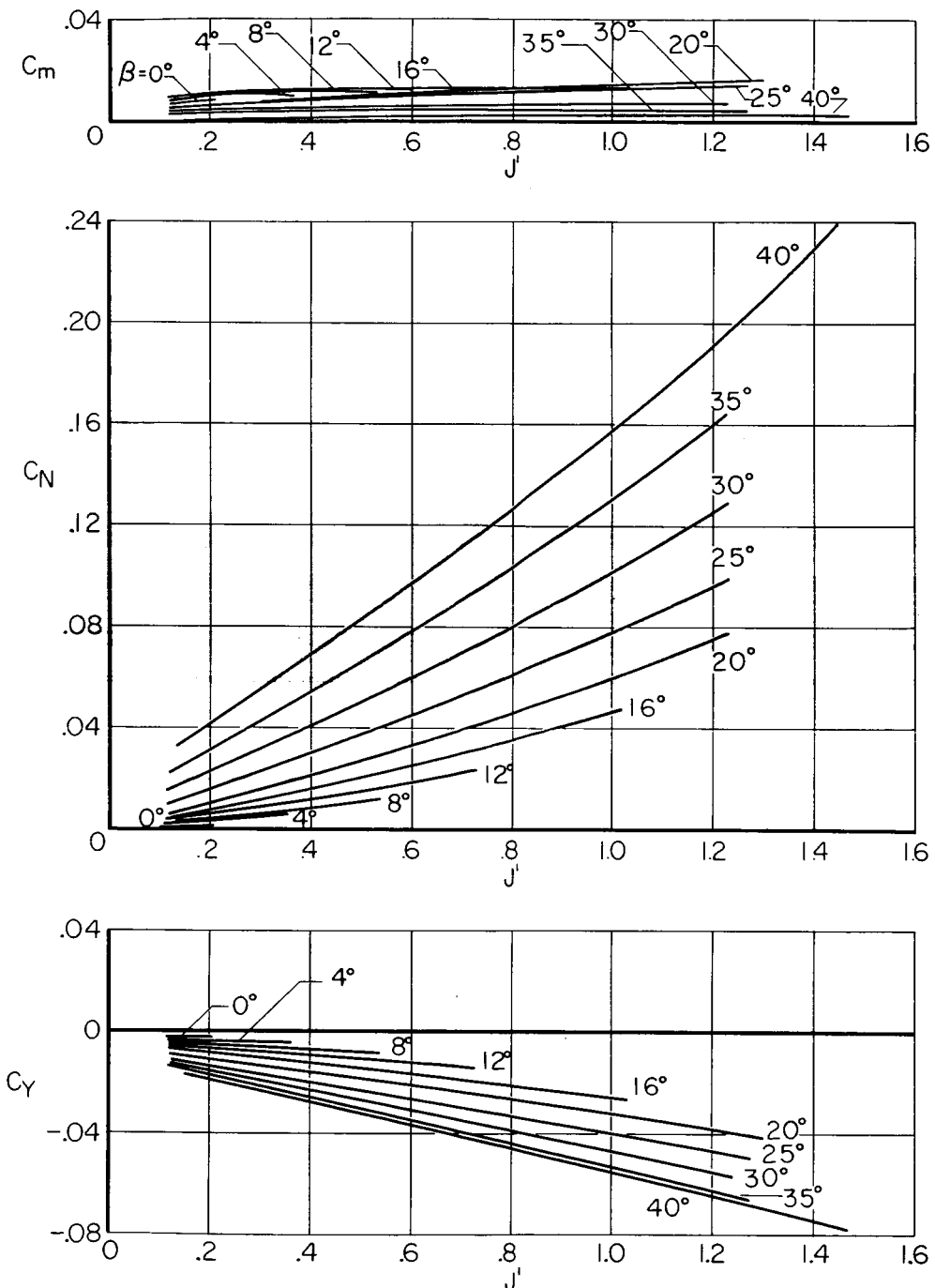
(b) Power coefficient C_P .

Figure 20.-- Continued.



(c) Pitching-moment coefficient C_m ; normal-force coefficient C_N ; yawing-moment coefficient C_Y .

Figure 20.- Concluded.

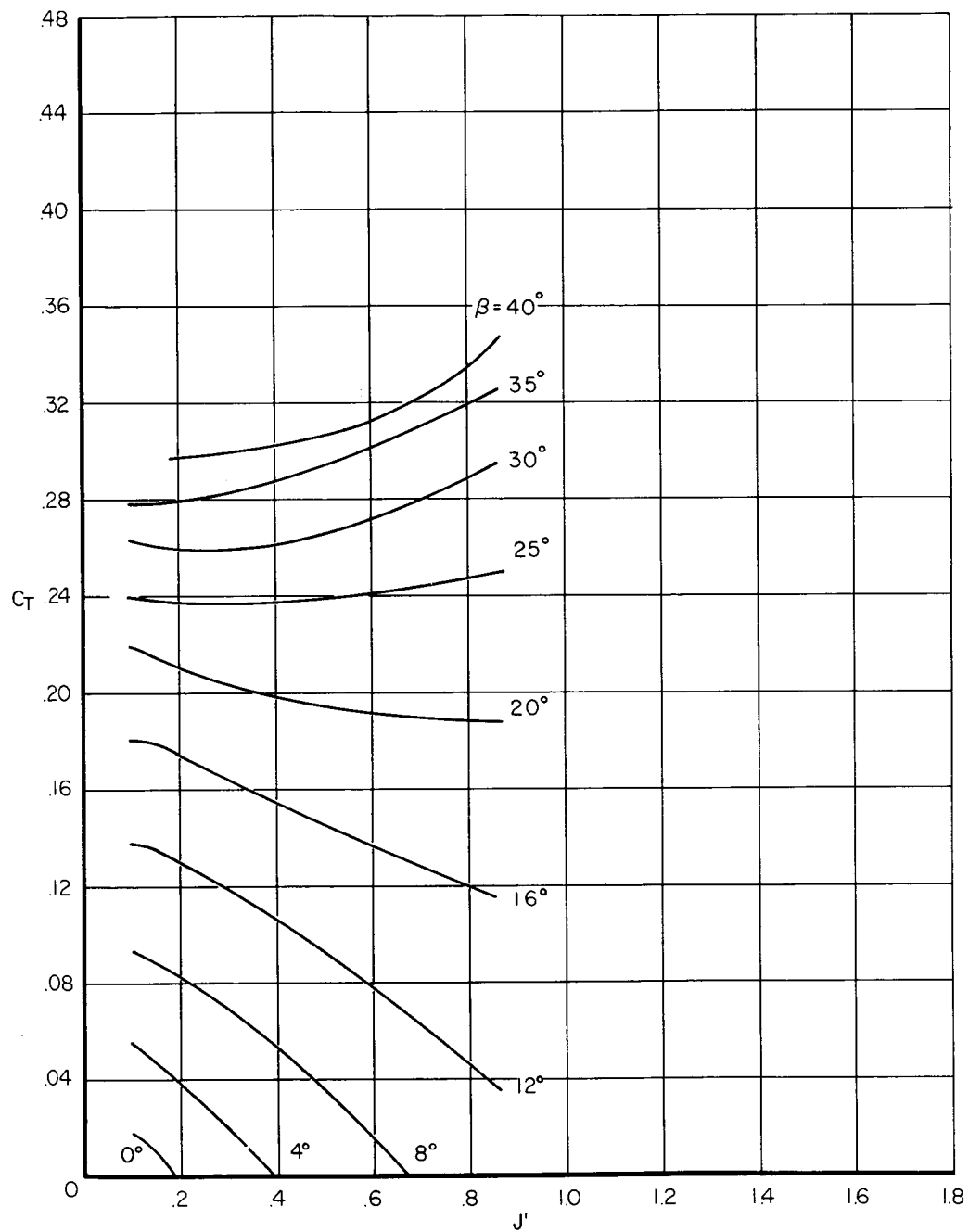
(a) Thrust coefficient C_T .

Figure 21.- Variation of the propeller performance parameters with modified advance ratio J' for several blade angles β ; $\alpha = 60^\circ$, propeller number 1.

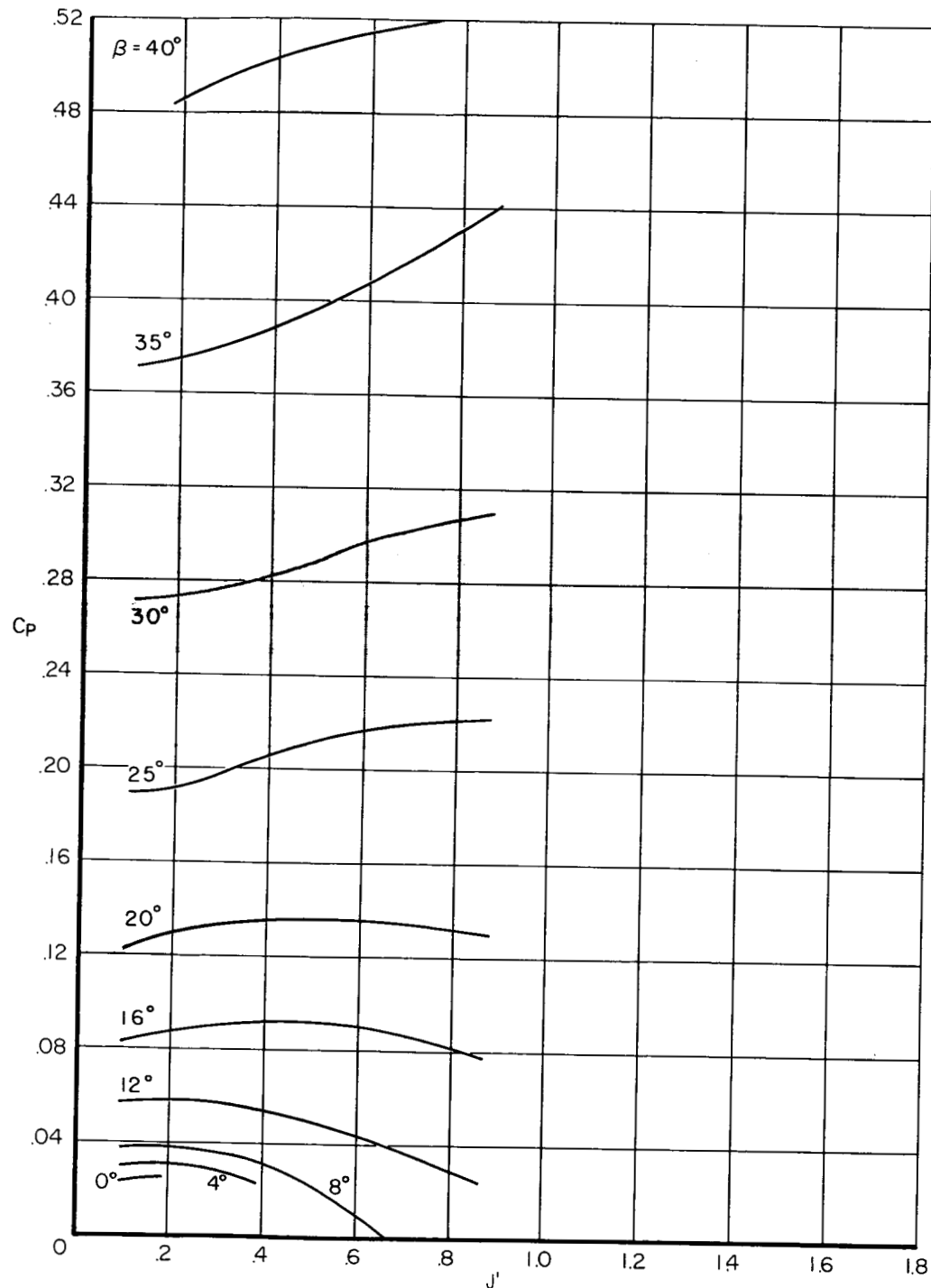
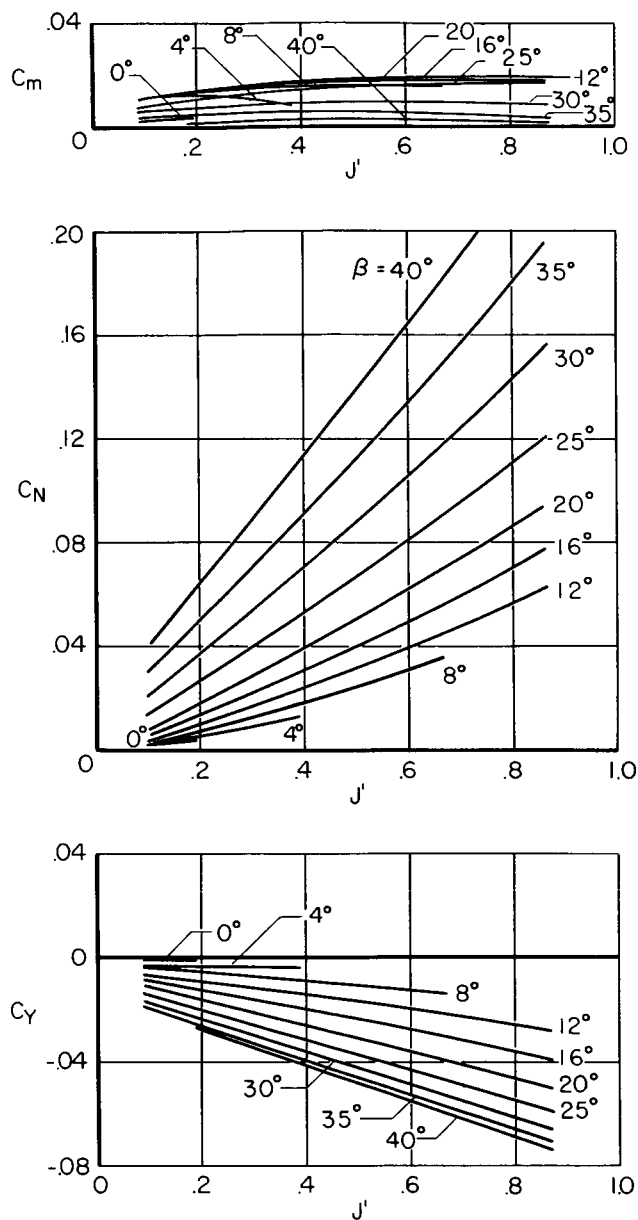
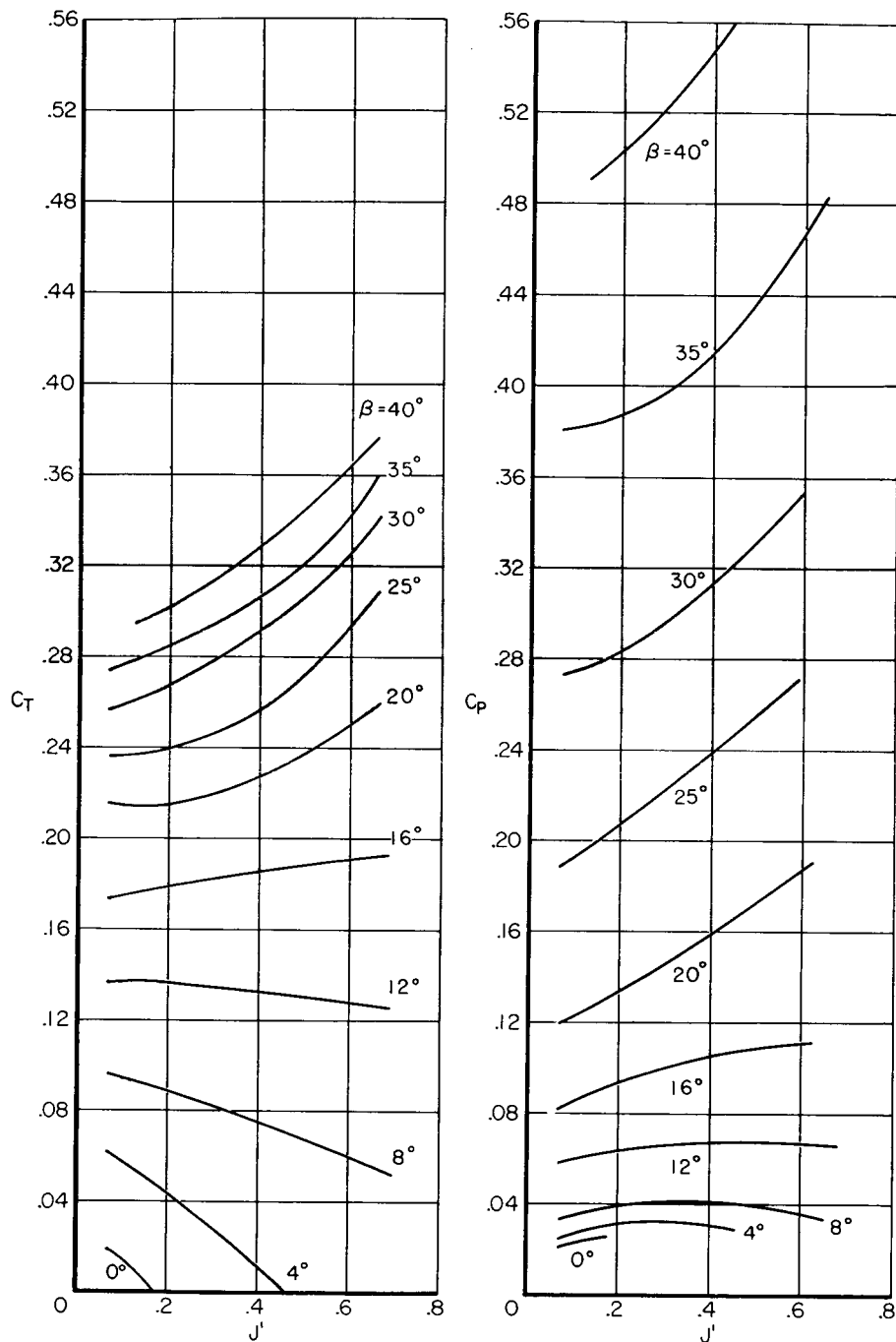
(b) Power coefficient C_P .

Figure 21.- Continued.



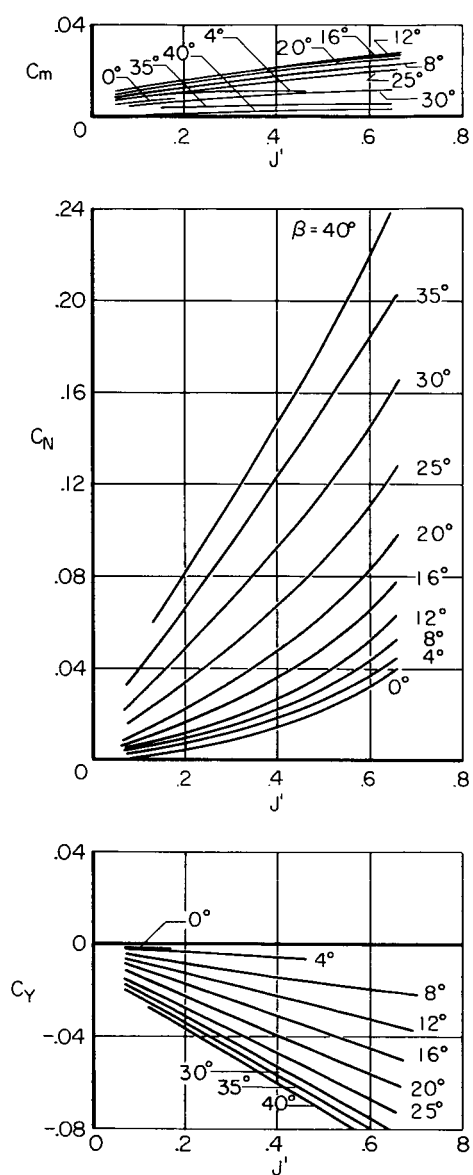
(c) Pitching-moment coefficient C_m ; normal-force coefficient C_N ; yawing-moment coefficient C_Y .

Figure 21.- Concluded.



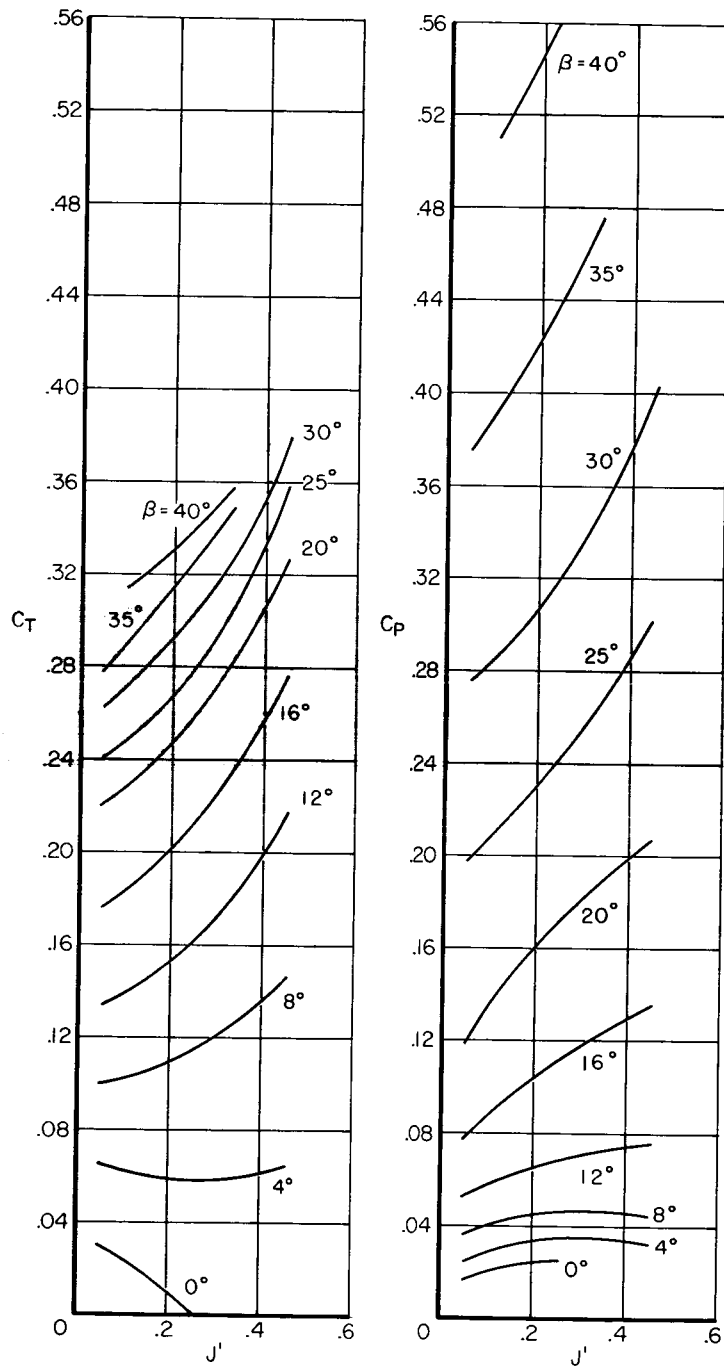
(a) Thrust coefficient C_T ; power coefficient C_P .

Figure 22.- Variation of the propeller performance parameters with modified advance ratio J' for several blade angles β ; $\alpha = 67.5^\circ$, propeller number 1.



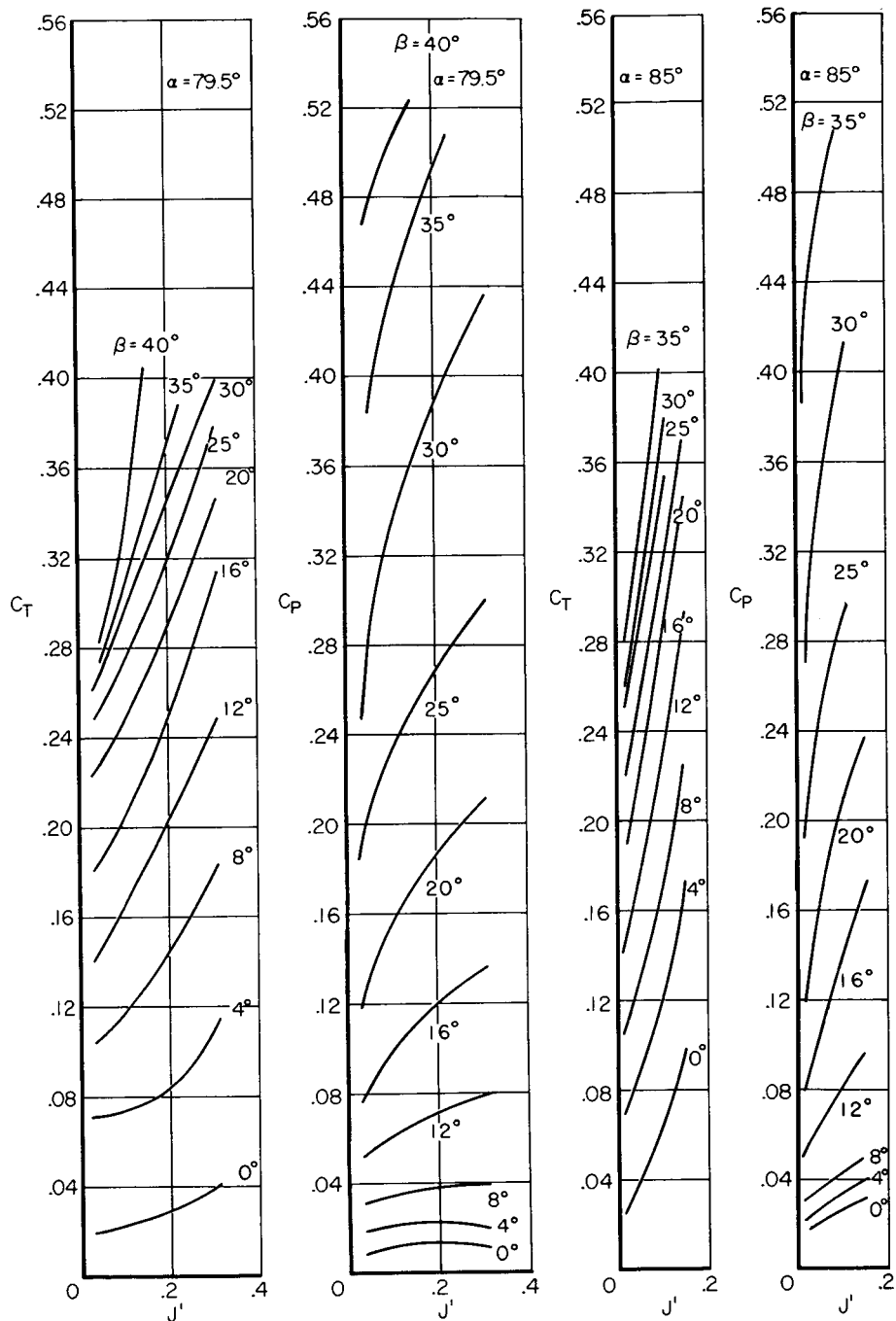
(b) Pitching-moment coefficient C_m ; normal-force coefficient C_N ; yawing-moment coefficient C_Y .

Figure 22.- Concluded.



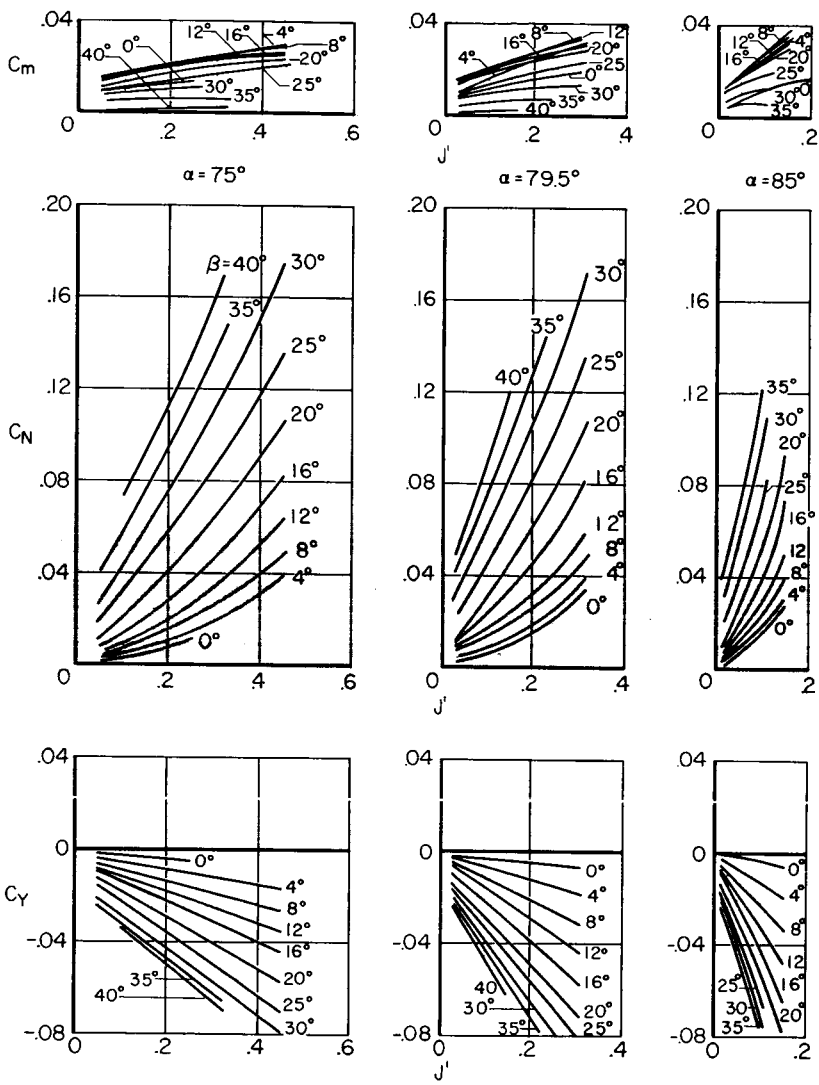
(a) Thrust coefficient C_T , $\alpha = 75^\circ$; power coefficient C_P , $\alpha = 75^\circ$.

Figure 23.- Variation of the propeller performance parameters with modified advance ratio J' for several blade angles β ; $\alpha = 75^\circ, 79.5^\circ$, and 85° , propeller number 1.



(b) Thrust coefficient C_T , $\alpha = 79.5^\circ$ and 85° ; power coefficient C_P , $\alpha = 79.5^\circ$ and 85° .

Figure 23.- Continued.



(c) Pitching-moment coefficient C_m , $\alpha = 75^\circ$, 79.5° , and 85° ; normal-force coefficient C_N , $\alpha = 75^\circ$, 79.5° , and 85° ; yawing-moment coefficient C_Y , $\alpha = 75^\circ$, 79.5° , and 85° .

Figure 23.- Concluded.

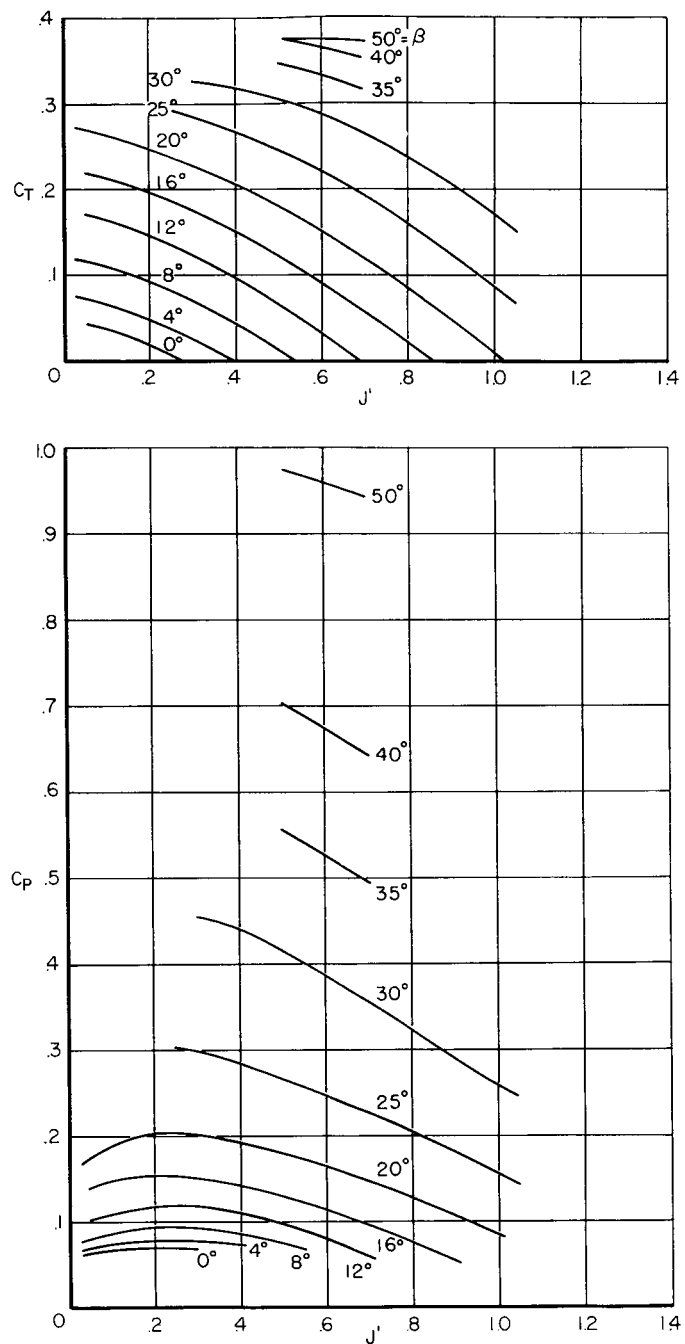
(a) Thrust coefficient C_T ; power coefficient C_P .

Figure 24.- Variation of the propeller performance parameters with modified advance ratio J' for several blade angles β ; $\alpha = 0^\circ$, propeller number 2.

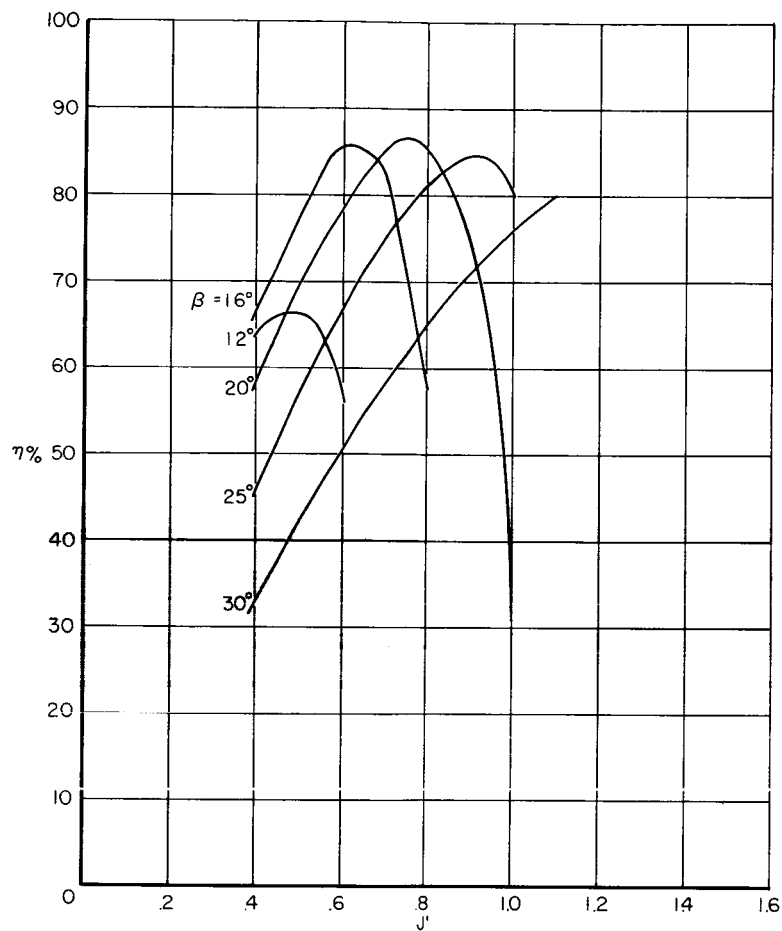
(b) Efficiency η .

Figure 24.- Concluded.

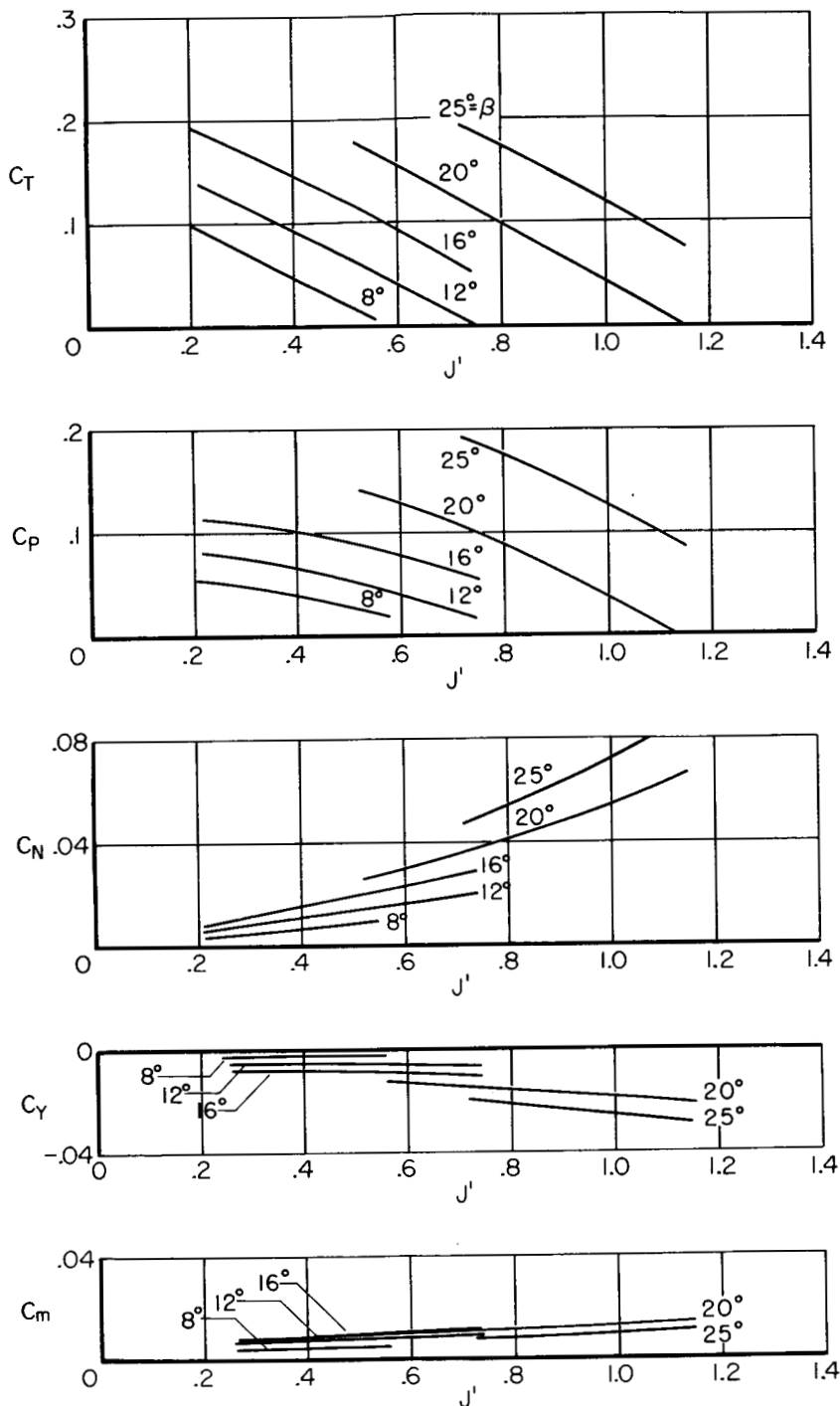


Figure 25.- Variation of the propeller performance parameters with modified advance ratio J' for several blade angles β ; $\alpha = 30^\circ$, propeller number 2.

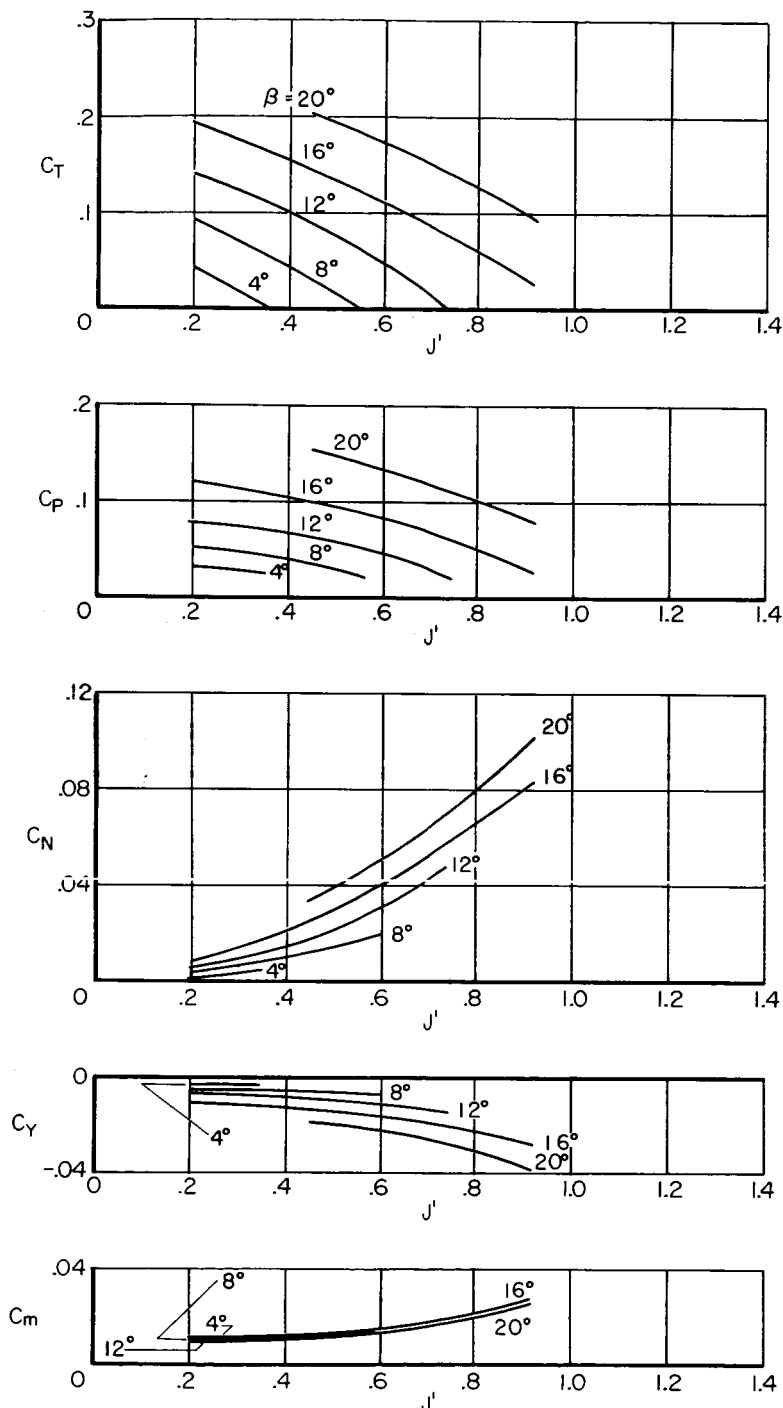


Figure 26.- Variation of the propeller performance parameters with modified advance ratio J' for several blade angles β ; $\alpha = 45^\circ$, propeller number 2.

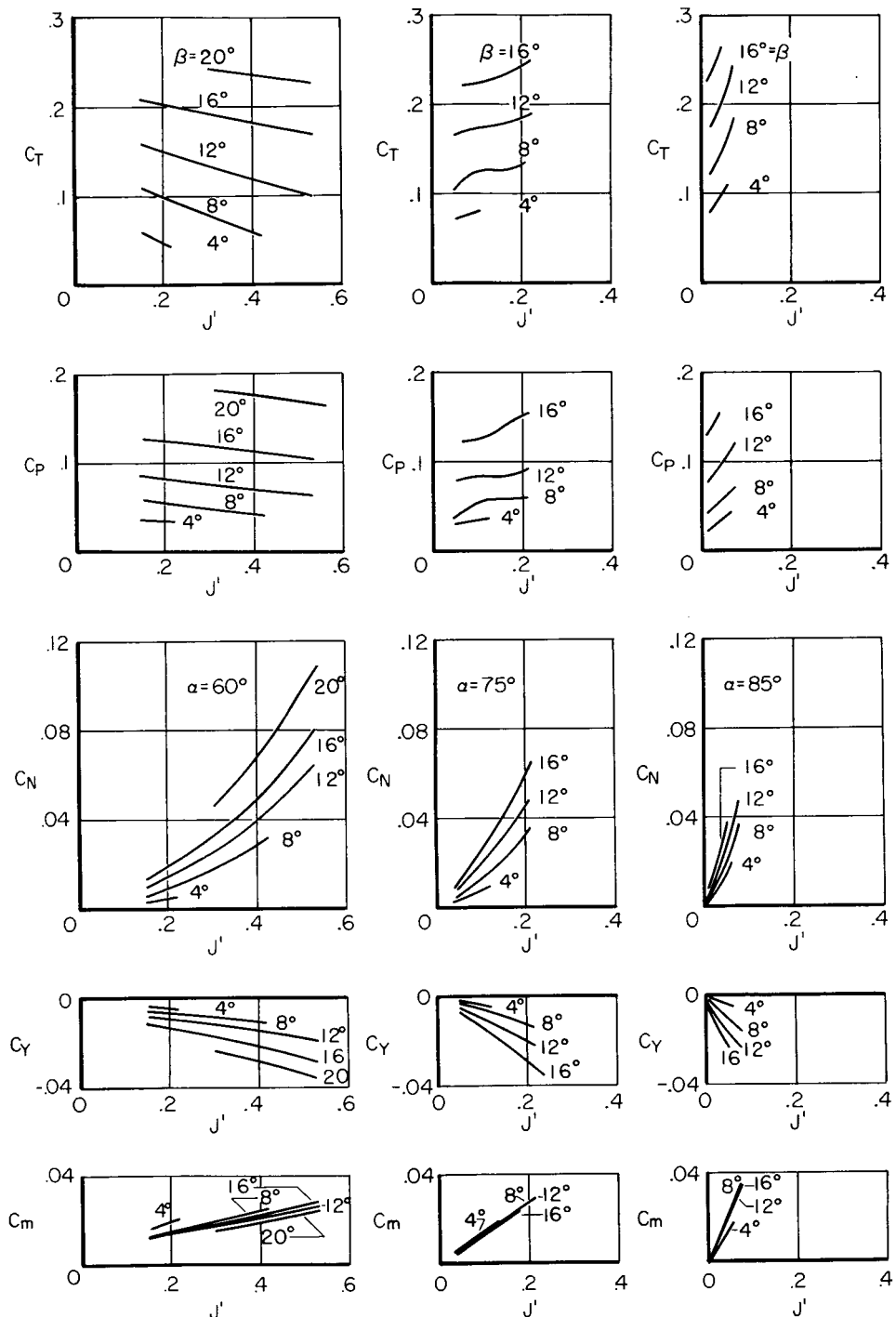
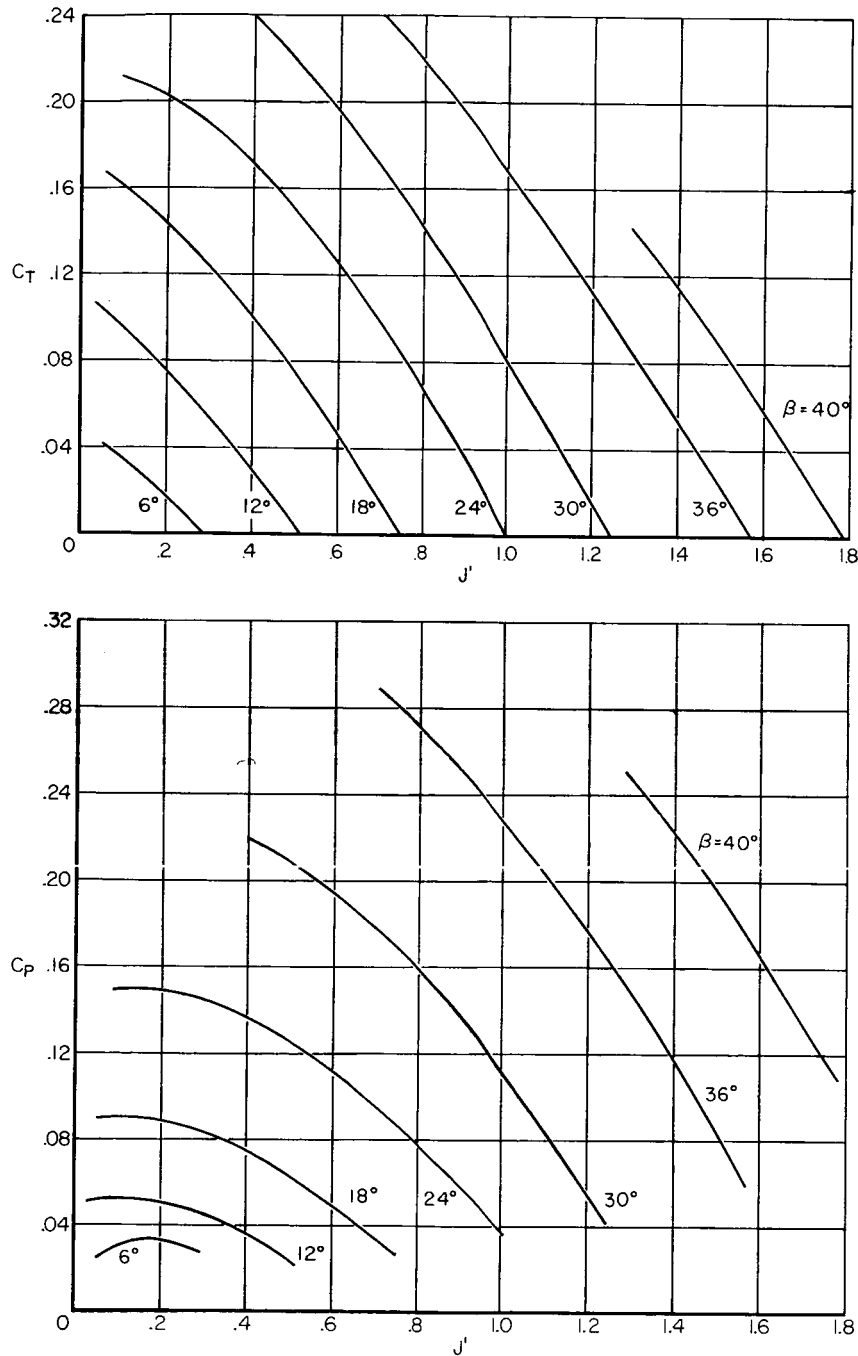


Figure 27.- Variation of the propeller performance parameters with modified advance ratio J' for several blade angles β ; $\alpha = 60^\circ$, 75° , and 85° , propeller number 2.



(a) Thrust coefficient C_T ; power coefficient C_P .

Figure 28.- Variation of the propeller performance parameters with modified advance ratio J' for several blade angles β ; $\alpha = 0^\circ$, propeller number 3.

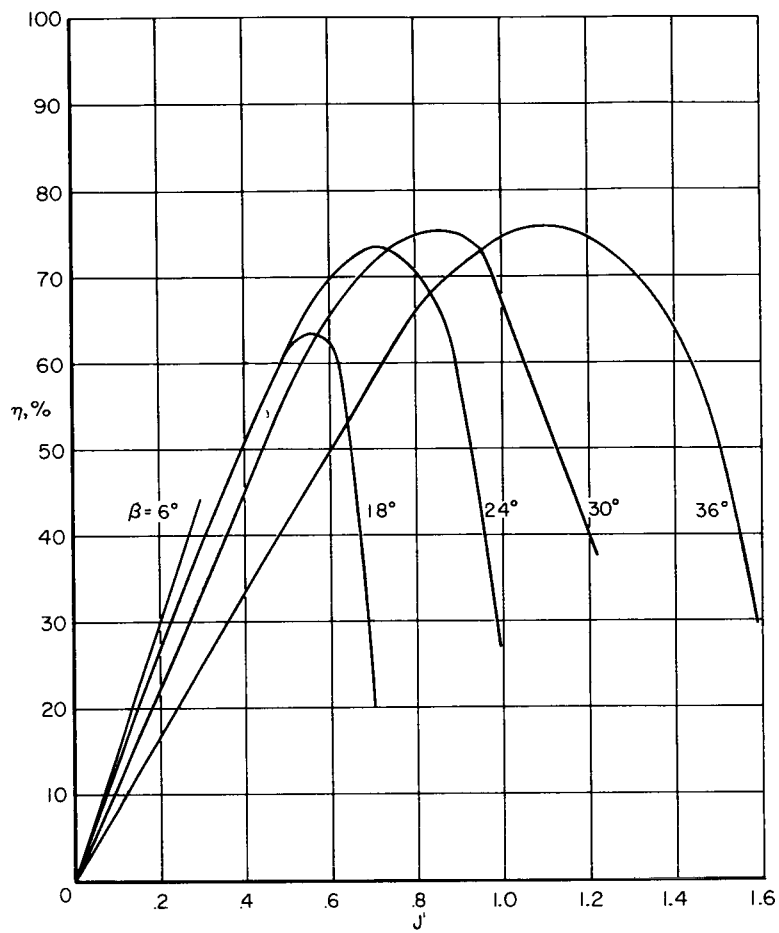
(b) Efficiency η .

Figure 28.- Concluded.

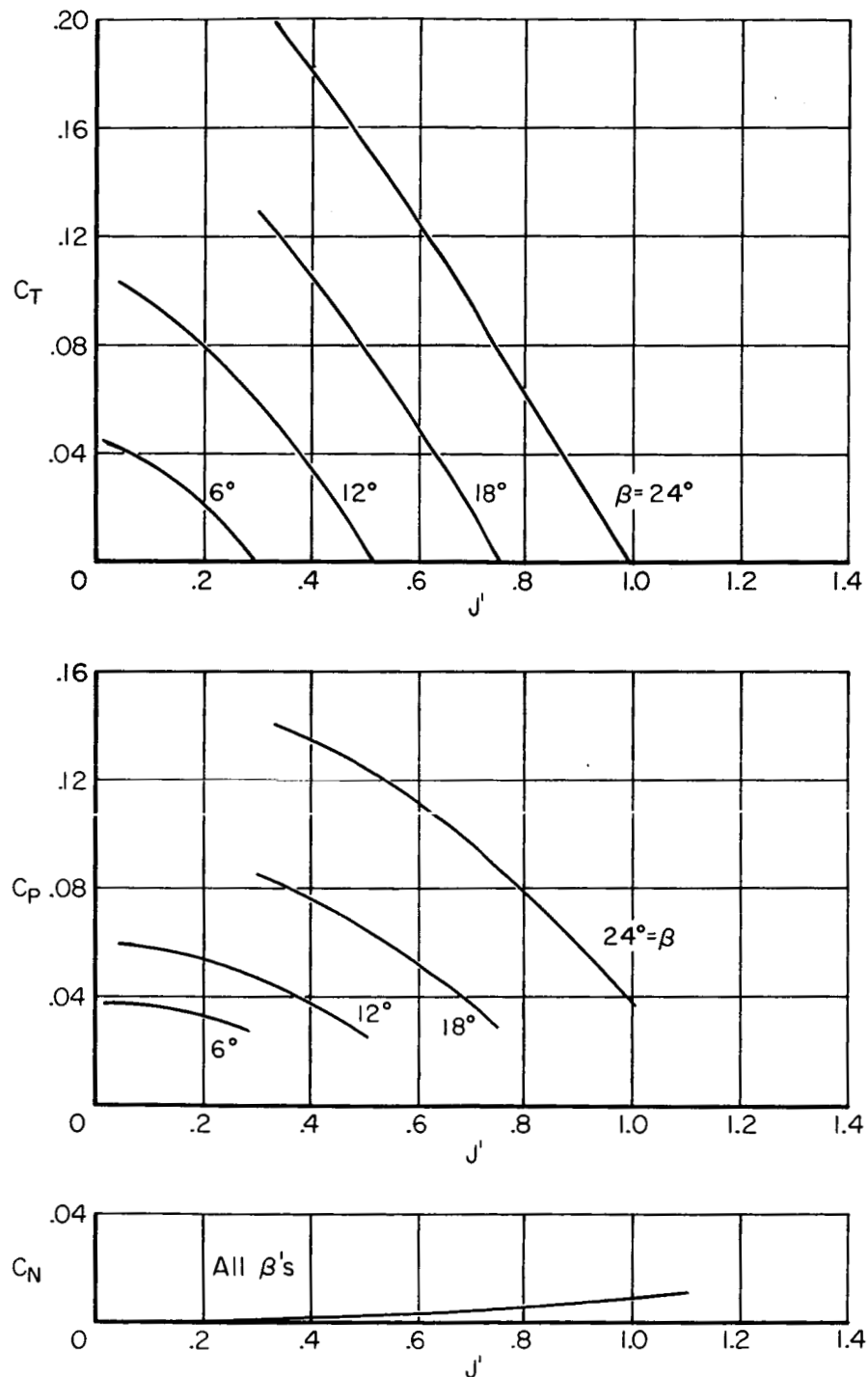


Figure 29.- Variation of the propeller performance parameters with modified advance ratio J' for several blade angles β ; $\alpha = 15^\circ$, propeller number 3.

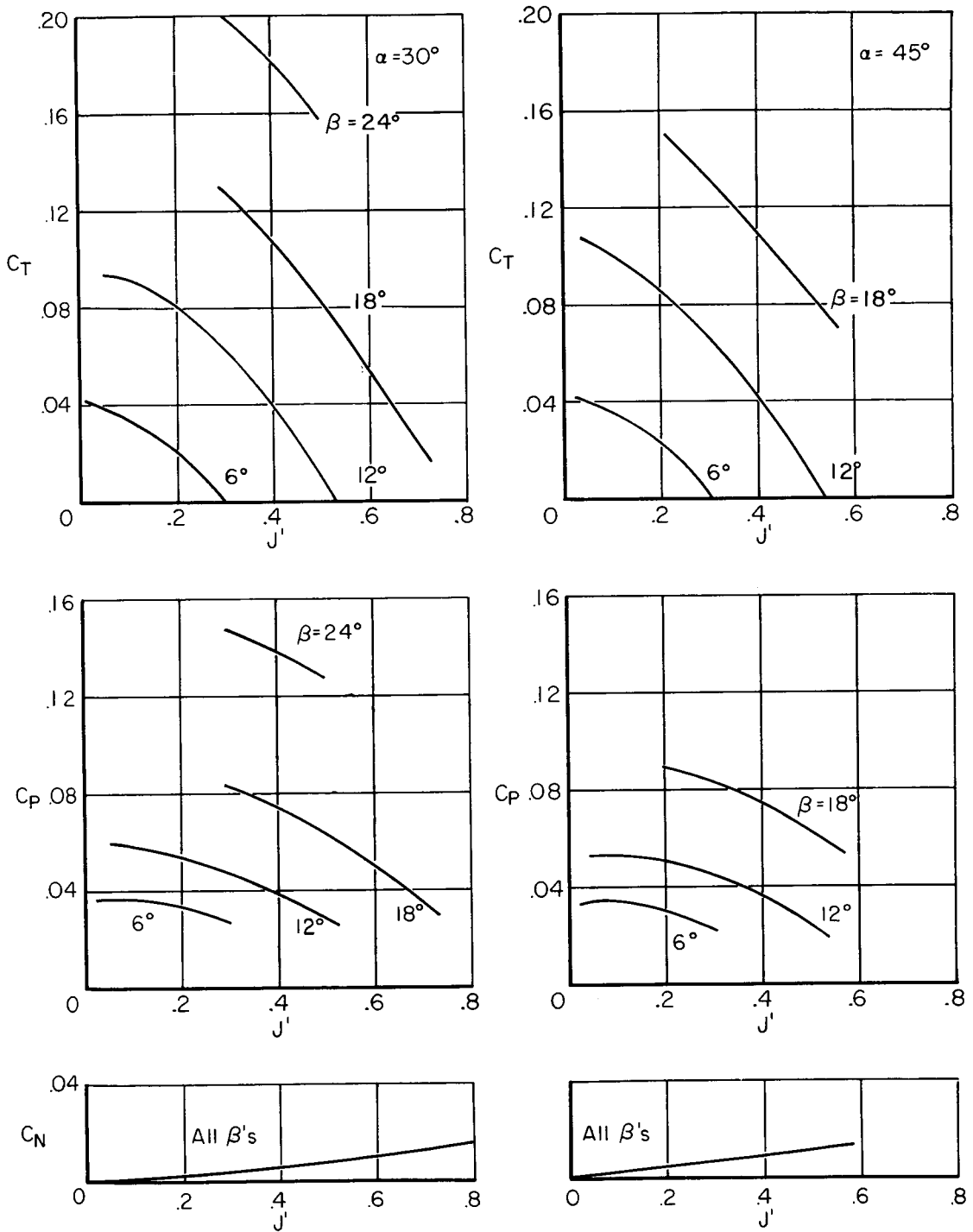


Figure 30.- Variation of the propeller performance parameters with modified advance ratio J' for several blade angles β ; $\alpha = 30^\circ$ and 45° , propeller number 3.

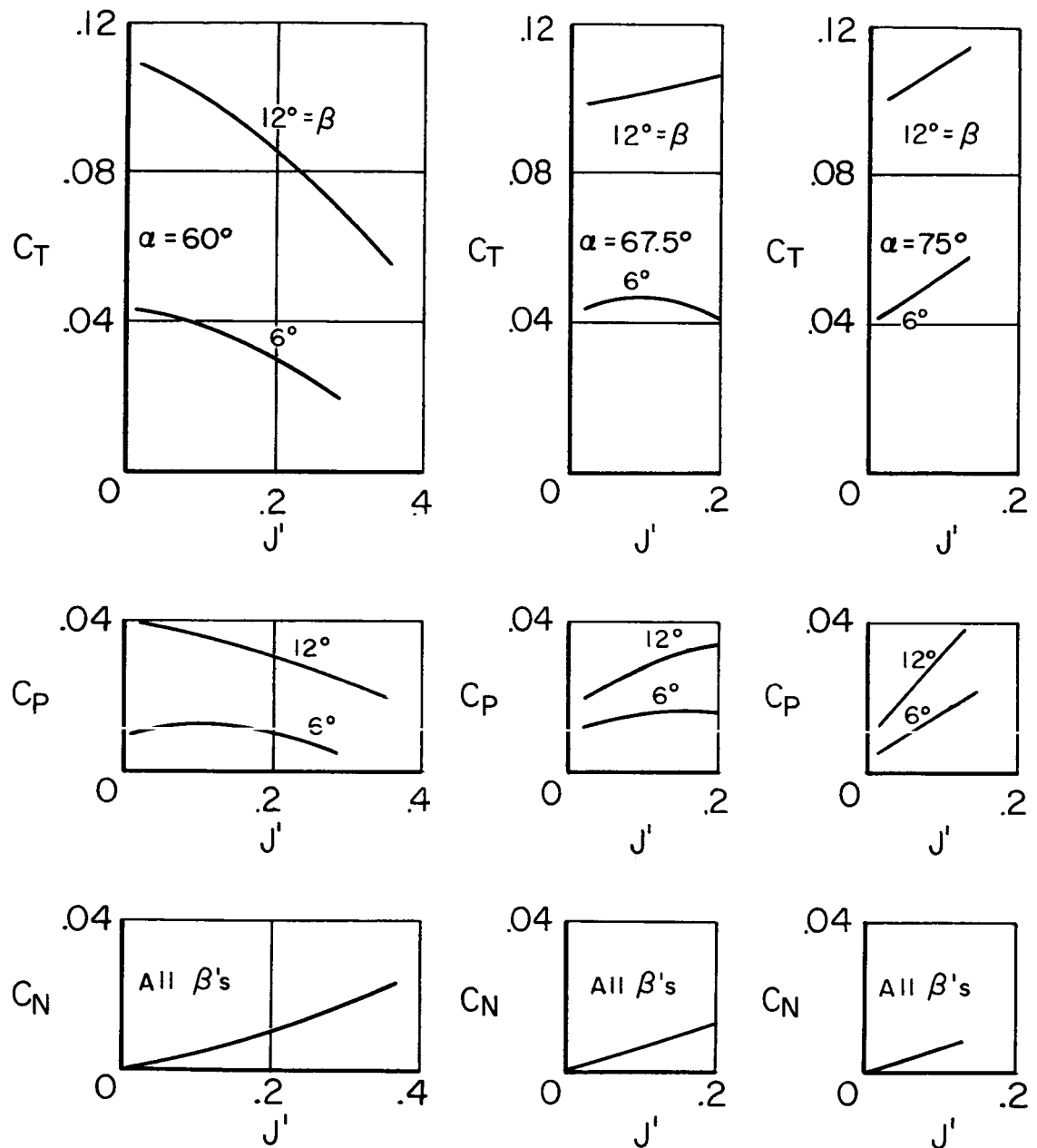


Figure 31.- Variation of the propeller performance parameters with modified advance ratio J' for several blade angles β ; $\alpha = 60^\circ$, 67.5° , and 75° , propeller number 3.